Pathophysiology of *KCNA2*-mediated epileptic encephalopathies and the effect of *SCN1A* variants on thalamocortical up-states

Dissertation

zur Erlangung des Grades eines
Doktors der Naturwissenschaften

der Mathematisch-Naturwissenschaftlichen Fakultät
und
der Medizinischen Fakultät
der Eberhard-Karls-Universität Tübingen

vorgelegt
von

Harshad Panikkaveettil Ashraf
aus Kerala, India

May - 2020

Tag der mündlichen Prüfung: 02.07.2020

Dekan der Math.-Nat. Fakultät: Prof. Dr. W. Rosenstiel
Dekan der Medizinischen Fakultät: Prof. Dr. I. B. Autenrieth

1. Berichterstatter: Prof. Dr. Holger Lerche

2. Berichterstatter: Prof. Dr. Cornelius Schwarz

Prüfungskommission: Prof. Dr. Holger Lerche

Prof. Dr. Cornelius Schwarz

Prof. Dr. Jan Benda

Prof. Dr. Thomas Euler

Erklärung / Declaration:

Ich erkläre, dass ich die zur Promotion eingereichte Arbeit mit dem

„Pathophysiology of *KCNA2*-mediated epileptic encephalopathies and the effect of *SCN1A* variants on thalamocortical up-states“

selbständig verfasst, nur die angegebenen Quellen und Hilfsmittel benutzt und wörtlich oder inhaltlich übernommene Stellen als solche gekennzeichnet habe. Ich versichere an Eides statt, dass diese Angaben wahr sind und dass ich nichts verschwiegen habe. Mir ist bekannt, dass die falsche Abgabe einer Versicherung an Eides statt mit Freiheitsstrafe bis zu drei Jahren oder mit Geldstrafe bestraft wird.

I hereby declare that I have produced the work entitled "Pathophysiology of KCNA2-mediated epileptic encephalopathies and the effect of SCN1A variants on thalamocortical up-states", submitted for the award of a doctorate, on my own (without external help), have used only the sources and aids indicated and have marked passages included from other works, whether verbatim or in content, as such. I swear upon oath that these statements are true and that I have not concealed anything. I am aware that making a false declaration under oath is punishable by a term of imprisonment of up to three years or by a fine.

Tübingen, den ....

Datum / Date Unterschrift /Signature

This is to my parents and teachers, who are the root and light of my life.

Contents

List of abbreviations

ACSF	Artificial cerebrospinal fluid
ADNFLE	Autosomal dominant nocturnal frontal lobe epilepsy
AHP	Afterhyperpolarization
AIS	Axon initial segment
AP	Action potential
BFNS	Benign familial neonatal seizures
CAE	Childhood absence epilepsy
CNS	Central nervous system
DEE	Developmental and epileptic encephalopathy
DS	Dyscognitive seizures
EA	Episodic ataxia
EDTA	Ethylenediaminetetraacetic acid
EEG	Electroencephalography
EGTA	Ethylene glycol tetraacetic acid
EoEE	Early-onset epileptic encephalopathy
ESES	Electrical status epilepticus of sleep
FDS	Focal dyscognitive seizures
FHM3	Familial hemiplegic migraine type 3
FS	Focal seizure
GABA	Gamma aminobutyric acid
GEFS+	Generalized epilepsy with febrile seizures plus
GGE	Genetic generalized epilepsy
G-LOF	Gain and Loss-of-function
GOF	Gain-of-function
GSW	Generalized spike and wave
GTCS	Generalized tonic–clonic seizure
HET	Heterozygous
HSP	Hereditary Spastic Paraplegias
ID	Intellectual disability
IGE	Idiopathic generalized epilepsy
ILAE	International League Against Epilepsy
IPSC	Inhibitory postsynaptic currents
ISI	Inter-spike intervals

IUE	*In utero* electroporation
JAE	Juvenile absence epilepsy
KO	Knock out
$K_V1.2$	Voltage gated potassium channel 1.2
LOF	Loss-of-function
MA	Myoclonic-atonic seizures
MC	Myoclonic seizures
MNTB	Medial nucleus of the trapezoid body
MUA	Multi-unit activity
$Na_V1.1$	Voltage gated sodium channel 1.1
NREM	Non-rapid-eye-movement
NRT	Reticular nucleus of thalamus
p/s	Penicillin streptomycin
PBS	phosphate-buffered saline
PCR	Polymerase chain reaction
RPM	Revolutions per minute
RTT	Rett syndrome
SEM	Standard error of the mean
SMEI	Severe myoclonic epilepsy of infancy
SSC L2/3	Somatosensory cortex layer two and three
SWS	Slow-wave sleep
Tau	Time constant
TC	Thalamocortical
VB	Ventrobasal complex
WT	Wild type

Summary

Understanding the pathophysiological consequences of different ion-channel encoding gene mutations in the evolution of epileptic seizures remains a major goal in epilepsy research. Even after understanding the complex mechanisms that underlie epileptogenesis, the comorbidities associated with epilepsy still need to be studied. The development of new effective treatment options is totally dependent on the knowledge of these mechanisms. In this context, my thesis aimed to address the following two aspects of epilepsies:

(1) The pathophysiological mechanisms and development of treatment strategies for *KCNA2*-mediated developmental and epileptic encephalopathies:

Developmental and epileptic encephalopathies (DEE) are disorders of early childhood, characterized by severe recurrent seizures and mental dysfunction. Often this progressive deterioration may be due to gene mutations induced effects or sometimes also to continuous seizures during development. *KCNA2* has been identified as one of the candidate genes in DEE that encodes the voltage-gated potassium channel $K_V1.2$, which is important in shaping neuronal repolarization. $K_V1.2$ expresses in both excitatory and inhibitory neurons of the central nervous system (CNS). In the present work, I intended to unravel the pathophysiological mechanisms of both loss- and gain-of-function (LOF/GOF) *KCNA2* variants for the morphological and electrophysiological properties of single neurons. Both forms of variants cause clinically distinguishable syndromes. Mouse models overexpressing (*in utero*) wildtype and mutated $K_V1.2$ channel subunits in somatosensory cortical layer 2/3 pyramidal neurons were used to get insights into the related pathophysiology. Electrophysiological and histochemical approaches were used to decipher single neuronal level changes. My results showed a reduction in dendritic arborization and action potential firing in $K_V1.2$ WT as well as GOF variant overexpressing neurons, probably due to a membrane hyperpolarization. Overexpression of LOF variant exhibited a considerable reduction in the number of APs probably due to the elongated repolarization phase, without significantly altering the morphological features as compared to control cells. The current study also analysed the application of therapeutic approaches using 4-Aminopyridine (4-AP) as a specific blocker for K_V1 and K_V4 potassium channels, which rescued the $K_V1.2$ WT overexpressing neurons from their hypoexcitablity. These findings provided the leads in addressing the therapeutic manipulation of *KCNA2* gene-related epileptic encephalopathy by using specific antagonist mechanisms.

(2) Effect of $Na_V1.1$ mutations on thalamocortical up-states studied in genetic mouse models:

Epilepsy and sleep are interrelated, and share the same thalamocortical (TC) loop as a regulatory mechanism. However, the interrelation between sleep and epilepsy at the molecular and cellular level is still unclear. The usage of antiepileptic drugs in patients has made it hard to understand this interconnection. Genetic mouse models carrying LOF and GOF mutations in *SCN1A* gene encoding $Na_V1.1$ are possible windows to open this reciprocal interaction. Mutations in $Na_V1.1$ channels have mainly altered inhibitory neuronal firing and thus led to uncontrolled firing in excitatory neurons and epilepsy. The characteristics of spontaneously generated TC up-states (<1Hz) within *in vitro* brain slices were studied through extracellular multi-unit (MU) neuronal recordings. The project had two objectives: (i) To understand the effect of *SCN1A* LOF on TC network dysfunction. (ii) To investigate the effect of *SCN1A* GOF (thus, an opposite molecular defect causing a rare sub-form of migraine) on TC up-states. I recorded TC up- and down-states from layer V neurons of somatosensory cortex (SSC) of acute and organotypic brain slices from *SCN1A* mouse. Recordings from both LOF and GOF conditions showed a reduction in the frequency of TC up states. This indicates the strong influence of inhibitory neurons in maintaining the balance of synchronized TC network firing, which is an important aspect of slow-wave sleep (SWS). However, this needs further validation experiments using *in vivo* models.

Overall, my thesis showed first pathophysiological neuronal mechanisms and 4-AP as an effective precision therapy (*in vitro*) in *KCNA2*-related DEE. The current work also showed an impact of *SCN1A* variants (LOF and GOF) on the TC network.

1. Introduction

1.1 Epilepsy: a general introduction

Epilepsy is one of the most common chronic neurological disorders which affects 50 million people worldwide. It is characterized by the occurrence of unprovoked recurrent seizures (at least two seizures > 24 hours apart) (Fisher *et al.*, 2014). According to the International League Against Epilepsy (ILAE), an epileptic seizure can be defined as a "transient occurrence of signs and/or symptoms due to abnormal excessive or synchronous neuronal activity in the brain" (Fisher *et al.*, 2005). The severity of these uncontrolled electrical discharges can vary from short attention lapses or muscle jerks to prolonged febrile convulsions with a frequency change from less than one per year to several per day. The epileptic seizures may lead to involuntary movement in parts of or the entire body and are sometimes accompanied by loss of consciousness as well as control of bowel or bladder function. The clinical symptoms of seizures one experiences depend on the affected part of the brain and etiologies (Berg *et al.*, 2010; McTague *et al.*, 2016; Scheffer *et al.*, 2017).

In 2017, the ILAE presented a revised three-level classification of epilepsy diagnosis based on seizure type, epilepsy type and epilepsy syndrome. These reports also inform about the epileptic comorbidities with detailed guidance for the selection of appropriate antiepileptic therapies. In the first level, epileptic seizures are classified according to their onset, such as focal, generalized and unknown. In the second level, epilepsies categorize into four: focal, generalized, combined generalized and focal, and unknown. In Focal (formerly partial) epilepsies or seizures, the seizure origin limited to small neuronal networks (a point around the structural lesion) within one hemisphere. Conversely, in generalized conditions, seizures originate from both hemispheres simultaneously. If the seizure origin is unable to locate in patients, it goes to the category of unknown. Under some conditions, patients show both generalized and focal seizures, this is included in the group of combined generalized and focal epilepsies. In epilepsy syndromes, seizure types are present with a cluster of features and incorporated with distinctive comorbidities such as intellectual and psychiatric dysfunction. Childhood absence epilepsy, West syndrome, Dravet syndrome, etc. are classical examples of epilepsy syndromes. An overview of the ILAE classification is depicted in Figure 1. Further classification has been carried out based on epilepsy etiology such as genetic, structural, infectious, metabolic and immune (Fisher *et al.*, 2017; Scheffer *et al.*, 2017).

Epileptic etiology usually varies with age. Childhood epilepsies are generally due to genetic predisposition, whereas in late adulthood, it is often due to structural or functional abnormalities. The underlying reason for the structural brain tissue damages may be genetic

or acquired, or both (e.g., brain trauma or prenatal or perinatal injuries, tumors, metabolic diseases, malformations of brain development, etc.). Other reasons like infections, metabolic, immune and unknown are also involved in etiologic classification. Genetic generalized epilepsies contribute about 30% of all etiologies. Genetic epilepsies are quite diverse and result directly from genetic mutations of known or presumed functionally important genes. Seizures with typical electroclinical presentations are interpreted as symptoms of genetic epilepsies (Heron *et al.*, 2007).

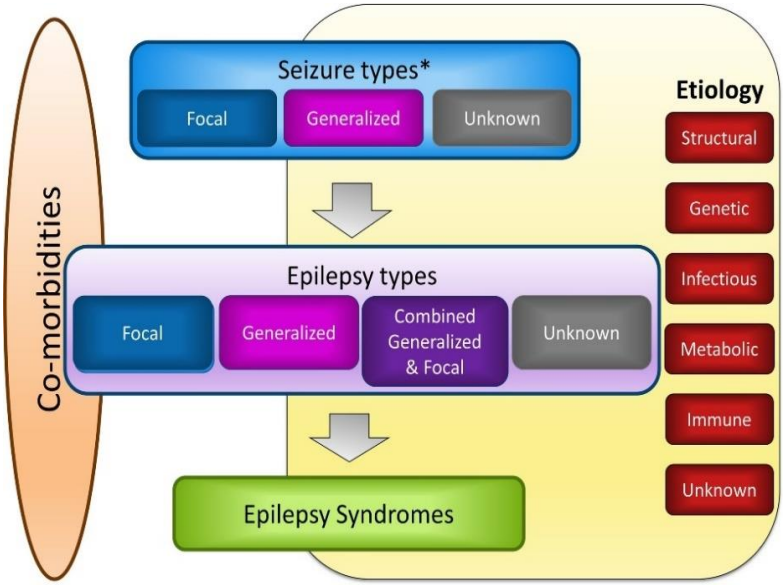

Figure 1. The revised ILAE classification of epilepsies: Epilepsies are classified into three-level according to the onset and origin of the seizures and epilepsy syndromes. It also includes the different types of etiology leading to epileptogenesis. Figure adapted from (Scheffer *et al.*, 2017).

1.1.1 Developmental and epileptic encephalopathies (DEE)

DEE is a disease condition in which severe genetic mutations are known to directly induce developmental consequences, apart from the effect of frequent epileptic seizures (Scheffer *et al.*, 2017). DEEs are usually associated with developmental delay or intellectual disability (ID) and other neuropsychiatric features. It has been estimated that DEE is the main reason for epileptic seizures during the first three years of life (Nieh and Sherr, 2014). Recent studies have shown the significant involvement of *de novo* mutations in many severe infantile and childhood epilepsies with DEE (Epi4K-Consortium *et al.*, 2013; He *et al.*, 2019). Especially *de novo* mutations in genes encoding Na^+ and K^+ ion-channel families, which are temporally and spatially interacting in a dynamic manner to generate action potentials, are largely involved in the DEE spectrum. Dravet syndrome represents a well-known example. In Dravet syndrome, >80% of cases are due to variants in the sodium channel $Na_V1.1$ subunit encoding gene (*SCN1A*), and as a secondary consequence, they induce developmental epileptic components. *De novo* mutations in the *KCNA2* gene have also been studied as a cause of DEE (Syrbe *et al.*, 2015; Masnada *et al.*, 2017).

Even though most of the mutations in DEE have been identified in ion-channel encoding genes, the complex mechanisms that underlie epileptogenesis are still unclear (e.g., as for the *KCNA2 gene* encoding $K_V1.2$). Additionally, in cases where the pathophysiology has been partially identified (*SCN1A* in Dravet syndrome), the mutation-induced neuronal network dysfunction has not been studied. However, such studies are crucial for the development of targeted therapeutic strategies. In my thesis, I am trying to contribute towards filling this knowledge gap by studying the disease mechanisms of *KCNA2*-related DEE as well as addressing the effect of *SCN1A* variants in thalamocortical network dysfunction.

1.2 The structure, function and biophysical properties of $K_V1.2$ channels

The *KCNA2* gene, which encodes the voltage-gated potassium channel subunit $K_V1.2$ belonging to the subfamily A, mediates an efficient repolarization of an action potential (AP) (Hodgkin and Huxley, 1952). $K_V1.2$ is one of the eight members in the shaker-related K_V1 channel family and was named after observing an abnormal "shaker" phenotype in *Drosophila* with an underlying shaker gene mutation (Salkoff and Wyman, 1981). The $K_V1.2$ subunit forms an integral part of the cell membrane, facilitates the rapid and selective K^+ ion flow through its conductive pore, thus plays a vital role in the generation and propagation of electrical impulses in the central nervous system (CNS). $K_V1.2$ subunits show low-threshold voltage-gated potassium currents and activate close to resting membrane potentials. They are crucial in regulating resting membrane potential by allowing the out-flow of intracellular K^+ ions in response to neuronal depolarization. They actively shape the duration and delay of axonal action potential (AP) initiation, thus regulate the frequency of action potentials in repetitive firing and the release of neurotransmitters at presynaptic terminals (Yellen, 2002; Dodson *et al.*, 2003; Clark *et al.*, 2009; Kuba *et al.*, 2015).

The ion selectivity and conductivity of the channels containing $K_V1.2$ subunits arise from their molecular architecture. A fully functional $K_V1.2$ channel is formed by an oligomerized assembly of four identical pore-forming α-subunits and may attach with regulatory beta subunits or other accessory proteins (Vacher *et al.*, 2008). Each subunit has six transmembrane (TM) segments (S1-S6). These transmembrane segments are linked through hydrophilic intra and extra-cellular loops, and keep both amino (N) and carboxy (C) termini on the intracellular side. The S4 region is enriched with multiple positively charged amino acids (Arginines or Lysines) and S1-S4 segments form its voltage-sensing domain. The loop between S5-S6 forms the symmetrically arranged selectivity ion conduction pore (Long *et al.*, 2005a, 2007) (a tetrameric architecture of 6TM is shown in Figure 2). Conformational changes in the S1-S4 domain during the voltage sensing are directly transferred to the pore region via

a helical linker and thus lead to the opening or closing of the narrow pore. The highly conserved selectivity filter is facilitated by five amino acids (Threonine, Valine, Glycine, Tyrosine, Glycine) and lined with oxygen atoms that provide four binding sites for K^+ ions. These precise structural features promote rapid K^+ conduction by solving the electrostatic stability of K^+ ions and avoiding unfavorable dielectric environment (Doyle *et al.*, 1998; Long *et al.*, 2005; Tombola *et al.*, 2005). The N-terminus (tetramerization domain-T1) determines the specificity of subunit assembly and channel modulation according to the intracellular signaling as well as it forms the platforms for beta-subunits binding and other protein-protein interaction (Shen and Pfaffinger, 1995; Kreusch *et al.*, 1998; Gulbis *et al.*, 2000). The C-terminus regulates the localization of the channel and its complex formation with other signaling molecules (Yellen, 2002; Khalili-Araghi *et al.*, 2006; Delemotte *et al.*, 2010).

In neurons, the K_V.1 subunit usually assembles into heteromeric channel forms. Either K_V1.2 co-assembles with identical tetramers and forms homotetrameric structure or heterotetrametric assembly with K_V1.1 or K_V1.4 subunits. The biophysical properties of K_V1.2 channels are determined and vary based on their α-subunit tetrameric formation with other K_V.1 channels (e.g., the heteromultimeric assembly of K_V1.2/K_V1.4 underlie pre-synaptic A-type K^+ currents) (Vacher *et al.*, 2008; Wang *et al.*, 2013). This complex expression pattern may be one of the reasons that makes it hard to elucidate the specific function of the K_V1.2 subunit.

K_V1.2 is included in the family of delayed rectifier channels that activate after a delay after the Na^+ channels and show a slow inactivation within a time scale of tens of milliseconds to a second. They activate relatively at the resting membrane potential (Shen *et al.*, 2004; Al-Sabi *et al.*, 2013). K_V1.2 exhibits two modes of activations, which are "slow" and "fast", and arise from the internal rearrangement within the voltage sensor (Horne *et al.*, 2010). These two distinct gating modes induce changes in the half activation ($V_{1/2}$) and the time constant (tau) of the channel. In slow gating, $V_{1/2}$ is around 16 mV with a tau of 90 ms at 35 mV, whereas fast mode shows a $V_{1/2}$ of around -19 mV with a tau of 4.5 ms (Rezazadeh *et al.*, 2007). The activation of K_V1.2 is use-dependent, which means channels can be shifted from a slow gating mode to a fast gating mode by delivering repetitive depolarizing pulses (Rezazadeh *et al.*, 2007; Baronas *et al.*, 2015). K_V1.2 limits its conductance in a time-dependent manner through a mechanism similar to C-type slow inactivation, which is sensitive to extracellular K^+ concentration. In C-type inactivation, the ion conductance is shut at the narrow selectivity filter itself rather than the closing induced by the N-terminus (N-type inactivation). The C-type is slower than the N-type inactivation and has a functional role in repetitive action potential firing (Yellen, 2002; Shen *et al.*, 2004; Suarez-Delgado *et al.*, 2019).

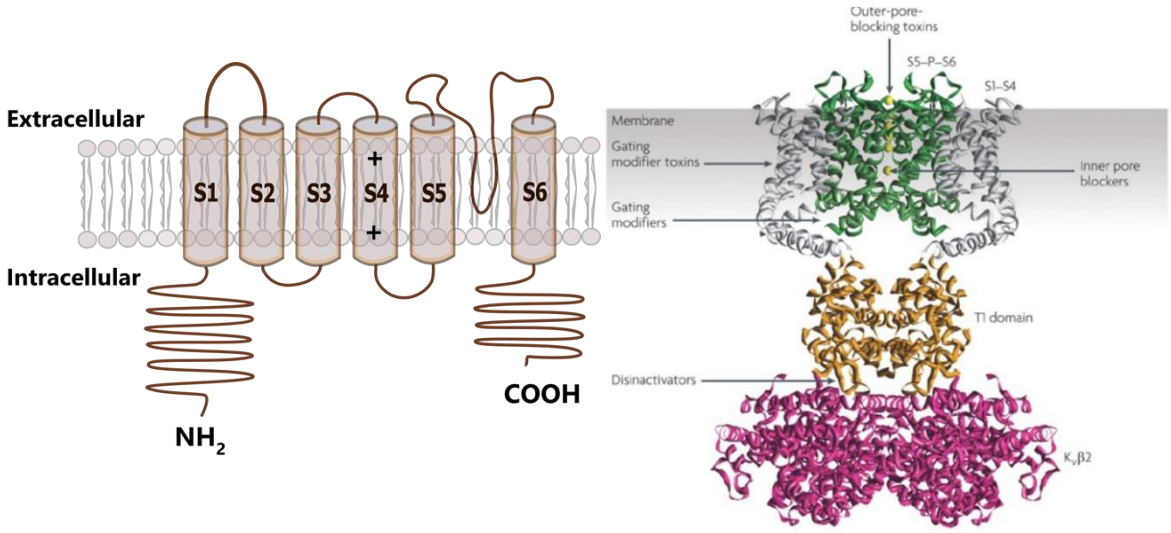

Figure 2. Molecular architecture of the K_V1.2 subunit: The orientation of six transmembrane segments (S1-S6) which forms the α-helix of the K_V1.2 tetrameric structure (left). Tetrameric assembly of K_V1.2 channel (right): S1-S4 segments form the voltage sensor part (sliver) and S5-S6 form an ion selectivity pore (green). N-terminus provides an avenue for β-subunit assembly by forming the T1 domain (golden) and K_Vβ2 auxiliary β-subunit assembly is shown in magenta. Two of the four subunits are shown here. Image (right) adapted from Long *et al.*, 2007.

K_V1.2 is ubiquitously expressed in both excitatory and inhibitory neurons of CNS (Nashmi *et al.*, 2000; Lorincz and Nusser, 2008; Trimmer, 2015). It is distributed in multiple subcellular compartments including axon initial segments, nodes of Ranvier and presynaptic terminal, thus regulates the neurophysiological functions such as action potential (AP) generation, axonal impulse conduction and neurotransmitter release (Dodson *et al.*, 2003; Robbins and Tempel, 2012; Rasband and Peles, 2016). The expression pattern of the K_V1.2 subunit showed considerable temporal variation during development (Prüss *et al.*, 2010). This expression and functional versatility of K_V1.2 in different neuroregulatory mechanisms including neuronal development and migration make it as the most prominent target in channelopathies (Zhang *et al.*, 2016) such as potential target for neuropathic pain treatment (Fan *et al.*, 2014), diabetic hyperalgesia (Wang *et al.*, 2015), ataxia and myoclonic epilepsy (Pena and Coimbra, 2015).

1.3 An overview of *KCNA2* channelopathy

The first human *KCNA2* channelopathy was reported in 2015 by Pena and Coimbra. The patient was a seven years old boy carrying a *de novo* mutation in *KCNA2* at c.890C>A, which causes the amino acid substitution p. Arg297Gln (R297Q). This mutation was located

in the voltage-sensing S4 transmembrane helix and the observed clinical phenotype was epileptic encephalopathy as a consequence of ataxia and myoclonic epilepsy. The neurodevelopment was normal until the first onset of an epileptic seizure. The brain magnetic resonance imaging (MRI) did not show any abnormalities. However, the electroencephalography (EEG) showed the burst of irregular spike slow waves at 2–2.5 cycles/s. Even though the study showed a clear phenotype, there was no information regarding the functional characterization of this mutation in the $K_V1.2$ channel (Pena and Coimbra, 2015). Parallel to this study, Syrbe *et al.* published a detailed clinical phenotype of four *KCNA2* variants and their functional effect on $K_V1.2$ channel properties including the previously reported R297Q mutation. Six unrelated patients carried four different *de novo* mutations (including two dominant-negative loss-of-function (LOF, including P405L variant) and two gain-of-function (GOF)). They showed normal brain developmental features until the first seizure onset. The MRI studies did not show any abnormalities in the brain structure of all patients, but delayed speech development and mild to moderate intellectual disability (ID) were observed. The four individuals carrying LOF showed seizure onset at the age of 8-17 months with abnormal epileptiform discharges in the electroencephalogram (EEG). However, the seizure outcome of all was seizure-free between 4-15 years of age. GOF mutation carrying patients showed severe phenotypes of DEE with early seizure onset and moderate to severe ataxia as well as seizures were found to be pharmaco-resistant which did not achieve any seizure freedom. Also, EEG showed a pattern of generalized epileptiform discharge (Syrbe *et al.*, 2015). After having a detailed description of clinical and functional features of *KCNA2* related variants, it is unclear why both LOF and GOF mutations lead to EE. In addition, a greater number of *KCNA2* mutations related to patient's data is required to better characterize significant genotype-phenotype relationships.

Another finding of a *KCNA2* mutation further expands its disease spectrum. Hundallah *et al.* reported a severe early-onset DEE case where the male infant developed frequent clonic and myoclonic seizures since the day of birth. They identified another *de novo KCNA2* (c.1120A > G (p. Thr374Ala)) mutation through whole-exome sequencing. No functional characterization at channel level was reported, however, the presence of dominant GOF was assumed. The MRI results were normal at the beginning but later showed supratentorial atrophy and delayed myelination (Hundallah *et al.*, 2016). Even though the authors assume the presence of GOF variants, the clinical phenotypes are almost identical to more patients carrying the same variant which was then shown as a severe combined gain and loss of function (G-LOF) that were later described in Masnada *et al.* studies (Masnada *et al.*, 2017).

A whole-exome sequencing study from Allen *et al.* carried out in an uncharacterized early-onset epileptic encephalopathy (EoEE) cohort and identified a novel *KCNA2* mutation. The *KCNA2* variant (c.869T>G; p. Leu290Arg) was located in the voltage sensor domain and a GOF effect was predicted. The patients showed early-onset generalized seizures (7 weeks) with clear cerebellar ataxia and moderated ID. Similar to the previous study, Allou *et al .* also identified a *de novo KCNA2* mutation in an infant with EE and showed close phenotypes of the Hanefeld variant of Rett syndrome (RTT). RTT is a brain disorder that leads to developmental problems in children, mostly affects language skills and hand use. Exome sequencing confirmed the location of missense variant (c.1223C>T; p. Val408Ala) in the pore-lining domain of the $K_V1.2$ subunit (Allou *et al.*, 2017). Both of the above-mentioned studies simultaneously announced the *KCNA2* candidacy for DEE and expanded its genetic heterogeneity.

Corbett *et al.* for the first time described the phenotypic spectrum of familial *KCNA2* mutation with pharmaco-responsive epilepsy. The study included seven affected individuals from a single-family over three generations. All seven patients carried the segregating dominant *KCNA2* mutation (P.255_257 del) that lead to epilepsy and inherited episodic ataxia (5 members). This was the first study that showed the effect of *KCNA2* mutations in episodic ataxia (EA). These findings expanded the inherited *KCNA2* variant phenotypic spectrum (Corbett *et al.*, 2016).

Hereditary Spastic Paraplegias (HSPs) is a spectrum of heterogeneous neurodegenerative disorders characterized by the gene mutations leading to the defected corticospinal connectivity and signaling. Helbig *et al.* for the first time showed an identical *KCNA2* missense mutation as a rare cause for HSPs in three unrelated families. Patients carried a dominant-negative mutation in the highly conserved R294 residue of the S4 voltage-sensing segment with substitution of arginine with histidine (c.881G>A (p.R294H)) (Helbig *et al.*, 2016). These findings suggest that some pathogenic *KCNA2* variants exhibit mutation-specific genotype-phenotype correlation. Manole and colleagues supported the same notion of *KCNA2*-related HSP distinctiveness by adding another patient data carrying the same recurrent *KCNA2* mutation with classic HSPs phenotypes (Manole *et al.*, 2017). Both of these studies expanded *KCNA2* channelopathy towards HSPs other than the DEE and ataxia.

Sachdev and colleagues presented data from three patients carrying two novel *KCNA2* mutations. The first patient carried previously described P405L mutation with electrical status epilepticus of sleep (ESES) EEG feature, which was not reported previously (Syrbe *et al.*, 2015). The second patient carried c.1195 G > A (p. Val399Met) *KCNA2* variant while the third patient with a *de novo* c.889 C > T (p. Arg297Trp) *KCNA2* gene mutation. This mutation was

in the same position as previously reported GOF (p. Arg297Gln) mutation and exhibited similar disease phenotype. This study showed the expansion of clinical phenotypes associated with gene mutations with the growth of the field (Sachdev *et al.*, 2017).

Masnada and colleagues presented the largest *KCNA2* cohort to date with the clinical and functional data from 23 patients (Masnada *et al.*, 2017). The study aimed to provide a clear and collective phenotypic spectrum of the novel and known *KCNA2* variants. It added a third distinct class of $K_V1.2$ channel protein dysfunction and its phenotype to the *KCNA2*-related encephalopathy spectrum. Previous reports had only discussed features of drastic GOF or dominant-negative LOF of *KCNA2* variants. This was the first report towards the third functional class showing the combination of GOF and LOF, in which the GOF effect is reduced by additional LOF (gain and loss-of-function; G-LOF). The gain to loss overcontrolled character included a hyperpolarized shift in steady-state activation and decreased current amplitude. The study involved fifteen new and eight known previously reported patient data from 11 females and 12 males with an average age of 12.9 years. The identified mutations involved ten missense (E157K, I263T, L290R, L293H, R297Q, L298F, L328V, T374A, G398C, P405L) and one truncation mutation (Q213*, found in S1/S2 loop). Most of the newly identified mutations (ten) were located in highly conserved functionally important transmembrane segments forming regions. One (Q357R) was found in the less conserved pore region. Even though all the above-mentioned patients carried three different channel phenotypes, they shared some overlapping clinical features with varying degrees of phenotypic severity. The commonly shared features were early temperature-sensitive seizure onset (within the first year of life) which is rare in case of G-LOF, impaired cognitive development, moderate cerebellar ataxia, difficulties in motor coordination and dysarthria. The distinctive features of LOF group involved predominant focal seizures with the activation of epileptiform activity during non-REM sleep with pronounced EEG abnormalities during infantile and childhood age (electrical status epilepticus of sleep (ESES)). Meanwhile, GOF group showed predominant generalized seizures together with severe ataxia. MRI results were normal for LOF while GOF was observed with progressive cerebellar atrophy whereas it began in the early childhood of the G-LOF group. The most concerned severe phenotype observed in G-LOF cases was the neonatal-epileptic onset with a strong intellectual disability. Overall, this comparative study suggests that LOF leads to milder phenotypes, GOF to severe and G-LOF to the most severe features. Interestingly, three recurrent *KCNA2* variants (R297Q, T374A, and P405L) are responsible for two-thirds of the pathogenic mutations in all identified *KCNA2* cases so far (Pena and Coimbra, 2015; Syrbe *et al.*, 2015; Corbett *et al.*, 2016; Hundallah *et al.*, 2016). This leads to the confusion that which factor (i.e., functional class or variant specificity)

determines the *KCNA2* related phenotypes. This compels the further involvement of a larger patient cohort to get a clear picture (Masnada *et al.*, 2017).

Masnada *et al.* (2017) further provided a hypothetical link of channel dysfunction within epileptogenesis. Their functional study in oocytes showed a hyperpolarized membrane potential in all GOF variants. This may cause an electrical silencing of neurons that carries this mutation. Considering other ion-channel dysfunctional studies (Reid *et al.*, 2009; Coppola and Moshé, 2012; Lerche *et al.*, 2013; Muona *et al.*, 2015), authors speculate that inhibitory neurons are primarily silenced cells in all cases of GOF, which led to a concurrent enhanced firing in excitatory pathway and thus epileptogenesis. In contrast to the previous view, the authors suggested that LOF affects the excitatory pathway due to the LOF-mediated impaired repolarization phase of an action potential. Both LOF and GOF can also alter the channel properties of $K_V1.2$ regardless of excitatory or inhibitory neuronal cell types. Collectively these assumptions strongly demand the neuronal level biophysical consequences analysis of three variants (R297Q, T374, and P405L), which represent three types of functional groups (LOF, GOF, G-LOF) in animal models. Animal models expressing these mutations by means of gene-targeted or overexpressed way (*in utero* : viral or electroporation) in specific brain regions will answer these questions to some extent. Further, they will also be useful to study the possible therapeutic antagonizing mechanisms.

1.3.1 *In vitro* models with genetic alterations associated with *KCNA2* channelopathy

Few animal models of *KCNA2*-related channelopathies have been studied previously. In 2007, Brew *et al.* reported the characterization of a possible LOF disease animal model (*Kcna2*-null (-/-) mice) lacking $K_V1.2$ with increased seizure susceptibility and reduced life span. Homozygous (-/-) $K_V1.2$ knockout mice had reduced life span as compared to WT (+/+ and) and heterozygous (+/-), and showed spontaneous generalized seizures as early as P14 and developmental *Kcna2* mRNA downregulation from P7. Heterozygous animals did not display spontaneous seizures but were more sensitive to a proconvulsant challenge compared to wild-type littermates. Direct whole-cell patch-clamp recordings from principle auditory neurons of the medial nucleus of the trapezoid body (MNTB) of *Kcna2* null mice showed hypo excitability (fired fewer APs) (Brew *et al.*, 2007).

In 2010, the so called Pingu mutant mouse model that carried a missense mutation in the *Kcna2* gene was reported. The amino acid substitution (I402T) in the S6 segment of $K_V1.2$ was induced through N-ethyl-N nitrosourea mutagenesis. The mutant mouse showed close LOF phenotypic proximity such as chronic motor incoordination equivalent to that found in

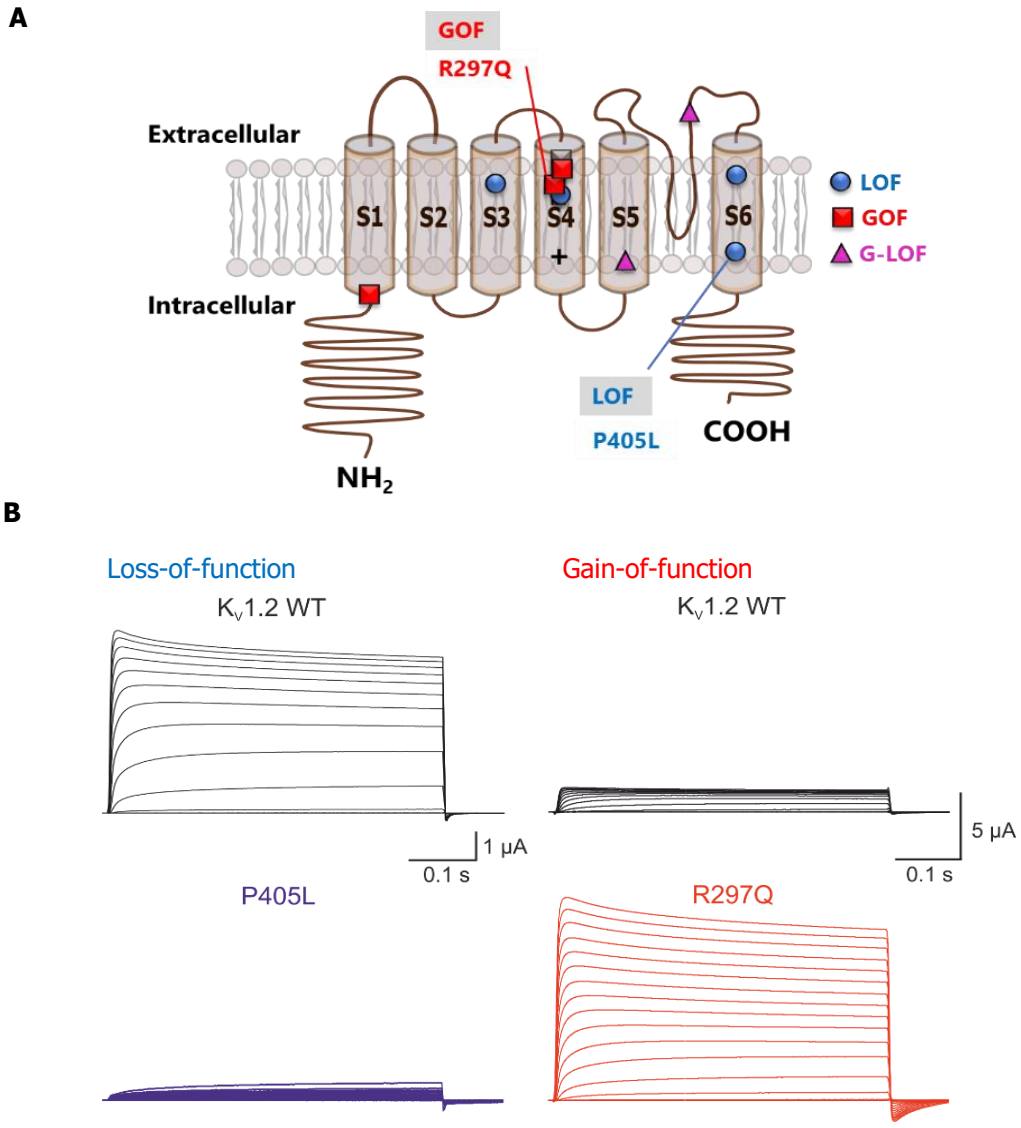

Figure 3. *KCNA2* mutations associated with DEE and their functional effect on $K_V1.2$: (A) Location of affected *KCNA2* variants on $K_V1.2$ subunit. LOF: blue, GOF: red and G-LOF: magenta, respectively. (B) Representative current traces show the functional effect of LOF (P405L) and GOF (GOF) on $K_V1.2$ channels recorded from *Xenopus* oocyte as a response of series of voltage steps (from −80 mV to +70 mV, 10 mV step). WT traces (black) at top, P405L (purple) and R297Q (red) at bottom respectively (image (3B) adapted from Syrbe *et al.*, 2015).

patients with DEE (Syrbe *et al.*, 2015). Both heterozygous and homozygous mutant mice displayed significant gait abnormalities. An increased frequency and amplitude of spontaneous GABAergic inhibitory postsynaptic currents (IPSCs), as well as reduced AP firing frequency, were observed in cerebellar Purkinje cells followed by an increased level of GABA release from cerebellar basket cells. The increased GABA release from basket cells may be the underlying mechanism of motor incoordination in Pingu mice. It was also shown that the non-targeted

pharmacological approach with the carbonic anhydrase inhibitor (acetazolamide), can rescue the motor incoordination (Xie *et al.*, 2010). These mouse models representing LOF and their cellular level firing patterns have increased the understanding regarding the complexity of the underlying mechanisms. To date, there are no reported mouse models with the *KCNA2* GOF variant, thus the cellular basis of excitability due to GOF *KCNA2* mutations is poorly understood.

In addition, there are currently no appropriate computational models or artificially induced drug models that are capable of elucidating the cellular level changes. Hence, in my thesis, I was trying to fill these knowledge gaps between $K_V1.2$ channel dysfunctions and underlying changes in cellular intrinsic firing properties. I have used the $K_V1.2$ channel over-expression approach with *in-utero* electroporation and studied the consequences of two *KCNA2* variants (R297Q (GOF) and P405L (LOF)) in transfected neurons (Figure 3B). These are the most recurrent *KCNA2* mutations observed in patients. In addition, studies were also undertaken to understand a mechanism-based therapeutic strategy with 4-aminopyridine (4 AP) (approved K^+ blocker) in *KCNA2* WT overexpressing (mimics GOF effect) neurons, which may help to maintain the neuronal excitation within the physiological limit.

1.4 *SCN1A*-related epileptic encephalopathies

Unlike *KCNA2*, in very few cases the pathophysiological mechanisms of ion-channel mutations leading to the seizure generation have been understood to a limited extent. One of the most important candidates among them is the *SCN1A* gene encoding the voltage-gated $Na_V1.1$ channel, which is known to be expressed in all parts of the central nervous system (Duflocq *et al.*, 2008; Catterall *et al.*, 2010). Two studies using $Na_V1.1$ knockout mice revealed strongly reduced Na^+ currents in dissociated cerebral bipolar inhibitory neurons, while excitatory neurons showed no or only small reduction in their sodium currents (Yu *et al.*, 2006; Kalume *et al.*, 2007). These experimental studies supported the hypothesis that $Na_V1.1$ is the major Na^+ channel in GABAergic interneurons. The firing activity of GABAergic interneurons is predominantly decreased by *SCN1A* variants leading to epileptic seizures. In neurons, $Na_V1.1$ is mainly located at the AIS of inhibitory neurons, which is the site for AP initiation (Duflocq *et al.*, 2008). Previously, members of our lab have performed a comprehensive characterization of an *SCN1A* mouse model carrying the human generalized epilepsy with febrile seizures plus (GEFS+) mutation (R1648H). They found ubiquitous disinhibition in the hippocampus and the thalamocortical loop presumably induced by an action potential firing deficit in axon initial segments of GABAergic interneurons as the cellular key mechanism. Consequently, enhanced network activity was observed in both the hippocampus and the

thalamocortical network, which provided an explanation for the occurrence of seizures (Hedrich *et al.*, 2014).

In addition to epilepsy-causing *SCN1A* variants, alterations in the $Na_V1.1$ channel can also cause a severe type of migraine with aura (familial hemiplegic migraine type 3, FHM3) (Dichgans *et al.*, 2005; Fan *et al.*, 2015). In contrast to LOF generated epilepsy-associated mutations, functional studies have suggested a GOF effect of migraine-associated mutations (Cestèle *et al.*, 2013; Fan *et al.*, 2015). In our group, there is a functionally characterized but unpublished FHM3 knock-in mouse model available, carrying a specific GOF mutation in the $Na_V1.1$ channel (L1649Q mutation in the voltage sensor of the channel, which was observed in patients) (Vanmolkot *et al.*, 2007; Cestèle *et al.*, 2013). It was observed that heterozygous animals did not exhibit any phenotypic alterations, whereas homozygous animals showed premature death between P15 and P25. The first results of firing patterns showed enhanced neuronal activity in hippocampal and cortical GABAergic interneurons of heterozygous animals as compared to their wild-type littermates indicating a GOF effect of the mutation. The adjacently located mutations in *SCN1A* (R1648H and L1649Q) are shown in Figure 4.

SCN1A-related disorders encompass a large spectrum of different phenotypes. Mutations in this gene can lead to generalized epilepsy with febrile seizures plus (GEFS+) (Escayg *et al.*, 2000) as the mildest syndrome caused by missense mutations and severe myoclonic epilepsy of infancy (SMEI) (Claes *et al.*, 2001) as the most severe form caused by nonsense mutations (Yu *et al.*, 2006; Ogiwara *et al.*, 2007, 2018). Dravet syndrome is a pharmaco-resistant form of *SCN1A*-related epileptic encephalopathy and heterozygous LOF mutations in this gene have been identified as a prominent reason for >80% cases. Various studies confirmed and widened the genetic role of *SCN1A* in the extreme variability of the developmental cognitive and physiological phenotypes (Buoni *et al.*, 2006; Ragona *et al.*, 2010). Sleep is one of the affected physiological phenomena among them.

Sleep and epilepsy are reciprocally interconnected. Seizures can adversely affect the quality and quantity of sleep, where sleep deprivation can act as a triggering factor for epileptic seizures (Balamurugan *et al.*, 2013). The hyper synchronization during the non-rapid-eye-movement (NREM) sleep is likely to lead towards the epileptiform discharges (Kataria and Vaughn, 2016). This may be due to the frequency similarity in both NREM sleep stages (0.1-4 Hz) and absence epilepsy (2.5-4 Hz). Patients with epilepsy showed sleep disorders such as daytime sleepiness, sleep apnea, etc. (Lanigar and Bandyopadhyay, 2017). The understanding of the mechanisms which connect this physiological function (sleep) and pathophysiological condition (epilepsy) is crucial in the proper management of epileptic seizures. However, the exact links between the effect of epilepsy-related variants and the neuronal network which

regulates sleep at the molecular and cellular level have not been clearly investigated. The direct evaluation of this complex relationship in patients may be out of experimental scope due to the usage of antiepileptic drugs. Thus, genetically modified mouse models carrying epilepsy-causing mutations will be an elucidative tool to understand this interrelation.

1.4.1 *SCN1A* defects and sleep

Two studies investigated the effects of the *SCN1A*-R1648H mutation on sleep, and found a reduction in non-REM sleep stages (reduced delta waves and spindles, increased awakening) (Papale *et al.*, 2013; Kalume *et al.*, 2015). However, it still needs to be investigated whether the disturbed sleep can be mainly explained by the dysfunction of interneurons leading to an impaired generation of sleep rhythms or the occurrence of seizure activity is an additional or the major cause of sleep alterations. In contrast, no comparable studies have been performed with *SCN1A* GOF mutations such as those found in FHM3 patients. Although clinical and animal data revealed potential cognitive impairments in other genetic subtypes of FHM (Freilinger *et al.*, 2008, 2011; Dilekoz *et al.*, 2015), no data on sleep architecture are specifically available for FHM3 patients till now. For both sleep and epilepsy, the thalamocortical network and its participating inhibitory neurons play a crucial role. Therefore, the epilepsy and FHM3 mouse model showing alterations within this network is a helpful tool to study the involvement of inhibitory neurons and the effects of seizures on sleep.

1.4.2 The thalamocortical network in the regulation of sleep and epilepsy

The thalamocortical (TC) network is an array of three interconnected neuronal populations located in both the thalamus and cortex. The three types consist of (i) thalamocortical neurons (TC-neurons) of the ventrobasal complex (VB), with axons extending into the cortex and also connected to reticular neurons, (ii) a thin layer of interconnected GABAergic neurons of thalamic reticular nucleus (NRT) which are specifically connected with TC-neurons and (iii) cortico-thalamic pyramidal neurons in cortical layer 5 with the axonal projection towards thalamic and reticular neurons in ventrobasal area (Steriade, 2000) (Figure 5). Reticular neurons are highly interconnected through their electrical synapses and have their own intrinsic oscillatory properties. These neurons inhibit thalamocortical activity via their direct connections to TC-neurons. The cyclic TC network activity starts with the pace making rhythmic inhibitory input generated in NRT, which is directly sent to the TC-neurons. This inhibitory input hyperpolarizes the TC-neurons and leads to the activation of T-type Ca^{2+} channels, thus induces a burst activity. These burst activities are further transferred to the cortex as well as to the neurons within the NRT. The TC-neurons input generates another round of oscillatory activity in cortex with the precise tuning of cortical interneurons, in turn

cortex further activates the neurons of NRT and TC-neurons (Krosigk *et al.*, 1993; Landisman *et al.*, 2002; Chang and Lowenstein, 2003; Fan *et al.*, 2017). This highly coherent cyclic oscillation due to the interaction of thalamus with cortical networks is important for the normal and abnormal functioning of the forebrain.

Sleep and epilepsy share the same TC loop as a regulatory mechanism (Steriade *et al.*, 1993). In physiological conditions, such as sleep, which is characterized by synchronized neuronal activities and is further categorized through the repeated occurrence of rapid eye movement (REM) sleep and non-REM sleep (consists of four consecutive stages including slow-wave sleep; SWS). During slow-wave sleep, these coordinated TC events induce rhythmic up- and down- states in the cortex. Up- and down- states of slow-wave oscillations are two preferred sub-threshold neuronal membrane potentials for action potential generation, where depolarized and hyperpolarized membrane potentials represent the up-state and down-state respectively (Steriade, 2000; Wilson, 2008). Up-states originate in the thalamus and are caused by reciprocal interactions between GABAergic neurons of the NRT, which function as a pacemaker, and glutamatergic TC projections mediating their synchronized propagation to cortical regions. The amplitude of cortical up-states is controlled by the activation of inhibitory neurons. The down-state is triggered by the activation of Ca^{2+}-dependent K^+ channels and the inactivation of persistent Na^+ currents. In pathological states, such as absence epilepsy (idiopathic generalized epilepsy), the TC network undergoes abnormal activities consisting of spike and wave discharges occurring at 2.5-4 Hz in the patient's EEG. This irregular pattern is due to the abolition of intra-NRT synaptic inhibition which changes synchronous activity into a hypersynchronous state and leads to seizure-like behavior (Huntsman *et al.*, 1999; Chang and Lowenstein, 2003; Huguenard, 2019).

The up- and down- state frequency (< 1Hz) corresponding to the SWS in the intact brain can also be recorded in thalamocortical slices (*in vitro*) (Sanchez-Vives and McCormick, 2000; Wilson, 2008; Diekelmann and Born, 2010). In electroencephalographic (EEG) recordings (*in vivo*), the slow-wave oscillations appear as periodic fluctuations of positive and negative waves. The *in vitro* and *in vivo* understanding of the progressive generation of these TC rhythmic recurrent activities can define the different sleep stages, hence these recordings can be used as a study tool to investigate the patterns altered by seizures of REM and non-REM sleep stages. Therefore, the current study aims to gain insight into the function of $Na_V1.1$ expressing neurons and the influence of both LOF (R1648H) and GOF (L1649Q) mutations on the regulation of TC up- and down- states.

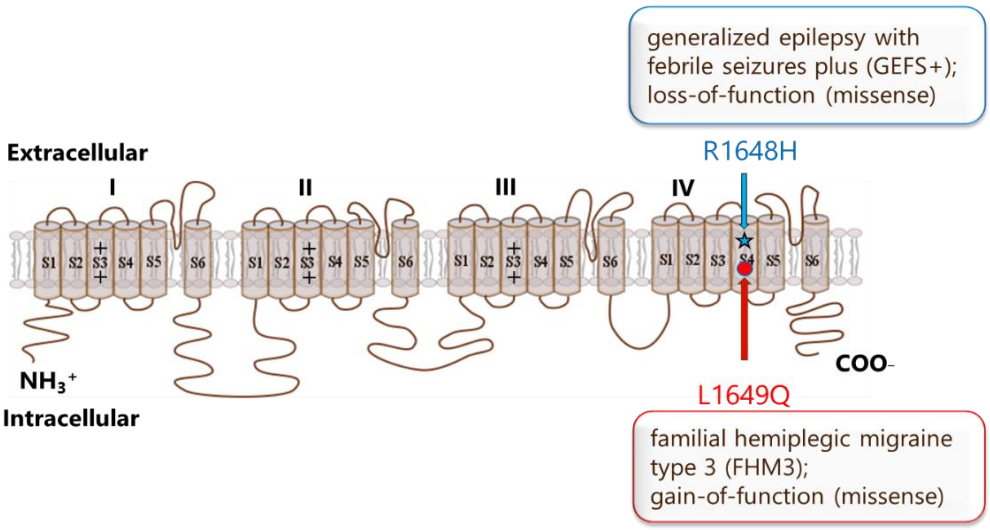

Figure 4. *SCN1A* LOF and GOF variants causing GEFS+ and FHM3: Two adjacently located Nav1.1 LOF and GOF variants are shown in the Nav1.1 channel subunit. Nav1.1 has four homologous domains (I, II, III and IV) that comprise the pore-forming alpha subunit of a voltage-gated sodium channel in which each domain contains six transmembrane segments (S1 to S6). The S4 segments act as a voltage sensor of the channel whereas S5-S6 segments form the pore region. LOF (R1648H) and GOF (L1649Q) variants are located in S4 leading to GEFS+ and FHM3, respectively.

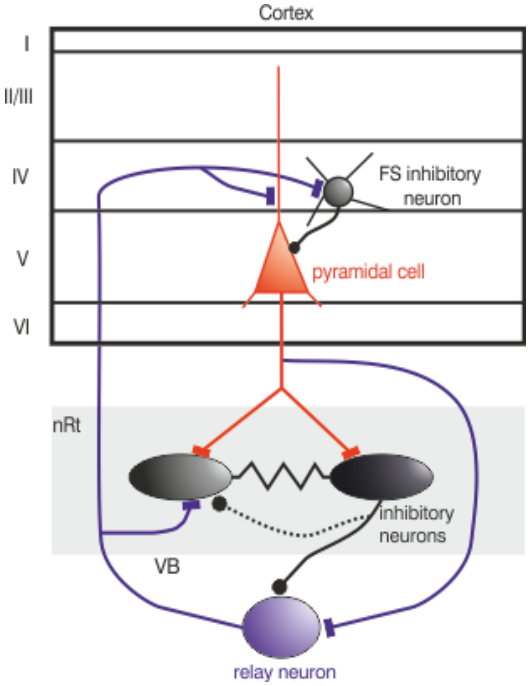

Figure 5. Thalamocortical network: TC network is formed by the array of three functionally different groups of neurons: (i) cortical Layer 5 pyramidal neurons, (ii) GABAergic neurons of nRT and (iii) relay neurons of VB. The relay neurons of VB receive inhibitory connections from the reciprocally interconnected inhibitory neurons of nRT and excitatory connections from pyramidal cells of the cortical layer 5. In turn, they send their excitatory inputs to the nRT neurons as well as back to the cortical neurons (pyramidal and fast-spiking interneurons) (image adapted from Hedrich *et al.*, 2014).

1.5 Research objectives:

The first part of the thesis is focused on understanding the pathophysiological mechanisms and the development of treatment options for *KCNA2*-related DEE. *KCNA2* knock-in/-out animals will be suitable experimental models; however, so far, no appropriate animal models are available. Taking this into consideration, I have used $K_V1.2$ WT as well as its LOF and GOF variants overexpressing (*in utero*) neuronal models to answer the following questions:

1) How does the overexpression of $K_V1.2$ WT and its LOF as well as GOF variants alter the intrinsic properties of somatosensory cortical layer 2/3 pyramidal neurons?
2) Are there any changes in morphological features of neurons overexpressing $K_V1.2$ WT, LOF and GOF channels subunits?

The second part of the thesis is set out to understand the effect of $Na_V1.1$ variants on the thalamocortical up- and down-states. Mouse models of human genetic epilepsies and FHM3 carrying either LOF or GOF mutations in the *SCN1A* gene have been used to answer the following questions:

1) How does *SCN1A* LOF mutations and thus affected interneurons alter TC up-states?
2) Does an opposite molecular defect, a GOF mutation, modify the TC up-states in different ways?

2. Materials and Methods

2.1 Molecular biology

2.1.1 Mutagenesis and cloning

The human $K_V1.2$ clones from the previous studies (Syrbe *et al.*, 2015; Masnada *et al.*, 2017) were used for subcloning the chicken beta-actin IRES-GFP (CBIG) construct. The human $K_V1.2$ in the pcDNA3.1 vector was provided by Stephan Grissmer (Institute of Applied Physiology, Ulm University). This vector was used for the synthesis of all $K_V1.2$ variants (R297Q and P405L) using $K_V1.2$ WT as a template for site-directed mutagenesis (PCR-based QuickChange method-TM-Agilent Technologies). Mutagenesis primers are listed in Table 1. The PCR was performed as follows: 50 ng DNA template, 2.5µl 10x reaction buffer, 0.5 µl 10 pmol/µl of each of the primer, 0.5 µl dNTPs, 0.5 µl PfuUltra Turbo polymerase, up to 25µl with Ampuwa water and products confirmed by agarose gel electrophoresis (1% agarose dissolved in Tris/Borate/EDTA; the solution supplemented with 20,000x Red safe dye-1x final dilution). The PCR products were used for bacterial transformation as detailed below. The mutated clones were confirmed by sequencing.

For the overexpression of channels in CHO cells and electroporation in embryos, human *KCNA2* wildtype or mutant cDNA was subcloned into a CBIG vector as an XhoI and PmeI fragment (a generous gift of JD Macklis, Harvard Medical School, plasmid map showed in Figure 6). The presence of the WT or mutant cDNA coding sequence was confirmed after the sequencing of the complete construct.

Table 1: List of primers used for *KCNA2* site-directed mutagenesis

Primer name (mutation)	*Sequence*
KCNA2 P405L F	5'- TAT TGC CTT ACT GGT CCC TGT C -3'
KCNA2 P405L R	5'- GAC AGG GAC CAG TAA GGC AAT A -3'
KCNA2 R297Q F	5'- CCG TGT CAT CCA GTT GGT AAG AGT -3'
KCNA2 R297Q R	5'- ACT CTT ACC AAC TGG ATG ACA CGG -3'

2.1.2 Transformation

5 µl of the PCR product from subcloning was collected and transformed into 50 µl of the Top 10 *E. coli* strain (ThermoFisher Scientific). The DNA mixed with the bacterial strain was incubated for 30 minutes on ice and then cells were heat-shocked for 30 S at 42°C. The cells were recovered on ice for 2 minutes. After recovery, 250 µl of pre-warmed SOC medium (Invitrogen) was added for outgrowth, and cells were incubated at 37°C and shaking was

done at 300 rpm for 60 min. After this, the cells were plated onto Agar plates containing Ampicillin (100 µg/ml Ampicillin; Agar plates: 20 ml LB medium including 1.5% Agar).

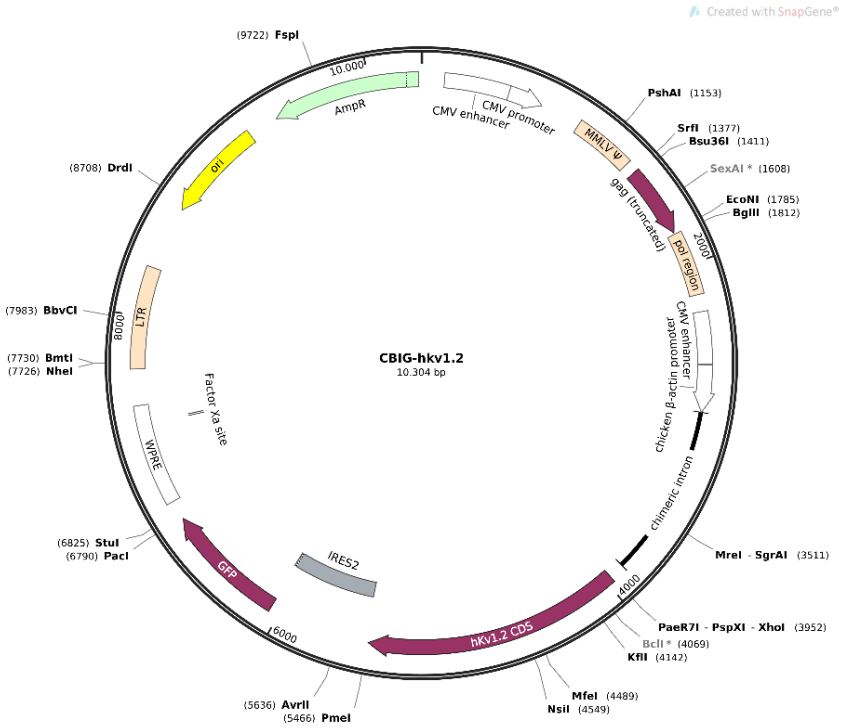

Figure 6. Plasmid map of CBIG vector

2.1.3 DNA purification and sequencing

Ampicillin resistant colonies that emerged on the LB plates were selectively picked and inoculated in 8 ml cell culture tubes containing LB medium (10 g/l B-tryptone, 5 g/l Bactoyeast, 10 g/l NaCl with pH 7.0 and autoclaved) supplemented with Ampicillin (100 µg/ml) and cultured overnight at 37°C. On the second day, mini-prep was performed to obtain plasmid-DNA from the bacterial cultures by using Illustra plasmid Prep Mini Spin kit (GE Healthcare), which was further used for the sequencing and preparation of a glycerol stock (1:1 ratio with 85% glycerol). After confirming the correct insertion of the mutations by Sanger sequencing (performed by GATC Biotech Company), the stored glycerol stocks were used for further preparation of plasmid DNA. Sequences obtained from GATC were analysed by CLC Sequence Viewer software (CLC Bio, QIAGEN). For a large amount of plasmid DNA, maxi-prep was performed using the Genopure plasmid Maxi prep kit (Roche). Concentration DNA was measured using the Nanodrop spectrophotometer (Thermo Scientific).

2.1.4 Genotyping

Mouse models carrying *SCN1A* LOF and GOF variants (R1648H and L1649Q) were used for acute and organotypic brain slice experiments. Animals were genotyped after every

preparation. Tails collected after the slice preparation were digested overnight at 55^0C in the presence of proteinase K in lysis buffer (expressed in mM: 50 Tris-HCl pH 7.5, 50 EDTA pH 8, 100 NaCl, 5 DTT, 0.5 Spermidine, 2 % SDS (v/v)) in a thermocycler with 300 rpm. After complete digestion, the DNA was precipitated in 100% of isopropanol, washed in 70% ethanol and dissolved in Ampuwa water. PCR reaction was performed using the primers listed in Table 2. The obtained product was visualized on 1-2% agarose gel. Specific control (samples of old WT or heterozygous animals) DNA of WT and heterozygous samples were used for the identification of WT or knock out (KO) bands. For the R1648H genotyping, an additional EcoR1 digestion step was performed. The expected size of the bands was 550bp for the WT and 400 bp for the KO allele. For L1649Q, the expected fragments were 197bp for the WT and 298 for the Knock-in (KI) allele.

Table 2: List of primers used for *SCN1A* mouse genotyping

Primer name	*Sequence*
R1648H KO-F	5′- TTGATGACTTCTTCACTGATTGAT -3′
R1649H KO-R	5′- ACCCAGGAAGGATATGATGATGTA -3′
R1649Q KO-F	5′- TAGTGTGCAAGCTTGAGAACG – 3′
R1649Q KO-R	5′- TCAGCTCCTTCAGTCCTTGC – 3′

2.2 Cell and organotypic brain slice culture

2.2.1 Chinese hamster ovary (CHO) cell culture and transfection of K_V1.2 channels

CHO cells were used to investigate the effect of 4-AP on K_V1.2 WT and mutant R297Q channels. CHO cells were cultured and maintained in Gibco® F-12 Nutrient Mixture (F12) medium at 37 °C and sub-cultured into 35 mm Petri dishes one day before transfection. At least 50% confluence of the cells was ensured, and the medium was changed before the transfection. "TransIT®-LT1" transfection reagent (mirusbio) was used as suggested by the company to transfect one µg of DNA into each dish. Electrophysiological recordings were performed after 24 hrs of post-transfection. Transfected cells were further split, seeded into 2-3 dishes and incubated in the F12 medium for 10-20 min before the recording.

2.2.2 Organotypic brain slice culture

After the preparation of TC slices (details in section 2.3.2) from P5 to P6 animals under sterile condition, sections were immediately transferred into a laminar flow hood. The day before slicing, 6-well culture plates were prepared by adding 1.2 ml of organotypic MEM culture medium (see recipes, Table 4) into each well and the culture inserts (Merck, Millipore) were placed on the top of the medium using straight tweezers to reverse the hydrophobicity

of polytetrafluoroethylene (PTFE) as well as to allow a proper feeding of the slices. These culturing plates were incubated overnight at 37 °C in a humidified 5% CO_2 atmosphere. Each slice was carefully placed on the PTFE membrane of the insert by using a sterile Pasteur pipette. The excess amount of aCSF was carefully removed with a pipette tip without damaging the brain tissue. The inserts were placed in the well plate without any air bubbles that were trapped between the PTFE membrane and the medium. The culture media was changed the day after the slicing procedure and then every 2-3 days until the experiments were completed.

Table 3: Extracellular and intracellular solutions used for CHO cells recordings

aCSF	Substance	Working concentration [mM]
Extracellular	NaCl	135
300-310 mOsm/l	KCl	5
pH = 7.4 with NaOH	$CaCl_2*2H_2O$	2
	$MgCl_2$	2
	HEPES	5
	Sucrose	10
Intracellular	Potassium fluoride	90
290-300 mOsm/l	KCl	10
pH = 7.2 with KOH	$CaCl_2*2H_2O$	1
	$MgCl_2$	1
	EGTA	11
	HEPES	10
	Na_2ATP	2

Table 4: MEM Media for organotypic brain slice culture

Ingredients	Working concentration	Company
Horse serum	20%	Gibco
L-Glutamate	1 mM	Gibco
Ascorbic acid	0.00125%	Sigma-Aldrich
Insulin	0.001 mg/ml	ThermoFisher scientific
$CaCl_2$	1 mM	Sigma-Aldrich
$MgSO_4$	2 mM	Sigma-Aldrich
D-glucose	13 mM	Sigma-Aldrich
Pen/Strep	1%	Biochrom, Berlin

2.3 Animal experiments

All animal experiments were approved and then performed under the regulation of the local animal care and use committee (Regierungspraesidium Tuebingen, Tuebingen, Germany). Mice from either sex with C57BL/6 background carrying specific mutations and its corresponding WT were used as listed below:

1) The C57BL.6J-*Scn1a* ^{tm1Aesc}/Hlerc strain carrying the *Scn1a*-R1648H mutation identified in a GEFS+ family. The mutation causes a wide-spread dis-inhibition in murine acute brain slices and spontaneous epileptic seizures among heterozygous mice and humans (Escayg *et al.*, 2000; Martin *et al.*, 2010; Hedrich *et al.*, 2014)

2) A mouse strain with the FHM3 gain-of-function mutation *Scn1a*-L1649Q, which causes premature death in homozygous animals as well as an enhanced firing of GABAergic interneurons.

Animals were housed at the Hertie Institute in the Core Facility *Transgene Tiere* (CFTT) and were kept under controlled conditions (temperature: 20-24°C; humidity:45-65%; 12 hours light-dark cycles with lights on at 6.00 a.m.; food and water provided ad libitum).

2.3.1 *In utero* electroporation (IUE)

IUE is a consistent way to overexpress or silence genes in the developing mouse brain. This method can be used as a critical alternative to time-consuming knock-out, knock-in and transgenic strategies to alter the mouse genome. After a successful injection of plasmid DNA solution to the lateral ventricle of embryonic neurogenic brain region, the application of electrical pulses allows the time-dependent transduction of DNA into the cell cytoplasm. The transfection of cells to targeted brain regions can be achieved through the specific positioning of the positive electrodes angle, whereas the age of embryos (embryonic days) decides which types of neurons are transfected (excitatory or inhibitory). The short application of electrical pulses opens transient electro-pores in the neuronal membrane and directs the negatively charged DNA molecules towards the positive pole of the electrode, thus enables the precise introduction into specific brain regions without affecting the rest of the embryo. Gain- and loss-of-function studies using IUE opens a possible and affordable window to characterize pathophysiological mechanisms controlling specific steps of brain development. Overall, IUE allows for a detailed analysis of developmental consequences in neuronal properties carrying specific mutations in the target gene (Saito and Nakatsuji, 2001; Tabata and Nakajima, 2001; Borrell *et al.*, 2004; Saito, 2006; Shimogori and Ogawa, 2008).

To understand the pathophysiological consequences of *KCNA2* mutations, IUE was used to integrate the $K_V1.2$ WT or mutant channels into neurons in intact networks. IUE was

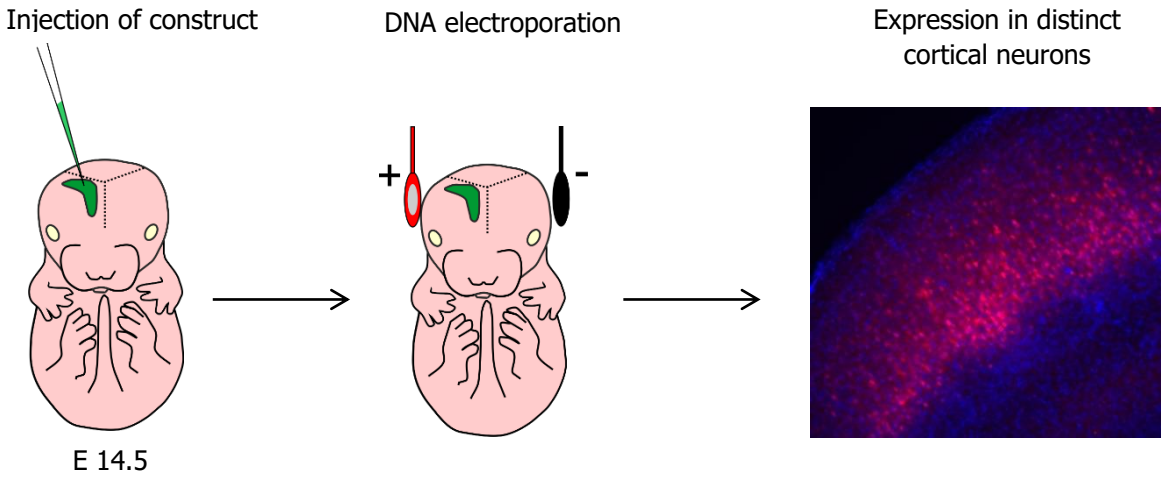

Figure 7. Schematic representation of directional IUE: Figure shows the injection of a DNA plasmid solution into the lateral ventricle of E14.5 embryos. The angle of the electrode is kept at 0^0 from the brain's horizontal plane to target the cortical ventricular zone. Image of slice shows an example of IUE transfected cells with the expression of IRES-tdTomato under CMV/β actin promoter in SSC L2/3 neurons and post hoc DAPI staining. The schematic used in this figure is from Dr. Ulrike Hedrich-Klimosch (Dept. of Neurology and Epileptology Tübingen).

performed at E 14.5, using 0^0 angle orientations of the electrode from the brain's horizontal plane to selectively target excitatory neurons of the somatosensory cortical layer 2/3 (SSC L2/3) (Figure 7). Purified DNA plasmids were prepared, as mentioned earlier (section 2.1). The plasmid DNA solutions were centrifuged at 14000 rpm for 10 min to remove the excess salt and endotoxin contents. The vector consists of $K_V1.2$(X) (encoding either $K_V1.2$-WT, -R297Q (GOF) or -P405L (LOF) mutant channels) and IRES-tdTomato under the control of a constitutively active CMV/β actin promoter. The equal concentration (2 µg/µl) of $K_V1.2$ (X) and IRES-tdTomato vector containing DNA solution were prepared in water and fast green (final concentration of 0.05 %; Sigma) was added to be able to visualize the injection of the DNA into the ventricle.

Timed pregnant BJ/6 strain mice were collected from the in-house animal facility of the Hertie Institute Tuebingen. All surgical procedures were performed under clean and sterile conditions. The mouse was anesthetized with the exposure of Isoflurane (Cp-Pharma, Burgdorf, Germany) before the injection of a mixture of Ketamine and Xylazine (0.625 mg per 10 g body weight, intraperitoneally). After achieving the complete loss of the righting reflex in animals, a drop of eye gel was applied on each eye to prevent the corneal eye dryness. After shaving the abdominal hair with an electric shaver, the mouse was transferred to a surgical mask with its back on the heating pad. The toe reflex was tested and confirmed the

complete loss of the righting reflex before the mouse was opened. The abdomen was cleaned with 70% ethanol, a 2-cm midline laparotomy was performed to carefully pull the embryonic chain out of the abdominal cavity and placed in wet surgical tissue, which covers the abdominal incision. From this point onwards, a sufficient amount of warm phosphate-buffered saline (PBS) was dispensed timely with an eyedropper to avoid the dryness of the uterus. The most accessible embryos were selected for the plasmid injection from the lateral side to keep track of electroporated embryos. A mouth-controlled pipette system (Aspirator tube assemblies, SIGMA-Aldrich) with previously pulled glass capillary microhematocrit tubes (Brand-GMBH) with a pinch off the tip with a forceps was used to inject 1-2 µl of DNA solution to the lateral ventricle of selected embryos. The position of the embryo inside the amniotic sac was adjusted carefully by using forceps to stabilize the head before the injection. The placing of the DNA solution was monitored with fast green. Electric pulses (five pulses of 30 V with 1 s intervals at 50 ms per pulse) were applied to the embryos through the uterus by holding the embryos with paddle electrodes with a 0^0 angle from the brain's horizontal plane using a CUY21 SC Square Wave electroporator (NEPAGENE). This position of the electrodes helped to selectively target somatosensory cortical layer 2/3 (SSC L2/3) excitatory neurons. After the complete electroporation of embryos, the abdominal cavity was filled with warm PBS and the uterine horn was placed in its original location. The abdominal muscle and skin incisions were sutured with vicryl absorbable sutures (Henry Schein Dental, Ethicon). Animals were then left to recover in a temperature maintained clean cage until they wake up. An approximate dose of pain killer RIMADYL (0.1 ml /10g body weight, subcutaneous injection) was given to the animals before transferring to the recovery cage. Mothers were monitored until the delivery and pups were screened and marked (with a non-harmful ink pen) under a fluorescent microscope to confirm the presence of electroporated cells at P2-3. These marked animals were later used to perform electrophysiological experiments.

2.3.2 Brain slice preparation and maintenance

Brain slices were prepared in two different methods for different experiments. For the patch-clamp recording of $K_V1.2$ electroporated mice, coronal sections were made from postnatal days 12 to 15 (P12-15). For acute extracellular recordings of TC up-states, slices were prepared from P13 to P20, while for organotypic brain slice cultures, P5 to P6 animals were used. The different slice preparation methods are described in detail below.

Acute brain slices were carefully prepared from *KCNA2*-electroporated mice to preserve the health of sections and the quality of neurons. After anesthesia with Isoflurane (Cp-Pharma, Burgdorf, Germany), following the complete lose reflex upon tail or paw pinching, animals

were quickly decapitated and brains were immersed in an ice-cold artificial cerebrospinal fluid containing (aCSF listed in Table 5), saturated with carbogen (95 % O_2, 5 % CO_2). Back part of the skull was immediately opened with a cut from caudal to the cerebellum and the skull was opened with a cut along the midline from the caudal end up to the olfactory bulbs without damaging the cortex. By using a fine forceps, the free edge of the skull on the open side of the midline was grabbed and the brain was gently scooped using a curved spatula. The brain was submerged in the ice-cold aCSF throughout this entire procedure. After removing the unwanted part from the caudal region, the brain was glued on a cutting plate with the ventral side down. A small agar piece was glued on the stage facing the back part to hold the brain in this conformation. The cutting plate was immediately transferred to the slicing chamber of a vibratome (Microm HM 650 V vibratome, Thermo Fisher Scientific). Coronal slices, each of 350 µm thickness, were cut in aCSF fluid. Slices were directly transferred to the tissue holding chamber, incubated for 1-1.5 hours at 37^0C temperature in a water bath and later transferred to room temperature prior to the experiments.

To record up-states from a preserved TC connectivity, TC brain slices were prepared according to a previously described method (Agmon and Connors, 1991). In this method, after the removal of the brain, it was placed on a glass ramp with a 10^0 slope. A vertical cut was made with a 55^0 angle at about one-third from the anterior part (Figure 8). This particular cut of the brain, using a 10° slope and a 55° angle, was made to allow the intact connectivity between the cortex and the thalamic area, including the NRT and the VB. The anterior part of the cut tissue was discarded while the cutting surface of the posterior part was glued onto a cutting stage (Figure 8). A small agar block was glued on the stage facing the ventral part to support the brain in this conformation and was placed in vibratome as the dorsal part of the brain facing the blade. Three to four 400 µM thalamocortical brain slices were cut and immediately transferred to the tissue holding chamber containing aCSF saturated with 95 % O_2 and 5 % CO_2. Slices were incubated for 1-1.5 hours at 37^0C and changed to room temperature before the experiments. For extracellular recordings, the slices were transferred into the submerged recording chamber (Warner instruments), continuously perfused with recording aCSF and experiments were performed at 34°C. For the organotypic TC brain slice culture, the same sectioning method was used, sections were prepared under sterile conditions and were immediately transferred into a laminar flow hood prior to the incubation.

2.4 Electrophysiological techniques

Electrophysiological methods have emerged as one of the best ways to understand the spatiotemporal information transfer in the nervous system (Sejnowski *et al.*, 2014). This

technique allows the precise understanding of the neurons from its single-channel level properties to whole organ level communication, which is essential in addressing the physiological and pathophysiological state of the nervous system. The voltage changes or electric currents, as the outcome of the accurate ion conductions through the neuronal surface membrane, enable neurons to integrate, propagate and transmit the information from one to another (Scanziani and Häusser, 2009). These electrical signals can acquire through extracellular electrode recordings or intracellular micropipettes recordings to make direct contact with the cell of interest. The micropipette measurements include intracellular recording where a sharp electrode penetrates the cell while for patch-clamp techniques, microelectrode forms a tight contact with the cell, without entering the cell.

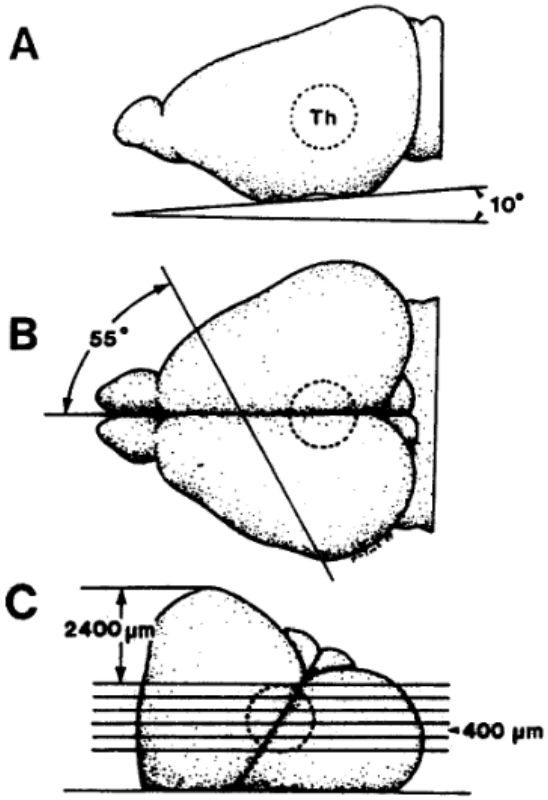

Figure 8. Preparation of acute thalamocortical brain slices: (**A**) The brain was placed at the 10^0 angle ramp. (**B**) The position of the vertical cut at 55^0 angles was made through the tissue. (**C**) The glued brain on the vibratome stage with the position of the slices containing the full TC connectivity. Figure adapted from (Agmon and Connors, 1991).

2.4.1 Patch-clamp recordings

This technique developed by Erwin Neher and Bert Sakmann in the late 1970s, which was later awarded the Nobel Prize in 1991, has given electrophysiologists new perspective. This invention allows us to record the high-resolution current from single ion-channels and to

understand their involvement in electrical information transfer in neurons. Patch-Clamp techniques involve a glass micropipette forming a tight giga-ohm (GΩ) seal with the cell membrane (Figure 9). The micropipette contains an electrode bathed in an electrolytic solution to conduct ions. The whole-cell recording is one of patch-clamp configurations, which involves rupturing a patch of the neuronal membrane with mild suction to allow low-resistance electrical access, enabling control of transmembrane voltage and recording currents through multiple channels simultaneously. On the other hand, it is also possible to pull a patch of membrane away from the neuron and evaluate currents through single channels via the inside-out or outside-out patch-clamp technique. Overall, the patch-clamp technique is one of the most challenging methods in laboratory work. The advancements in this technique have made it possible to study the two configurations of patch-clamp, such as whole-cell voltage clamp and current clamp in a single patch set up using the same electrical amplifier.

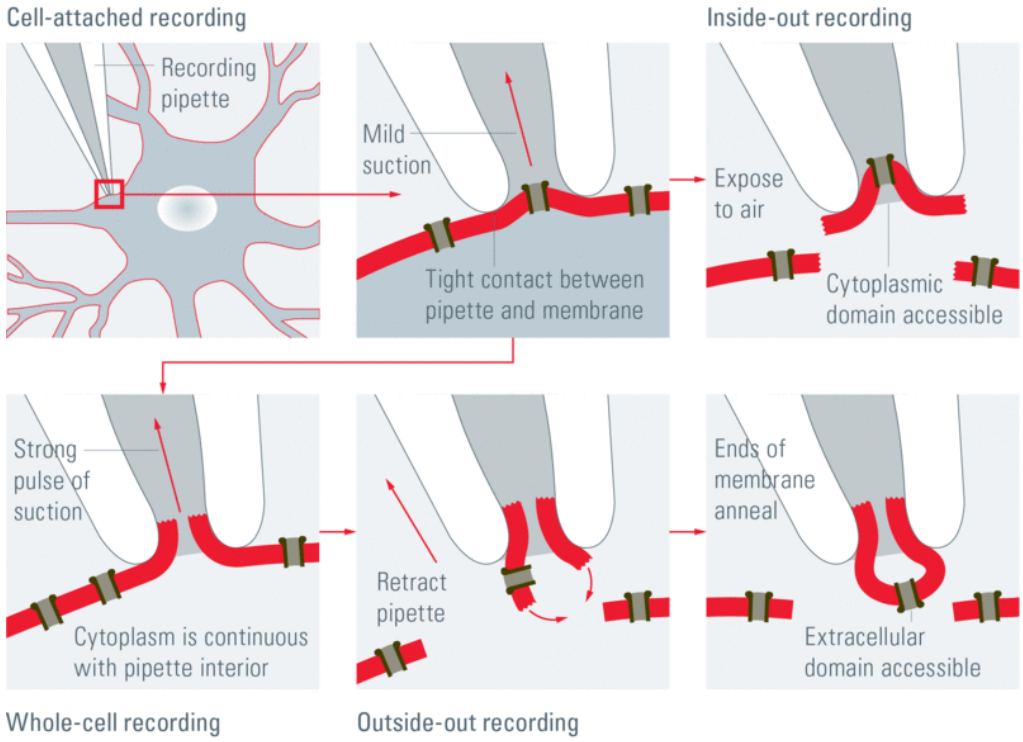

Figure 9. The four patch-clamp recording configuration: Cell-attached, whole-cell, inside-out and outside-out. Image source: Patch me if you can – What is the patch-Clamp Technique? puzzledponderer.wordpress.com

2.4.2 Voltage-clamp recordings

In whole-cell voltage-clamp experiments, the investigator controls the membrane voltage in a cell and measures the transmembrane current required to maintain that voltage. In the simplest scenario, it can be defined by keeping the voltage constant across a piece of

membrane attached to a pipette (small membrane patch to a whole-cell) and record current. This voltage control (command voltage) and its maintenance at different voltage levels are achieved through a simple amplifier, which can inject a specific amount of current when required. The injected current will be proportionate to the current escaping through open ion channels, allowing the amplifier to calculate the amount of current passing through open membrane-bound ion-channels.

In the present study, the whole-cell configuration was mainly used to understand the effect of 4-AP in mammalian CHO cells overexpressing $K_V1.2$ WT and mutant R297Q channels. Further, the potassium current in *in utero* electroporated neurons was also studied. Transfected cells (as mentioned in section 2.2.1) were further split, seeded into 2-3 dishes and incubated in the F12 medium for 10-20 min before recording. A perfusion insert (AutoMate Scientific) was carefully introduced into the Petri dish before mounting on the microscopic stage. Transfected cells were visualized and the expression of GFP was confirmed using an inverted fluorescent microscope (Leica Biosystems, Wetzlar, Germany). Whole-cell patch-clamp recordings were performed using an Axo-patch 200B amplifier, a Digidata 1440A digitizer and data were acquired using Clampex 10.2 acquisition software (Molecular Devices). Leakage and capacitive currents were automatically subtracted online using the P/4 subtraction protocol. The series resistance and membrane capacitance were compensated up to 85%. Recorded data were filtered at 2 kHz and sampled at 5 kHz. All recordings were performed at room temperature. The recordings were made in the extracellular bath solutions (Table 3) with glass pipette (borosilicate glass with a tip resistance of 2.5 - 3.5 MΩ) filled with an internal solution (Table 3). The liquid junction potential was calculated as +7.7 mV at 23°C, but not corrected. Potassium currents were recorded at a holding-potential of −90 mV and then depolarizing voltage steps were applied with an increment of 10 mV from -110 mV to 60 mV for 500 ms. The average currents amplitude was measured within the last 100 ms of 500 ms epoch for the analysis. These data points were further used to determine the current-to-voltage and conductance-to-voltage relationships in both *KCNA2* wild-type and *KCNA2*-R297Q before and after the application of 4-AP. A Minipuls peristaltic pump (Gilson) was used to provide a constant in- and out-flow (~3-4 ml/min) of bath solution containing different concentrations of 4-AP (Sigma-Aldrich). An incubation time of 5 min was always followed after the application of the drug.

2.4.3 Current clamp recordings

The current-clamp method measures the resulting transmembrane potential (voltage) from an injection of current or spontaneous ion-channel activity. In the current-clamp mode,

the voltage changes are analysed using an amplifier system, which monitors the voltage drop initiated by current injection along with an in-series resistor. The current clamp allows an investigator to inject simulated but realistic current waveforms into a cell and monitor the membrane effect. This technique is very accurate and ideal for the evaluation of critical cellular events such as action potentials.

Current-clamp experiments were used to study the overexpression effect of $K_V1.2$ WT, its LOF and GOF variants on intrinsic firing properties of neurons. Whole-cell patch-clamp recordings of excitatory neurons of SSC L2/3 were made in a submerged-type recording chamber with temperature-controlled (34°C) aCSF supply saturated with carbogen (95 % O_2 and 5 % CO_2). The chamber was fixed on a movable (motor controlled) top plate of the recording stage with micromanipulators (Scientifica, UK). The movable stage was fitted to an upright fluorescent microscope (BX61WI Microscope, Olympus, UK). Neurons (including fluorescently labeled) and the position of the electrodes were monitored with Cellsens imaging software (Olympus, UK). Recordings were obtained with Multiclamp 700B (Molecular Devices), amplifiers, a Digidata 1420 digitizer (Molecular Devices) and pClamp 10.3 software (Molecular Devices). Signals were recorded with a sampling rate of 100 kHz and low pass filtered at 30 kHz. Series resistance was monitored as <20 MΩ during the experiments. Cells showing unstable series resistance above 20 MΩ or resting membrane potentials were discarded. Extracellular and intracellular solutions that were used for current- and voltage-clamp experiments are summarized in Table 5. The pipettes were pulled from borosilicate glass (Science Products GmbH) using a Sutter P97 Puller (Sutter Instruments) with resistances of 3–5 MΩ. Liquid junction potential was calculated as -1.5 mV at 34^0C but was not corrected.

After establishing the whole-cell configuration in voltage-clamp mode, the mode was changed into current-clamp and the balanced bridge compensation. For current-clamp recordings except for the resting membrane potential and the input resistance, cells were held at -70 mV. After 2 min of stable gap-free recording, hyperpolarizing (from -10 to -110 pA for 500 ms) or depolarizing current injections (from -50 to 300 pA for 800 ms and 500) were applied to measure the input resistance or evoke action potential (AP) trains. Single APs were recorded with a threshold current injection with 5 ms duration. After the completion of the current-clamp recordings, the mode was shifted to voltage-clamp and K_V currents were recorded without the presence of any specific blockers. After finishing the entire protocols, pipettes were carefully detached from the cell and slices were fixed immediately with 4% paraformaldehyde (PFA) to preserve biocytin (Sigma) filled fluorescently labeled neurons.

Table 5: Brain slicing and recording solutions

aCSF for electrophysiological recordings	Ingredients	Working concentration [mM]
Slicing aCSF	NaCl	125
300-310 mOsm/l	$NaHCO_3$	25
pH = 7.4	KCl	2.5
	$NaH_2PO_4*H_2O$	1.25
	$CaCl_2*2H_2O$	1
	$MgCl_2$	7
	Glucose	10
Current clamp recording aCSF	NaCl	125
300-310 mOsm/l	$NaHCO_3$	25
pH = 7.4	KCl	2.5
	$NaH_2PO_4*H_2O$	1.25
	$CaCl_2*2H_2O$	2
	$MgCl_2$	1
	Glucose	10
Up-states recording aCSF	NaCl	126
300-310 mOsm/l	$NaHCO_3$	26
pH = 7.4	KCl	5
	$NaH_2PO_4*H_2O$	1.25
	$CaCl_2*2H_2O$	1
	$MgSO_4*7H_2O$	1
	Glucose	20
Intracellular solutions for Current-clamp recordings		
290-300 mOsm/l	KCl	5
pH = 7.2 with KOH	ATP-Mg	4
	Phosphocreatine	10
	GTP-Na	0.3
	HEPES	10
	K-Gluconate	125
	$MgCl_2*6H_2O$	2
	EGTA	10
	Biocytin*HCl,	0.2%

2.4.4 Extracellular multi-unit recordings

With extracellular recordings, the transient electrical potential from the extracellular space of neurons can be recorded. When using extracellular electrodes, the recordings represent multi-unit (MU) extracellular neuronal population activity from specific parts of the brain allowing to understand network-level changes in neuronal populations. Multi-unit (MU) recordings can show the long-lasting network discharges from a neuronal population as an up-state (in case the depolarized plateau potential lasts more than 300 ms). MU field potential recordings were performed for TC slices in a recording chamber (Warner Instruments, Harvard biosciences. Inc) with continuously perfused (~ 10 ml/min) aCSF (Table 5) at 30^0C. Recordings were obtained using 0.5-1 MΩ borosilicate glass microelectrodes (Science Products GmbH) filled with aCSF. The microelectrodes were placed in deep layers of the SSC, layer 5 and NRT (Figure 10). Waveform signals were acquired using in-house built head stages that were connected to the AC amplifier Model 1700 (A-M Systems, USA), Digidata 1420 digitizer (Molecular Devices) and integrator from NPI (Model INR-011). Data were acquired using pClamp 10.3 software (Molecular Devices). Signals were amplified 10,000-fold and bandpass filtered (0.25-1.5 Hz).

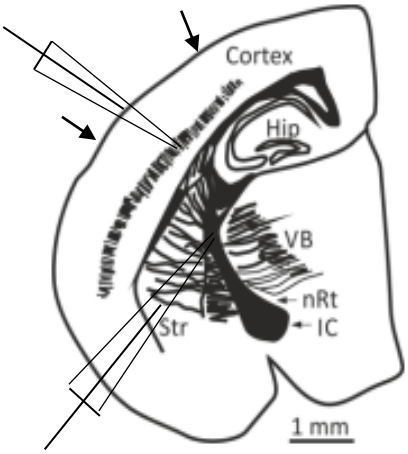

Figure 10. A thalamocortical brain slice with two extracellular recording electrodes: One electrode is placed in the cortex (layer V) and one in the NRT. Image modified from (Agmon and Connors, 1991).

2.5 Immunohistochemical staining

Sections fixed for 24 hours after the electrophysiological recordings were incubated overnight in PBS. After each antibody incubation, a washing step was performed with PBS (3X-10 min interval in every washing step), and sections were subsequently blocked for one hour in blocking medium (PBS with 6% normal goat serum and 0.6% Triton X-100) at room

temperature. After blocking, sections were incubated with a monoclonal antibody against GFP (Invitrogen; 1:500) for one hour at room temperature and then overnight at 4°C. On the next day, sections were incubated of 2 hours at room temperature with secondary Alexa Fluor 488-conjugated goat anti-mouse antibodies (dilution 1:500; Invitrogen). Then, slices were incubated for 6 hours at room temperature with cy3 conjugated streptavidin (Sigma; dilution 1:200 in PBS with 0.3% Triton X-100). After a washing step, slices were stained with DAPI for 2 min (Sigma-Aldrich; dilution 1:5000) to identify the nuclei. After the final washing step, sections were air-dried and mounted with fluoromount-G (Southern Biotech), glass cover-slipped and visualized on a Leica TCS SP8 confocal laser-scanning microscope (Bensheim, Germany) using a 40x/1.3NA oil-immersion objective.

2.6 Neuronal 3D-reconstruction and morphological assessment

The morphological reconstruction of neurons using image processing is an important aspect to understand neuronal health and development. It allows to study the developmental changes emerging in neuronal morphology due to the specific ion-channel mutations. In this study, I have used the aforementioned technique to assess the $K_V1.2$ WT and its LOF and GOF variants channel overexpression induced changes in the dendritic arborization. For the 3D-reconstruction of neurons, high-resolution Z-stack tile scans of the slices were acquired after the immunohistochemical staining of biocytin filled or GFP-labeled neurons (Figure 11). The Cy3 fluorescence and GFP signal were excited at 548 and 488 nm, respectively, using a tunable white light laser. The emissions were detected between 555 nm and 615 nm for Cy3, and between 493 nm and 530 nm for GFP. Neurons (biocytin filled) lacking dendritic arborization more than 2/3 due to the sectioning were avoided in the analysis. The position of layer 2/3 pyramidal neurons was confirmed by the orientation of apical dendrites and by measuring the distance from their soma to the pia as 250-350 µm. The slices were imaged at the following resolution: voxel size: 0.2481 × 0.2481× 0.7 μm^3 (Width: 240 µm Height: 240 µm). The tile scans were stitched using the inbuild stitching option of LAS X imaging software (Leica microsystems). Neuronal reconstruction was performed using semi-automated open ware Neuromantic v1.7.5. (Myatt *et al.*, 2012). The apical and the basal dendrites were identified manually and represented with the colors orange (apical dendrites) and magenta (basal dendrites) (Figure 12.A). The axons could not be traced in each neuron; therefore, they were not involved in the assessment of morphological features.

2.7 Data analysis

Electrophysiological traces recorded during experiments were displayed offline with the Clampfit software pClamp version 10.7 (Molecular Devices). The analysis was performed

using Clampfit 10.7 (Molecular device), Excel (Microsoft), SigmaPlot 12.5 (SYSTAT software) and Origin (Origin-lab). Morphological analysis was performed with Neuromatic software; the Sholl and skeleton analysis were performed in image J software using the Simple Neurite Tracer plugin (F. Frangi *et al.* 1998).

2.7.1 Current-clamp analysis

In current-clamp experiments, passive membrane properties such as resting membrane potential, input resistance and membrane time constant as well as active cellular events of action potentials were studied. The particular method used for the analysis of each intrinsic cellular properties are mentioned below:

a. Resting membrane potential (R_m) (mV): R_m was calculated as an average potential of the last 100 ms from the first 2 min gap-free recording without injecting any current in the current-clamp mode.

b. Input resistance (R_{in}) (MΩ): R_{in} was calculated as a slope of the linear fit to the steady-state voltage response to different current injections (0 mV t0 –110 mV). It was measured by injecting brief hyperpolarizing current pulses (500 ms) at R_m of small amplitude (10 mV) from 0 - 110 mV. The voltage deflection was considered only at the end of the voltage response (300 - 400 ms) to avoid the influence of a sag potential.

c. The membrane time constant (τ) (ms): The membrane time constant is considered as the time taken for the membrane to repolarize after a small current injection of fixed amplitude and duration. It was calculated by fitting the single exponential to the first 100 ms of the voltage response of injecting -50 pA hyperpolarizing current (Figure 14C).

d. The action potential threshold (mV): The threshold potential was calculated as the voltage at which an AP was initiated (as assessed by measuring the rising slope of membrane voltage). It was measured from an action potential fired at minimum injected current amplitude as a response of 5 ms long depolarizing current. The AP threshold was measured as the membrane potential at which the dV/dt exceeded 20 V/S.

e. AP amplitude (mV): The AP amplitude was defined as the voltage that indicated the height of the AP. It was calculated as the voltage difference between the AP threshold and the AP peak (see Figure 15A) and measured from 5 ms threshold current injection.

f. AP half-width (ms): The AP half-width was calculated as the AP duration at the membrane voltage halfway between the AP threshold and AP peak (see Figure 15A). To analyse this parameter, the 5 ms current injection protocol was used.

g. Afterhyperpolarization (AHP) amplitude (mV) and duration (ms): the AHP amplitude was defined as the difference between the potential level at the AP threshold and the end of

hyperpolarization (see Figure 18A). The time taken from the AP threshold level to reach the peak of the end of hyperpolarization was considered as the duration. The endpoint of the hyperpolarization was considered as a potential in which the first derivative was coming back to the point of zero (see Figure 18C). The AP train elicited by the current injection (800 ms duration) of 125 pA amplitude was used for the measurement. For the calculation of the duration of the repolarization (ms), the same criteria used to determine the end of hyperpolarization was considered, but the AP peak was considered as the beginning (see Figure 18C).

h. Rheo-base (nA), AP number and area under the curve (AUC): the Rheo-base is the minimum current injected that is needed to elicit an AP with an infinite duration. It was derived from the episodic current injection (500 or 800 ms duration, 25 pA amplitude) from -50 pA to 300 pA. The same protocol was used for the calculation of the AP number. This AP number and current injection ratio were further used to calculate the AUC.

i. Adaptation ratio (proportion): The adaptation ratio represents the ratio of durations between late and early AP inter-spike intervals (ISI) on an AP train and gives information about the temporal distribution of spikes during a train. The adaptation ratio on an 800 ms pulse exceeding 175 pA, using $1 - (F_{L200ms}/F_{I200ms})$ was measured, with F_{L200ms} and F_{I200ms} corresponding to the firing frequencies recorded during the last and the first 200 ms period of the step, respectively.

2.7.2 Voltage-clamp analysis

For the voltage-clamp experiment of CHO cells, the membrane potential was episodically depolarized using a step protocol for a duration of 500 ms (from -110 mV to 60mV with an increment of 10 mV) from a holding potential of -90 mV. For the neurons, the holding potential was -70mV and the depolarizing episodes were injected up to 20 mV with a 10 mV increment. The current amplitude was calculated as the average when they reached the steady-state of the trace (300-400 ms). A Boltzmann equation was fit to the data points as mentioned below to calculate the activation curve.

$$G(V) = Gmax/(1 + \exp[(V - V½)/k])$$

where G (V) = $I/(V\text{-}V_{rev})$ is the conductance, I is the current amplitude at potential V, V_{rev} is the K^+ reversal potential, G_{max} is the maximal conductance, $V_{½}$ is the voltage at which the activation is half-maximal, and k is the slope factor (a positive number for activation).

2.7.3 MUA-extracellular analysis

The integrated traces of up-states recorded as extracellular multi-unit activity (MUA) were further used for manual analysis. Since the recording from NRT was silent, only up-states recorded from SSC L5 were used for analysis. The plateau depolarizations (up-states) followed by hyperpolarization (down-states) spontaneously occurred and lasted for at least 300 ms, were considered as an up-state event. Up-states shorter than 300 ms were excluded from further analysis. The frequency of up-states was calculated from traces of 20 min duration. The period between an up-state onset and offset was considered as the duration of the event (Figure 23A).

2.7.4 Morphological analysis

The reconstructed neurons from the Neuromantic were further used for morphological assessment with Sholl and skeleton analysis. In Sholl analysis, concentric spheres were automatically placed around the cell by keeping the soma as a centre. To analyse the dendritic complexity, intersections of the dendrite with spheres were counted from the soma at every 10 µM (SHOLL, 1953). The maximum diameter of the sphere used to cover the entire dendrites of neurons was considered as a cell radius. The total branch length and the sum of total branches were calculated in the render and skeleton analysis part of Simple Neurite Tracer plugin for image J. Neuro-skeleton (without soma) from the reconstructed neurons was only used for skeleton analysis.

2.8 Statistical analysis

All statistical analyses were performed in Excel (Microsoft), SigmaPlot 12.5 (SYSTAT software) and Origin 2020 (Origin lab). All data have undergone a test for normal distribution with the Shapiro-Wilk test. Statistical analyses to compare two groups were performed using paired (before and after effect) or unpaired Student's t-test (normally distributed data) or Mann-Whitney rank-sum (not-normally distributed data). Three or more groups were compared using one-way ANOVA with Bonferroni's post hoc test (for normally distributed data) and ANOVA on ranks with Dunn's post hoc test (for not normally distributed data). Two-way ANOVA was adopted to compare the effects of 4-AP application between WT and mutant channels. Statistical significance is indicated in the figures with the following symbols: *$p<0.05$, **$p<0.01$, ***$p<0.001$.

3. Results

3.1 Understanding the pathophysiology of *KCNA2* mediated epilepsies

3.1.1 Overexpression of K_V1.2 WT, LOF and GOF variants in pyramidal neurons of the somatosensory cortical layer 2/3 (SSC L 2/3)

Epilepsy patients carrying *KCNA2* variants have shown distinctive clinical phenotypes including febrile or afebrile seizures, focal, generalized tonic-clonic seizures, absence and generalized myoclonic seizures. These diverse seizure types and related phenotypic variability indicate that *KCNA2* variants may impair different functional brain regions such as neocortical, hippocampal and thalamic structures. Till now, no information is available regarding the effect of *KCNA2* mutations on the intrinsic firing properties of neurons as well as the involved cellular and local network in the processes of seizure initiation. To fill this knowledge gap, I have examined the electrophysiological and morphological properties of neurons overexpressing K_V1.2 wild type (WT) channels, LOF and GOF variants, leading to *KCNA2*-mediated epilepsies in patients. The somatosensory cortex (SSC) has been identified as a fundamental structure in the generation and propagation of spike-and-wave discharges in absence seizures of rat models (Meeren *et al.*, 2002; Polack *et al.*, 2007) and detailed analysis of its involvement is crucial to unravel the *KCNA2* pathology. Another critical factor is the ubiquitous expression of K_V1.2 in both excitatory and inhibitory neurons (Nashmi *et al.*, 2000; Lorincz and Nusser, 2008; Trimmer, 2015) increasing the complexity in understanding seizure generating mechanisms. Considering the aforementioned facts, I have started my study by primarily focusing on SSC L2/3 pyramidal neurons of P12-P15 mice.

In utero electroporation (IUE) allows the overexpression of ion-channels in specific brain regions and facilitates to modify only a subset of pyramidal neurons at an early developmental stage, therefore abolishing the complications of global excitability changes (Chen *et al.*, 2014). To target SSC L2/3 pyramidal neurons, IUE was performed at embryonic day (E) 14.5, which enabled the optimal overexpression of K_V1.2 WT and its variants (R297Q, P405L) in the targeted brain region. The morphology and the localization of transfected neurons were identified through the co-transfection of a td-Tomato expressing fluorescent protein together with GFP-tagged K_V1.2 channels. Previous studies have shown that the co-transfecting efficiency of two plasmids with IUE exceeds 90% (Siddiqi *et al.*, 2012). The morphological orientation parameters, such as the projection of apical dendrites towards pia matter and the distance of the soma from the pia, were also used to confirm the pyramidal cells in SSC L2/3. Overexpression of K_V1.2 WT channels in SSC L2/3 pyramidal neurons (GFP positive) are shown in Figure 11. During the whole-cell patch-clamp recording (P12-P15), the

recorded neurons were filled with biocytin and then used for post-hoc immune staining and morphological analysis.

3.1.2 K_V1.2 WT and GOF overexpression alter the morphological features of SSC L 2/3 pyramidal neurons

Severe genetic ion-channel variants can directly induce neuro-developmental consequences (Scheffer *et al.*, 2017). Patients carrying *KCNA2* mutations were also observed with a delay or a stagnation of psychomotor development (Masnada *et al.*, 2017). This developmental impairment may be connected to the morphological alterations that occurred at an individual neuronal level in the brain. One of our collaborators, Prof. Dr. Olga Garaschuk's lab also made such observation that K_V1.2 WT channel overexpression can alter morphology in olfactory bulb neurons (unpublished, personal communication between the research groups). These observations motivated me to first elucidate the morphological changes in neurons due to the overexpression of K_V1.2 channels by keeping untransfected neurons as a control in the electroporated area.

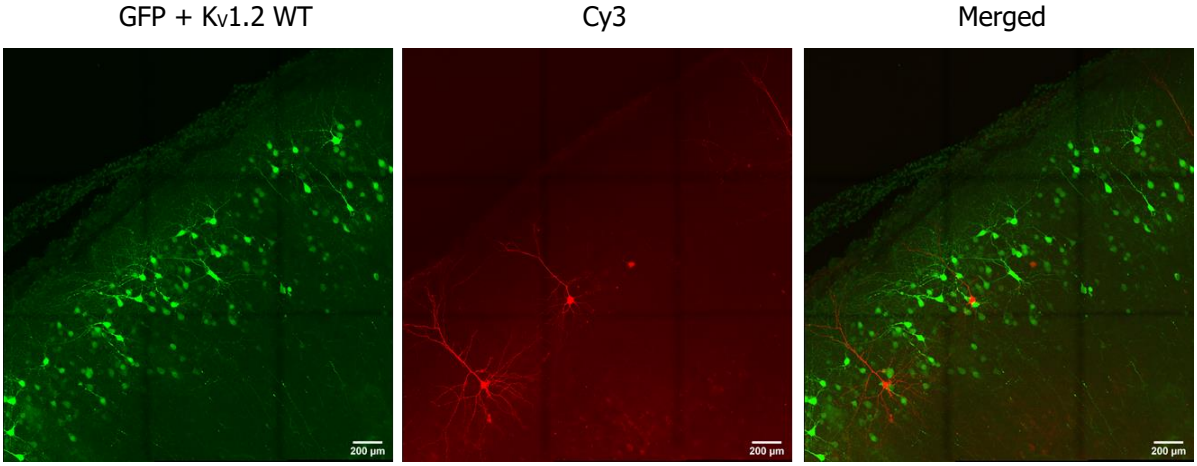

Figure 11. Overexpression of K_V1.2 WT in SSC L2/3 pyramidal neurons: Representative confocal images of K_V1.2 WT transfected pyramidal neurons in the SSC L2/3 (green) obtained by single electroporation performed at E14.5. Sections were counter-stained with GFP and streptavidin conjugated with Cy3 (red) for neurons filled with biocytin via the patch pipette. Three images indicate GFP, Cy3 and their merged images respectively, with a scale bar of 200 µm.

For studying the neuronal morphological features, high-resolution confocal images were acquired and 3D reconstructed. Pyramidal neurons were filled with biocytin during whole-cell recording, which was sufficient to study the clear presence of apical and basal dendritic compartments. These 3D reconstructed neurons were later used to perform Sholl and skeleton analysis (Figure 12A). Statistical significance was calculated for the entire Sholl profile showed

that neurons overexpressing $K_V1.2$ WT ($P < 0.01$) and R297Q ($P < 0.001$) variant were overall smaller and had less dendritic arborizations as compared to controls (untransfected neighboring neurons in the electroporated area; one-way repeated measures ANOVA followed by Bonferroni's post hoc test). The results are shown in Figure 12B indicating the number of intersections occur at fixed distances (10 µm) from the soma in concentric Sholl spheres. The diameter of Sholl circle, calculated from the soma which covers the entire dendrites of neurons, was also significantly reduced in R297Q as compared to controls ($P < 0.05$); one-way ANOVA with Bonferroni's post hoc test) (Table 6). The detailed skeleton analysis of $K_V1.2$ WT and R297Q showed a significant reduction in the extent of tertiary branching and length of overall dendrites, however, the overexpression of the P405L variant did not induce any morphological changes as compared to control cells. The total branch length calculated from skeleton analysis demonstrated a significant reduction in the neurites of R297Q overexpressing neurons ($P < 0.01$) as compared to control and P405L (Figure 12D); one-way ANOVA with Bonferroni's post hoc test, while in WT ($P < 0.05$) overexpressing cells the branch length was significantly reduced in comparison to neurons overexpressing the P405L variant (Table 6). The number of branches were also significantly reduced in R297Q ($P < 0.05$) cells as compared to control and P405L; one-way ANOVA with Bonferroni's post hoc test) (Table 6).

Table 6: Details of Sholl and skeleton analyses comparing cell radius, total branch length and number of branches among four neuronal groups

Morphological parameters	Control (n=10)	WT (n=4)	R297Q (n=6)	P405L (n=4)
Cell radius (µm)	328 ± 38.92	202 ± 30.10	172 ± 17.59 a*	313 ± 24.62
Total branch length (µm)	3743 ± 489	2259 ± 360 b*	1553 ± 244 a**, b**	4697 ± 654
Number of branches	204 ± 26.25	129 ± 13.60	88 ± 17.56 a*, b*	224 ± 26.85

Data are presented as mean ± SEM. a* denotes values are significantly different from control values. b* denotes values are significantly different from P405L values. *p < 0.05 and **p<0.01, n: Number of cells used in morphological analysis.

The next aim was to assess the overexpression-induced specific changes in apical versus basal dendritic compartments. A separate skeleton analysis (without soma) was performed for both apical and basal dendrites (Figure 13), and a significant reduction of the apical dendritic branch length was observed in R297Q ($P < 0.05$) overexpressing neurons compared to controls; ANOVA on ranks with Dunn's post hoc test. The total number of apical dendrites were also significantly reduced in R297Q ($P < 0.05$) compared to controls; one-way ANOVA with Bonferroni's post hoc test) (Table 7). The comparison of the total basal branch length showed a reduction in R297Q ($P < 0.05$) compared to neurons overexpressing the P405L variant; one-

way ANOVA with Bonferroni's post hoc test) (Table 7). The total number of basal branches did not significantly change among the four groups; one-way ANOVA with Bonferroni's post hoc test) (Table 7). Taken together, these results suggest that the overexpression of the $K_V1.2$ GOF variant induces morphological alterations in the dendritic morphology, which affected both apical and basal dendritic compartments. However, LOF variant overexpression did not show any significant changes in the dendritic arborization as compared to control cells.

Table 7: Summary of specific changes due to the overexpression $K_V1.2$ channels in apical versus basal dendritic compartments

Morphological parameters	Control (n=10)	WT (n=4)	R297Q (n=6)	P405L (n=4)
		Apical dendrites		
Branch length (µm)	2017 ± 446	897 ± 91	432 ± 187 a*, b*	2114 ± 147
Number of branches	100 ± 16.48	55 ± 6.56	27 ± 12.88 a*	95 ± 25.64
		Basal dendrites		
Branch length (µm)	1727 ± 274	1363 ± 311	1121 ± 121 b*	2584 ± 539
Number of branches	104 ± 18.67	75 ± 9.78	61 ± 10.12	129 ± 10.84

Data are presented as mean ± SEM. a* denotes values are significantly different from control values. b* denotes values are significantly different from P405L values. *p < 0.05, n: Number of cells used in morphological analysis.

3.1.3 $K_V1.2$ R297Q and P405L overexpression changes the neuronal passive membrane properties in SSC L2/3 pyramidal neurons

Ion-channel specificity and its density in neurons affect passive membrane properties and consequently their information coding ability. Changes in passive membrane properties due to the ion-channel density directly influence the synaptic or sensory inputs and therefore, the information processing capabilities of neurons (Sengupta *et al.*, 2013). Morphological changes due to severe ion-channel variants can also directly impair the passive membrane properties. In order to understand the effect of overexpression of $K_V1.2$ WT channels and its variants on passive membrane properties, the resting membrane potential (R_m), input resistance (R_{in}) and membrane time constant-Tau (abbreviated τ) were analyzed (Figure 14; Table 8) in neurons overexpressing $K_V1.2$ WT, R297Q and P405L variants.

Channels containing the $K_V1.2$ subunit show low-threshold voltage-gated potassium currents and activate close to R_m. They are crucial in regulating R_m, therefore I explored how the overexpression of $K_V1.2$ subunits modulate the R_m. The R_m was measured from gap-free recording without injecting any current in the current-clamp mode. The values of R_m measured

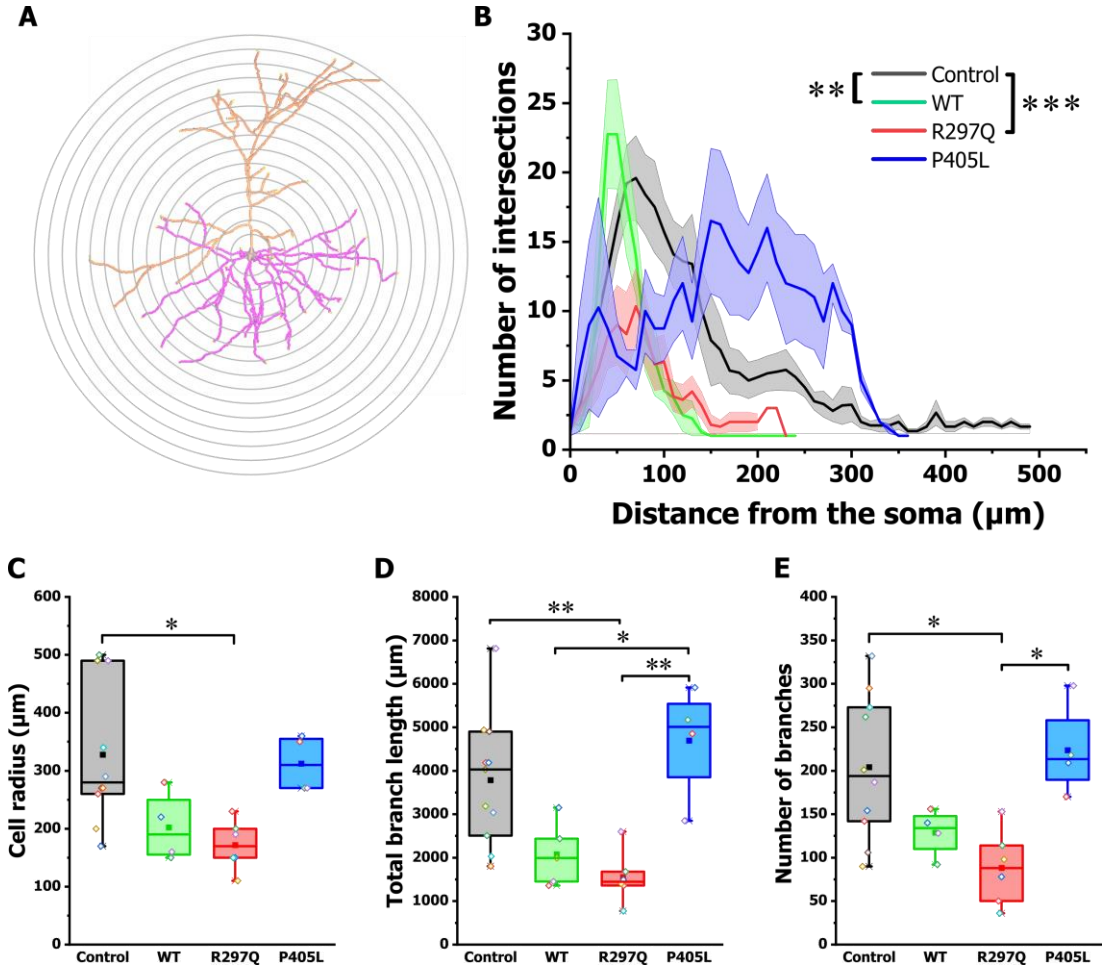

Figure 12. Effect of $K_V1.2$ WT, its LOF and GOF variants overexpression in dendritic morphology: (**A**) Schematic representation of the Sholl analysis of a 3D reconstructed control neuron. The apical dendrites are presented in orange and the basal dendrites in magenta. Each addition of concentric sphere radii is 10 µm. (**B**) The overall number of dendritic intersections as a function of the distance away from the soma (in µm). There was a statistically significant difference between control and WT ($P < 0.01$) as well as control and R297Q ($P < 0.001$); one-way repeated measures ANOVA followed by Bonferroni's post hoc test. (**C**) Cell radius measured from control, WT, R297Q and P405L. Statistical significance was tested by one-way ANOVA with Bonferroni's post hoc test, control : R297Q ($P < 0.05$). (**D**) The branch length calculated from control, WT, R297Q and P405L and statistical difference were (control, P405L : R297Q, $P < 0.01$, WT : P405L, $P < 0.05$) calculated with one-way ANOVA with Bonferroni's post hoc test. (**E**) Box plots comparing total number of dendritic branches from control, WT, R297Q and P405L. The significant difference (control, P405L : R297Q, $P < 0.05$) was calculated with one-way ANOVA with Bonferroni's post hoc test. All data from each group are shown in the box plot. The lower and upper whiskers show the minimum and maximum values. The lower and upper borders of the boxes represent 25th and 75th percentiles respectively. Center lines represent median, whereas center boxes represent numerical mean.

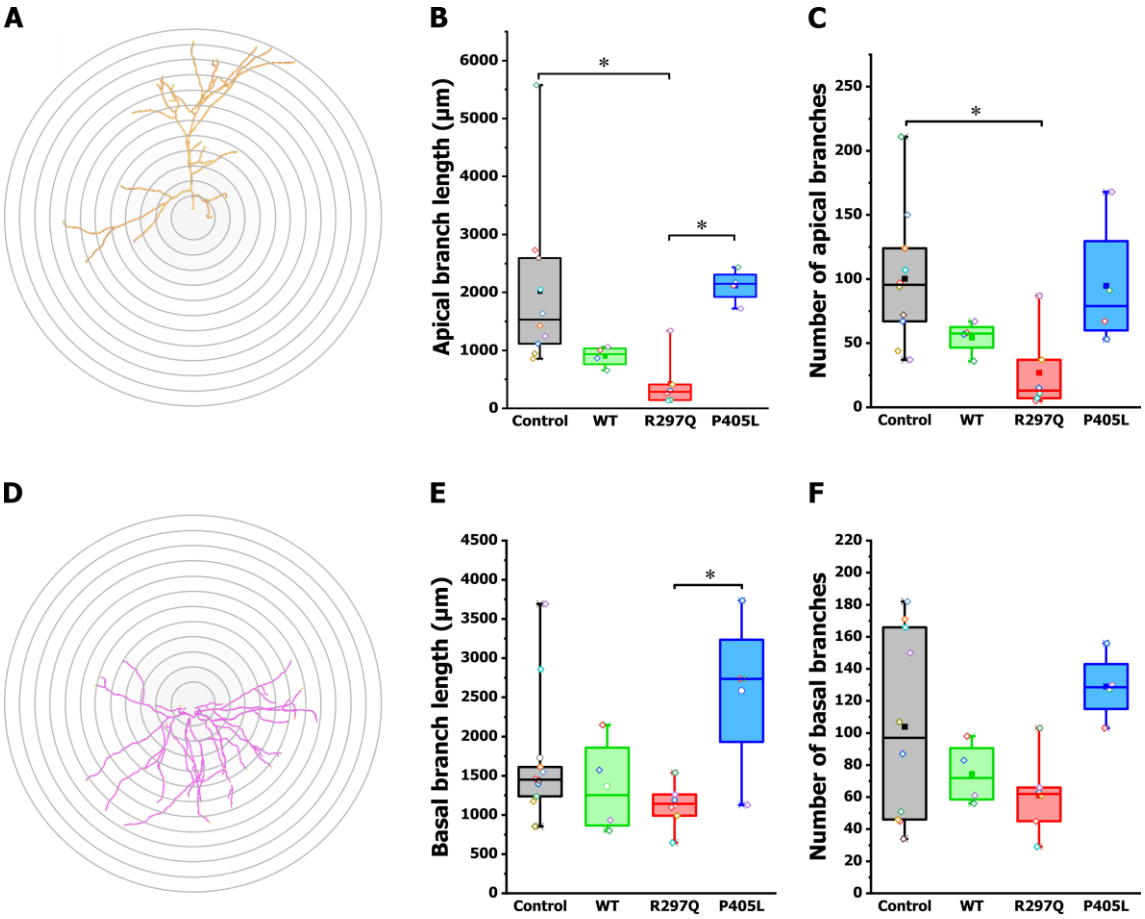

Figure 13. Specific changes due to the overexpression $K_V1.2$ channels in apical versus basal dendritic compartments: (**A**) Schematic representation of separate skeleton analysis for the apical dendrites presented in orange. (**B**) Box plots comparing the apical branch length from control, WT, R297Q and P405L, statistical difference among groups were calculated using ANOVA on ranks with Dunn's post hoc test (control, P405L : R297Q, $P < 0.05$). (**C**) Box plots comparing the total number of apical branches from control, WT, R297Q and P405L, statistical significance were calculated using one-way ANOVA with Bonferroni's post hoc test (control : R297Q, $P < 0.05$). (**D**) Schematic representation of separate skeleton analysis for the basal dendrites presented in magenta. (**E**) Total basal branch length comparison among four groups with a significant difference in R297Q ($P < 0.05$) compared to P405L overexpressing neurons; one-way ANOVA with Bonferroni's post hoc test). (**F**) The total number of basal branches, which did not show any significant difference among four groups (control, WT, R297Q and P405L; one-way ANOVA with Bonferroni's post hoc test). All data from each group are shown in the box plot. The lower and upper whiskers show the minimum and maximum values. The lower and upper borders of the boxes represent 25th and 75th percentiles respectively. Center lines represent median, whereas center boxes represent numerical mean.

from four groups of cells varied from -60 mV to -77 mV (Table 8) and no cell showed spontaneous firing. Cells overexpressing WT and R297Q $K_V1.2$ channels showed a significantly more hyperpolarized membrane potential compared to the P405L overexpressing neurons (WT : P405L, $P < 0.01$, R297Q : P405L, $P < 0.05$; ANOVA on ranks with Dunn's post hoc test). The measured R_{in} values among the four groups showed a reduction in R297Q than the P405L ($P < 0.05$; one-way ANOVA with Bonferroni's post hoc test) (Table 8). Finally, the membrane time constant-Tau was also analyzed to understand the voltage attenuation in $K_V1.2$ channels overexpressing neurons as a response towards the current injection. The Tau values were compared using ANOVA on ranks with Dunn's post hoc test and showed a significant change among the four groups (control : WT, $P < 0.01$; control : R297Q, $P < 0.01$; P405L : WT, $P < 0.001$; and P405L : R297Q, $P < 0.001$) (Table 8). All the data indicate the strong influence of $K_V1.2$ R297Q and P405L overexpression on passive membrane properties.

Table 8: Summary of changes in passive membrane properties due to the $K_V1.2$ channels overexpression

Neuronal types	Rm (mV)	Rin (MΩ)	Tau (ms)	Cell (n)
Control	-71.7 ± 0.5	238.8 ± 10.5	23.3 ± 1.2	35
WT	-73.2 ± 0.7 b**	216.0 ± 11.5	17.3 ± 0.8 a**, b***	19
R297Q	-73.4 ± 0.9 b*	194.7 ± 21.4 b*	15.1 ± 1.4 a**, b***	9
P405L	-68.7 ± 1.1	260.4 ± 13.4	26.5 ± 1.8	19

Data are presented as mean ± SEM. a* denotes values are significantly different from control values. b* denotes values are significantly different from P405L values. *p < 0.05, **p<0.01 and ***p<0.001, n: Number of recorded neurons.

3.1.4 $K_V1.2$ WT, R297Q and P405L overexpression lead to changes in action potential (AP) properties

$K_V1.2$ channels are located in multiple cellular compartments, including the AIS, where they regulate the axonal resting membrane potential (Robbins and Tempel, 2012). To understand the role of $K_V1.2$ on AP properties, I investigated the single AP properties of neurons overexpressing $K_V1.2$ WT, R297Q and P405L channel subunits (Figure 15). APs were recorded following a brief current pulse injection with a threshold current amplitude to fire a single AP (5 ms). The injected current threshold to fire a single AP remained the same in all four groups. In addition, the AP threshold did not show any significant changes among the four groups (Table 9, one-way ANOVA with Bonferroni's post hoc test). The next question was whether the overexpression of $K_V1.2$ subunits influences the repolarization phase of APs. The AP amplitude was determined as a potential difference (in mV) from the AP threshold to the peak of the AP (Figure 15A). The analyzed data revealed that the AP amplitude was significantly reduced in

neurons overexpressing the R297Q variant ($P < 0.05$; one-way ANOVA with Bonferroni's post hoc test, Table 9).

$K_V1.2$ subunits may increase the speed of the repolarization phase by enhancing the out-flow of K^+ ions. To further investigate this, the half-width of the AP was measured, which was found to be significantly reduced in neurons overexpressing WT subunits compared to controls ($P < 0.05$; ANOVA on ranks with Dunn's post hoc test, Table 9). In addition to the single AP parameters, I have also measured the rheobase as a minimum current injection to elicit single AP in an AP train with an infinite duration (< 300 ms). This indicated how the excitability of the cells was reduced due to the overexpression of $K_V1.2$ subunits. The rheobase was determined by a current injection with a duration of 500 ms or 800 ms, and in both cases, it remained the same. Groupwise comparison (control : 0.06 ± 0.00 nA, n= 35; WT : 0.08 ± 0.01 nA, n =18; R297Q : 0.11 ± 0.01 nA, n = 6 and P405L 0.06 ± 0.01, n =19; ANOVA on ranks with Dunn's post hoc test) showed that the rheobase was increased for neurons overexpressing the R297Q variant (control : R297Q, $P < 0.001$ and P405L : R297Q, $P < 0.01$) (Figure 16B).

Table 9: Summary of AP changes due to the overexpression of $K_V1.2$ WT, R297Q and P405L

Neuronal types	Current threshold (nA)	AP-threshold (mV)	AP amplitude (mV)	AP half-width (ms)	Cell (n)
Control	0.4 ± 0.02	-44.7 ± 0.6	78.8 ± 1.4	1.78 ± 0.08	35
WT	0.3 ± 0.03	-43.4 ± 0.8	76.8 ± 2.3	1.36 ± 0.12*	19
R297Q	0.3 ± 0.03	-43.0 ± 1.6	69.0 ± 4.2*	1.54 ± 0.16	9
P405L	0.4 ± 0.02	-42.6 ± 0.8	77.6 ± 1.9	1.78 ± 0.17	19

Data are presented as mean ± SEM. * marked values are significantly different from the control values, *p<0.05. n: Number of recorded neurons.

Overall, these AP properties showed that overexpression of the R297Q variant triggers the repolarization phase of an AP earlier than control, WT and P405L. Also, a significantly higher amount of current was required to elicit an AP in R297Q overexpressing neurons.

3.1.5 Effect of $K_V1.2$ WT, R297Q and P405L overexpression on AP firing

The $K_V1.2$ subunits are expressed in SSC L2/3 pyramidal neurons, however, it is not clear how the neuronal AP repetitive firings are affected by the disease-causing variants of $K_V1.2$. The K_V1 channel family strongly regulates the repolarization phase and may also influence repetitive AP firing by inducing a long-lasting afterhyperpolarization (Pathak *et al.*, 2016). To examine these characteristics of $K_V1.2$ channel subunits in SSC L2/3 pyramidal neurons, cells overexpressing $K_V1.2$ WT, R297Q and P405L subunits were depolarized to different potentials by injecting currents of -50 pA to 300 pA for 500 or 800 ms. The firing patterns were identical in both current protocols with different duration. Control neurons (non-transfected neurons in

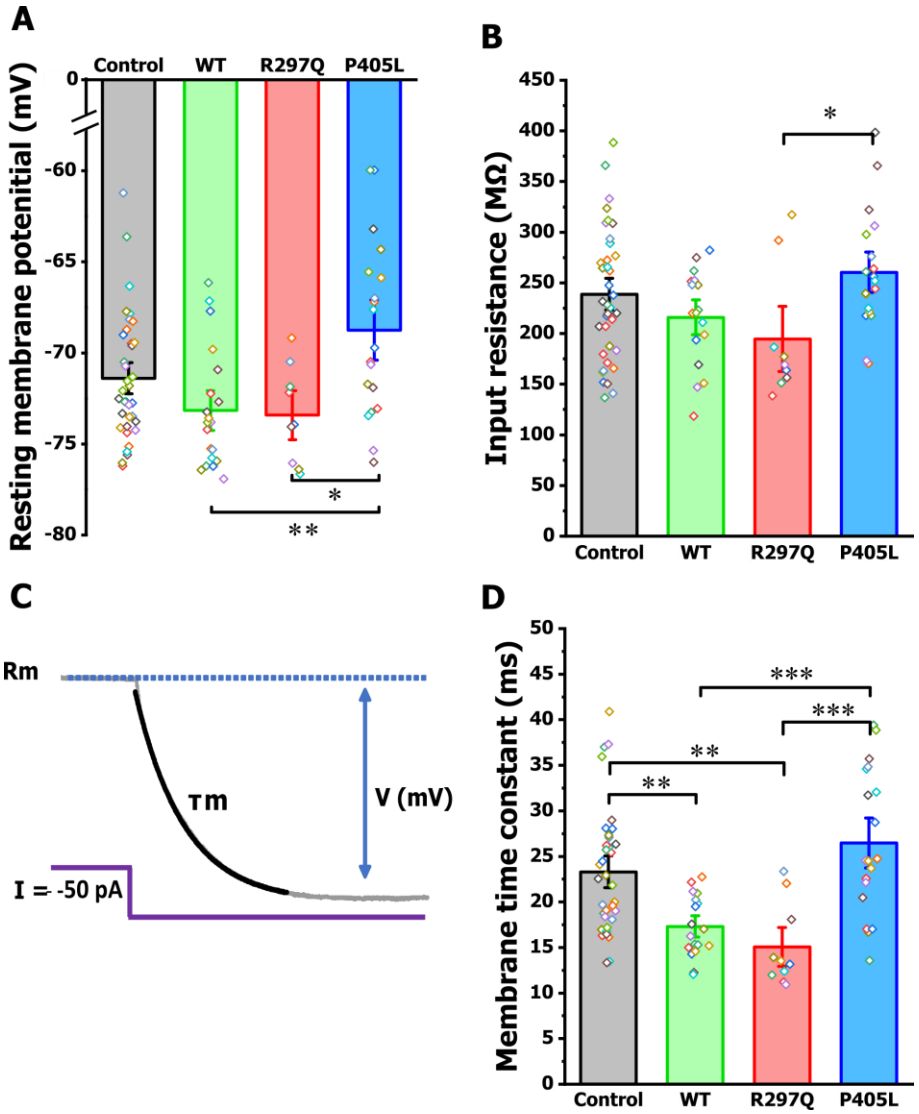

Figure 14. Modulation of passive membrane properties due to the overexpression of $K_V1.2$ Wt, its LOF and GOF variants: (**A**) Resting membrane potential measured from control (n = 35), WT (n = 19), R297Q (n = 9) and P405L (n = 19). A statistically significant hyperpolarized R_m was observed for WT and R297Q overexpressing neurons as compared to neurons overexpressing the P405L variant (WT : P405L, $P < 0.01$, R297Q : P405L, $P < 0.05$; ANOVA on ranks with Dunn's post hoc test). (**B**) The measured variation in input resistance among control, WT, R297Q and P405L. The R297Q showed a significant reduction in R_{in} as compared to the P405L ($P < 0.05$; one-way ANOVA with Bonferroni's post hoc test). (**C**) Schematic representation of the method used for the membrane time constant calculation. A thick black line shows the single exponential fit to the first 100 ms of the voltage response (V) of injecting -50 pA (purple) hyperpolarizing current from R_m. (**D**) Differences in the membrane time constant in four groups are as follows: control, WT, R297Q and P405L. The group-wise comparison using ANOVA on ranks with Dunn's post hoc test showed a significant variation among the four groups (control : WT, $P < 0.01$; control : R297Q, $P < 0.01$; P405L : WT, $P < 0.001$; and P405L : R297Q, $P < 0.001$). All data are shown as mean ± SEM and plotted as bar graph. The colored dots represent each data point.

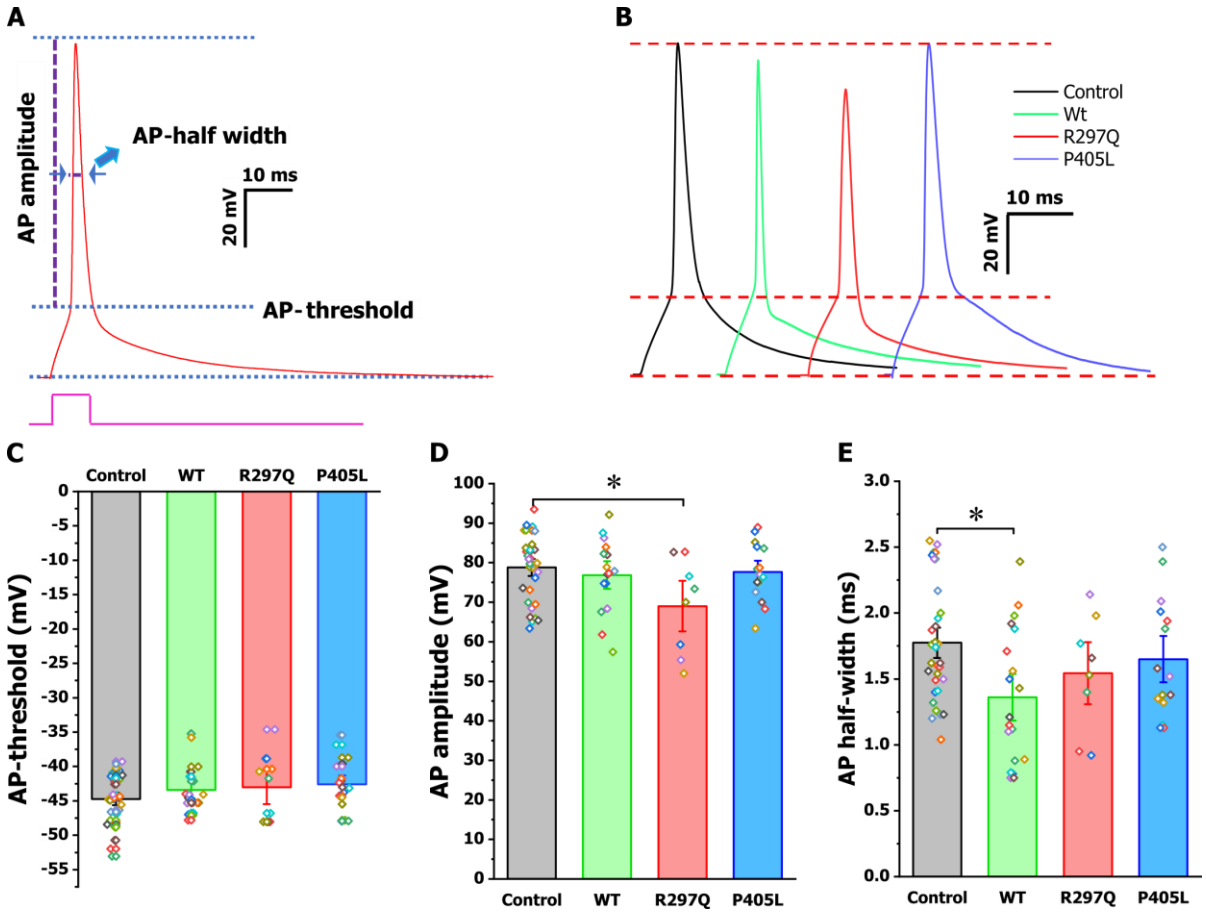

Figure 15. Changes in single AP properties due to the overexpression of K_V1.2 WT, R297Q and P405L: (**A**) Schematic representation of AP parameters. The AP threshold was determined as the membrane potential at which the dV/dt exceeded 20 V/S. The difference in the potential from the threshold to AP peak was defined as the AP amplitude. The AP width at the membrane voltage halfway between the AP threshold and AP peak was considered as the AP half-width. (**B**) Representative voltage traces of single APs from all four groups: control (black), WT (green), R297Q (red) and P405L (blue). (**C**) Bar graphs showing the AP threshold determined for control (n = 35), WT (n = 19), R297Q (n = 9) and P405L (n = 19). No statistically significant difference was observed among the different groups (one-way ANOVA with Bonferroni's post hoc test). (**D**) Graphical representation of the AP amplitude determined for control, WT, R297Q and P405L. A statistically significant reduction in the AP amplitude of neurons overexpressing the mutant R297Q K_V1.2 subunit was observed ($P < 0.05$; one-way ANOVA with Bonferroni's post hoc test). (**E**) Bar graphs show the AP half-width calculated from control and K_V1.2 subunits overexpressing cells. The AP half-width was significantly reduced in cells overexpressing K_V1.2 WT channels compared to controls ($P < 0.05$; ANOVA on ranks with Dunn's post hoc test). All data are shown as mean ± SEM.

close proximity to the electroporated area) showed a regular firing pattern of pyramidal neurons. However, the neurons transfected with $K_V1.2$ WT subunits fired only 3-4 APs and the cells overexpressing mutant $K_V1.2$ R297Q subunits exhibited only 1-2 APs. The voltage at which the firing block was observed in cells overexpressing the WT (30.20 ± 1.39, n = 15) and mutant R297Q subunits (19.71 ± 2.48, n = 6) varied significantly ($P < 0.001$, student's t-test, Figure 17). Also, the reduction in the input resistance, described in the previous section (3.1.3) supports the hypothesis of reduced excitability of neurons overexpressing the R297Q variant.

The P405L overexpressing neurons also showed a considerably reduced number of APs in comparison to controls (Figure 16C, AP firing pattern from 500 ms duration current injection). The number of APs fired during a 100 pA current injection were: control cells, 6.53 ± 0.80, n = 35; WT cells, 3.77 ± 1.08, n = 18; R297Q, 1.16 ± 0.61, n = 6; and P405L cells, 5.73 ± 1.22, n = 19; $P < 0.05$, ANOVA on ranks with Dunn's post hoc test. For 200 pA current injection: control cells, 14.05 ± 0.85, n = 35; WT cells, 4.66 ± 1.14, n = 18; R297Q, 3.66 ± 0.72, n = 6; P405L cells, 13.42 ± 1.45, n = 19; $P < 0.001$, ANOVA on ranks with Dunn's post hoc test. Overall, the statistical comparison among all four groups, which was performed by calculating the area under the curve of the AP number as a response to different current injections (from -50 pA- 300 pA, 500 ms) showed significant differences (control : WT, $P < 0.001$; control : R297Q, $P < 0.001$; P405L : WT, $P < 0.01$; P405L : R297Q, $P < 0.01$; ANOVA on ranks with Dunn's post hoc test). Together, these findings suggest that $K_V1.2$ plays an important role in repetitive neuronal firing activity in SSC L2/3 pyramidal neurons and can induce changes in AHP.

3.1.6 Overexpression of the mutant P405L subunit prolongs the repolarization phase of an AP

After the investigation of the repetitive firing properties of neurons overexpressing $K_V1.2$ WT, R297Q and P405L subunits, it was found that neurons overexpressing $K_V1.2$ WT and R297Q subunits fired a reduced number of APs. This reduction is due to the enhanced K^+ out-flow mediating the inability of cells to reach again the firing threshold (WT) because of which, neurons were unable to recover from the enhanced repolarization phase after 2-3 APs (R297Q). The decreased AP number in neurons overexpressing the P405L has a different explanation. Here the prolonged AP leads to a slower repolarization, thereby prolonging the time until the next AP can be elicited.

To understand the eventual influence of calcium-activated potassium channels in the elongated repolarization of neurons overexpressing the P405L variant, I have compared the

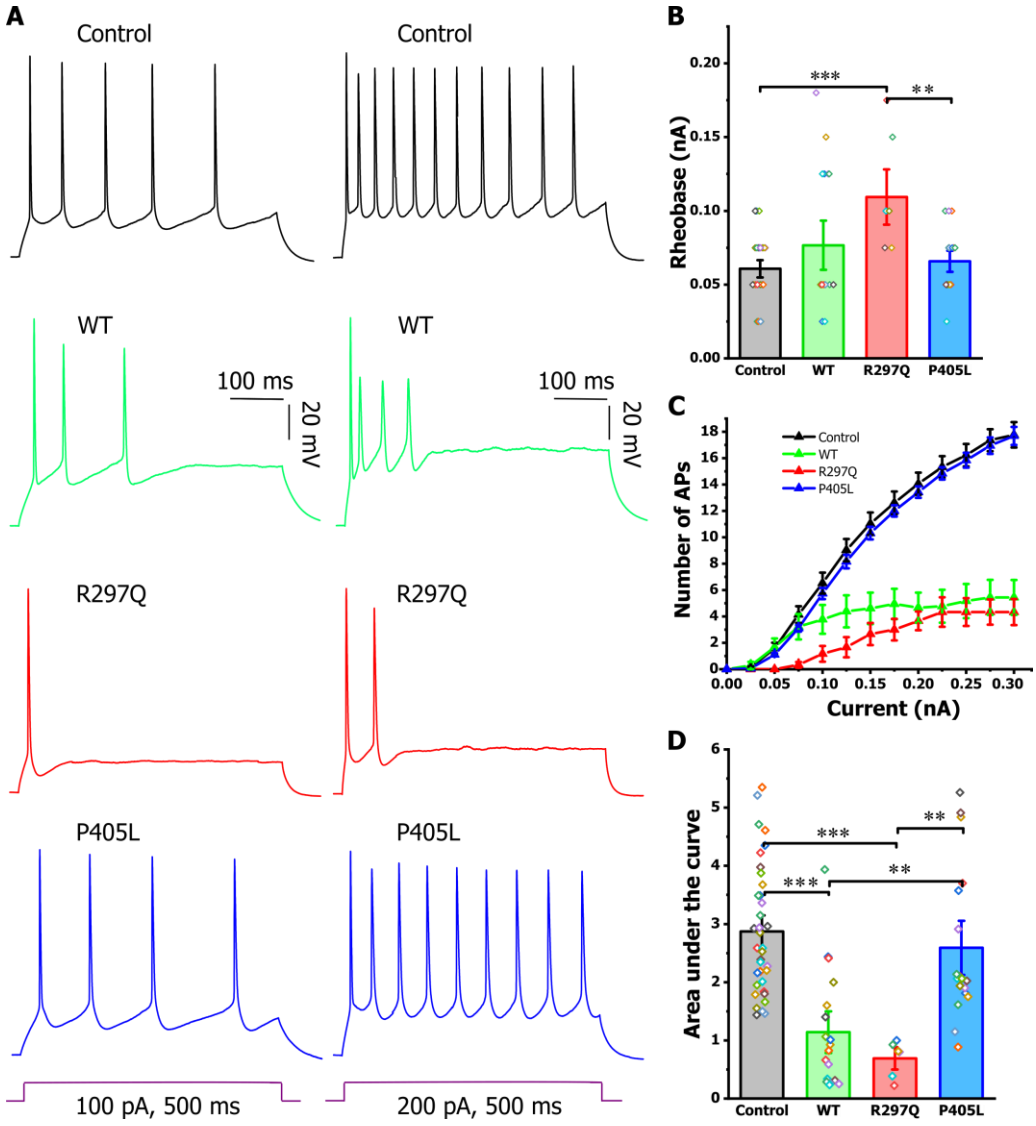

Figure 16. Changes in AP repetitive firing properties due to the overexpression of $K_V1.2$ WT, R297Q and P405L: (**A**) Representative voltage responses to two current injection steps (500 ms, 100 pA and 200 pA) in SSC L2/3 pyramidal neurons from control (black), WT (green), R297Q (red) and P405L (blue) overexpressing neurons. Membrane potential was held at -70 mV by injecting a small direct current (DC) through the recording pipette. (**B**) The rheobase measured from a current injection of the duration of 500 ms. Groupwise comparison among control, WT, R297Q and P405L with ANOVA on ranks with Dunn's post hoc test showed that R297Q cells only fired at significantly higher current injection steps compared to controls and P405L (control : R297Q, $P < 0.001$ and P405L : R297Q, $P < 0.01$). (**C**) Summary graphs show the effect of $K_V1.2$ WT, R297Q and P405L subunits overexpression on AP number as a response towards different current injection from -50 pA- 300 pA, 500 ms. Control, n = 35; WT, n = 18; R297Q, n = 6; P405L, n = 19. (**D**) The area under the curve derived from graphs shown in **C**: Statistically significant differences are as follows: control : WT, $P < 0.001$; control : R297Q, $P < 0.001$; P405L : WT, $P < 0.01$; P405L : R297Q, $P < 0.01$; one-way ANOVA on ranks with Dunn's post hoc test. All data are shown as mean ± SEM and the colored dots represent each data point.

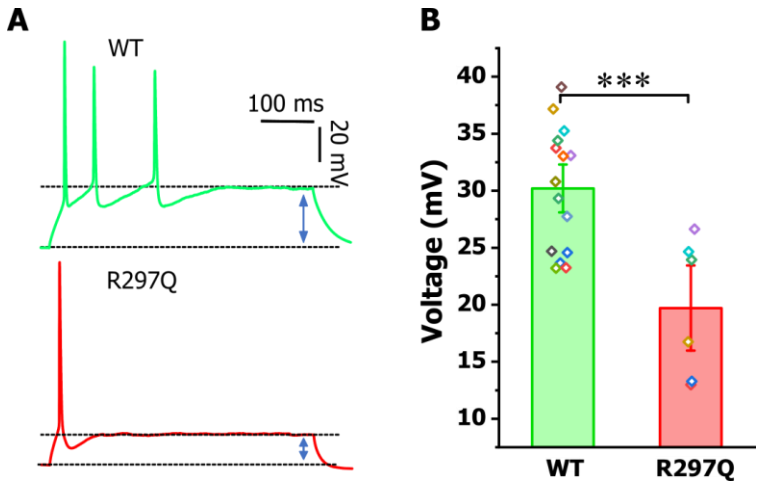

Figure 17. Voltage at which a firing block was observed in K_V1.2 WT and R297Q overexpressing neurons: (**A**) Schematic shows the measurement of the voltage at which the firing block was observed. Voltage was measured as difference from the holding potential of -70mV to the firing block (indicated with black line) (WT, green; R297Q, red) (**B**) The bar graph shows the difference in voltage at which firing block was observed from WT (n = 15) and R297Q (n = 6), ($P < 0.001$; student's t-test). All data are shown as mean ± SEM.

AHP amplitude and the duration of the repolarization phase (Figure 18) among the four neuronal groups (control, WT, R297Q and P405L). The first three APs from the repetitive AP firing as a response to 125 pA current injection, with a duration of 800 ms was used to perform the analysis. The AHP amplitude was calculated as the difference in voltage between the AP threshold and the end of hyperpolarization (Figure 18A). The duration of the repolarization phase of an AP was measured as a difference in time from the AP peak (start point) to the end of hyperpolarizing potential in which the first derivative of the AP was coming back to zero (endpoint) (Figure 18C). The statistical comparison among the four groups showed a significantly increased AHP in P405L overexpressing neurons as compared to controls : 1st AP ($P < 0.05$; ANOVA on ranks with Dunn's post hoc test), 2nd AP ($P < 0.05$; ANOVA on ranks with Dunn's post hoc test) and 3rd AP ($P < 0.01$; ANOVA on ranks with Dunn's post hoc test) (Table 10). The duration analysis also showed an elongated repolarization phase in neurons overexpressing the P405L variant in comparison to controls (1st AP, $P < 0.001$; ANOVA on ranks with Dunn's post hoc test. 2nd AP, $P < 0.05$; ANOVA on ranks with Dunn's post hoc test and 3rd AP, $P < 0.05$; ANOVA on ranks with Dunn's post hoc test). All details are shown in Table 10. In addition, the cells overexpressing WT subunits showed a significantly reduced repolarization phase of all 3 APs in comparison to controls ($P < 0.001$; ANOVA on ranks with Dunn's post hoc test) (Figure 18). These data suggest that overexpression of the P405L variant elongates the AHP and the entire repolarization phase of APs.

Table 10: Summary of AHP and duration of repolarization from 1st, 2nd and 3rd AP.

Cell types	After-hyperpolarization amplitude (mV)			Duration of repolarization (ms)			Cell (n)
	1st AP	2nd AP	3rd AP	1st AP	2nd AP	3rd AP	
Control	6.9 ± 0.8	12.9 ± 0.4	12.3 ± 0.5	13.3 ± 0.8	16.8 ± 1	17.2 ±0.8	30
WT	7.9 ± 1.4	13.5 ± 0.7	14.5 ± 0.8	5.3 ± 0.4***	9.2 ±1***	9.2±2***	11
R297Q	8.7 ± 1.3	14.2 ± 0.7	16.1 ± 1.2	13.2 ± 2.2	18.3 ± 1	17.9 ±1.4	5
P405L	12.9 ± 1.6*	16.5 ± 1.6*	16.5 ±1.6**	22.8±2.7***	21.6 ± 2*	22 ±1.9*	15

Data are presented as mean ± SEM. * marked values are significantly different from the control values, *p<0.05, **p<0.01 and ***p<0.001. n: Number of recorded neurons.

To further validate the hypothesis of the P405L overexpression effect on the elongated repolarization of neurons, the K_V1 channel family were blocked in control cells by the application of 4-AP, which caused a higher AP firing frequency in SSC L2/3 pyramidal neurons. The duration was calculated as mentioned in the previous section (Figure 18C). Statistical comparison of the repolarization duration in the first three APs of a current trace (125 pA, 800 ms) among control (n = 30), P405L (n = 15) and control + 4-AP (n = 5), showed a significant increase in neurons overexpressing the P405L variant (as explained earlier) and not in 4-AP applied control cells (Figure 19A). Differences between the control and the P405L were calculated: 1st AP; $P < 0.001$; ANOVA on ranks with Dunn's post hoc test, 2nd AP; $P < 0.05$; ANOVA on ranks with Dunn's post hoc test and 3rd AP; $P < 0.05$; ANOVA on ranks with Dunn's post hoc test (Figure 19A). The application of 4-AP slightly increased the duration of the repolarization in control neurons but not that significant as in P405L overexpressing neurons (Duration of the repolarization in control cells after the application of 4-AP: 1st AP = 19.95 ± 1.95 ms, 2nd AP = 19.46 ± 2.39 ms and 3rd AP = 19.57 ± 2.46 ms). These results suggest a specific role of mutant $K_V1.2$ LOF (P405L) subunits in prolonging the repolarization phase of an AP and regulating neuronal firing.

The next question raised after observing the P405L overexpression effect on the repolarization phase was how P405L overexpression can affect the neuronal spike adaptation? Previous result showed that cells exhibit a strong adaptation with enhanced AHP, and this increased AHP amplitude has been observed in neurons overexpressing the P405L variant. It has been shown before that a blockade of the delayed rectifier potassium current (I_K) with 4-AP (50 µM) reduces spike adaptation in callosal-projecting neurons of the visual cortex (Locke and Nerbonne, 1997). The spike adaptation in control, P405L and control with 4-AP cells was calculated from the AP train as a response of 175 pA current injection with 800 ms duration.

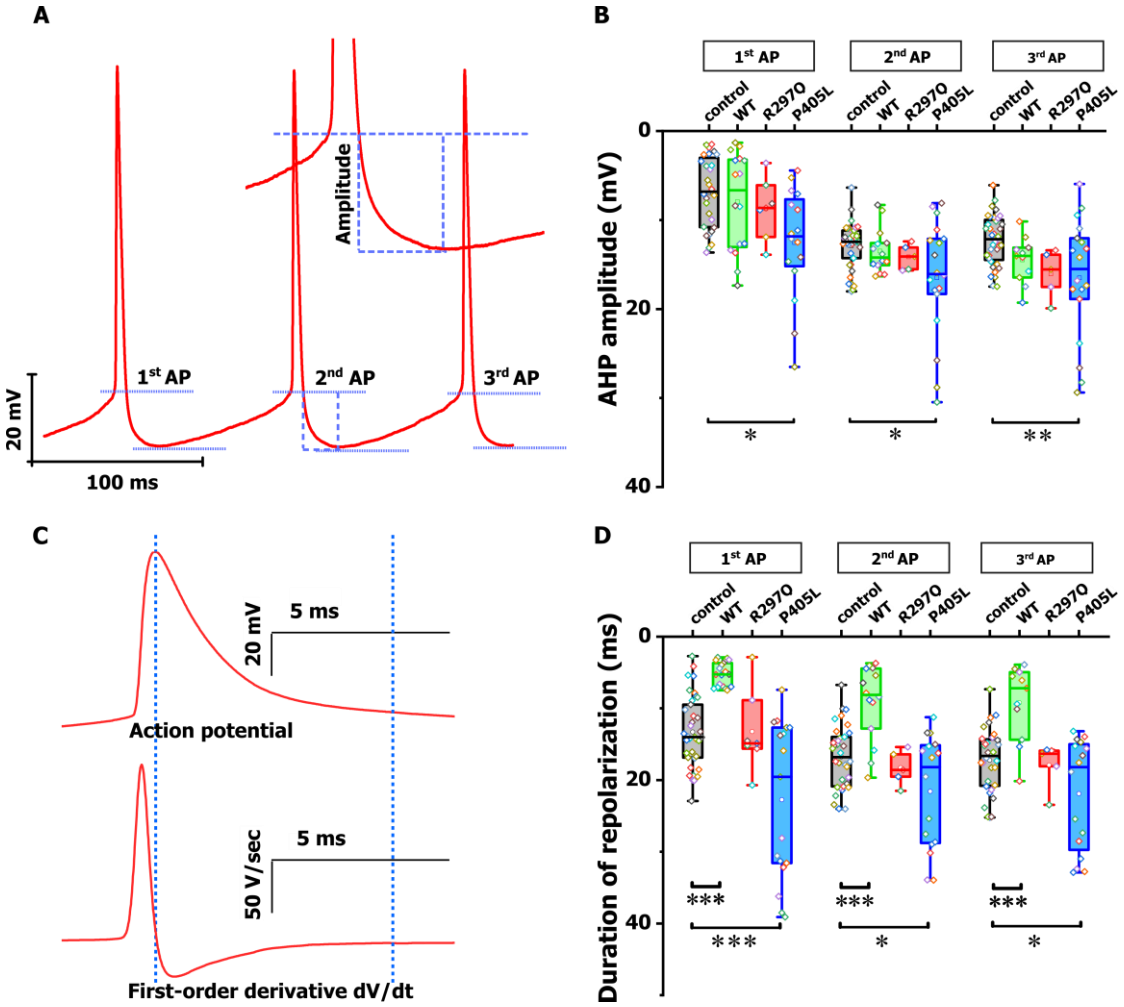

Figure 18. Changes in the AHP and the repolarization phase of APs due to the overexpression of K_V1.2 WT, R297Q and P405L: (**A**) Schematic shows the method used for the determination of AHP in 1ST, 2nd and 3rd APs from AP firing response of current injection (125 pA, 800 ms). The AHP amplitude was shown between the two blue dotted lines as a difference in voltage between the AP threshold and the end of hyperpolarization. (**B**) Box plot shows the AHP amplitude comparison among control (n = 30), WT (n = 11), R297Q (n=5) and P405L (n = 15). The statistical results (1st AP, $P < 0.05$; ANOVA on ranks with Dunn's post hoc test, 2nd AP, $P < 0.05$; ANOVA on ranks with Dunn's post hoc test and 3rd AP, $P < 0.01$; ANOVA on ranks with Dunn's post hoc test) showed an increase AHP in the P405L overexpressing neurons. (**C**) Schematic shows the method used for the calculation of the duration of the repolarization as a difference in time between the AP peak (start point) and the end of hyperpolarizing potential in which the first derivative was coming back to zero (as an endpoint). (**D**) The duration of the repolarization phase calculated for control, WT, R297Q and P405L. Significantly prolonged repolarization was observed in P405L as compared to controls (1st AP, $P < 0.001$; ANOVA on ranks with Dunn's post hoc test, 2nd AP, $P < 0.05$; one-way ANOVA on ranks with Dunn's post hoc test and 3rd AP, $P < 0.05$; ANOVA on ranks with Dunn's post hoc test). Concurrently, neurons overexpressing the K_V1.2 WT showed a significantly reduced repolarization phase as compared to controls in all 3 APs ($P < 0.001$; ANOVA on ranks with Dunn's post hoc test).

The values of the spike adaptations for three groups were as follows control : 0.31 ± 0.02, n = 30, P405L : 0.22 ± 0.02, n = 15 and control + 4-AP : 0.26 ± 0.04, n = 5. AP trains showed significantly reduced spike adaption in neurons overexpressing the P405L variant as compared to the control cells (P < 0.05; one-way ANOVA with Bonferroni's post hoc test) (Figure 19B). These results indicate that the overexpression of mutant P405L $K_V1.2$ subunits enhances the duration of the repolarization phase together with an elongated AHP. In addition, P405L overexpression reduces spike adaptation. Similarly, also in control neurons, a considerably reduced spike adaptation was observed after the blockade of I_K with 4-AP. However, equivalent examination in a P405L gene-targeted mouse model, pharmacological experiments with specific $K_V1.2$ antagonists and the usage of calcium-activated potassium channel blocker are required to validate this notion.

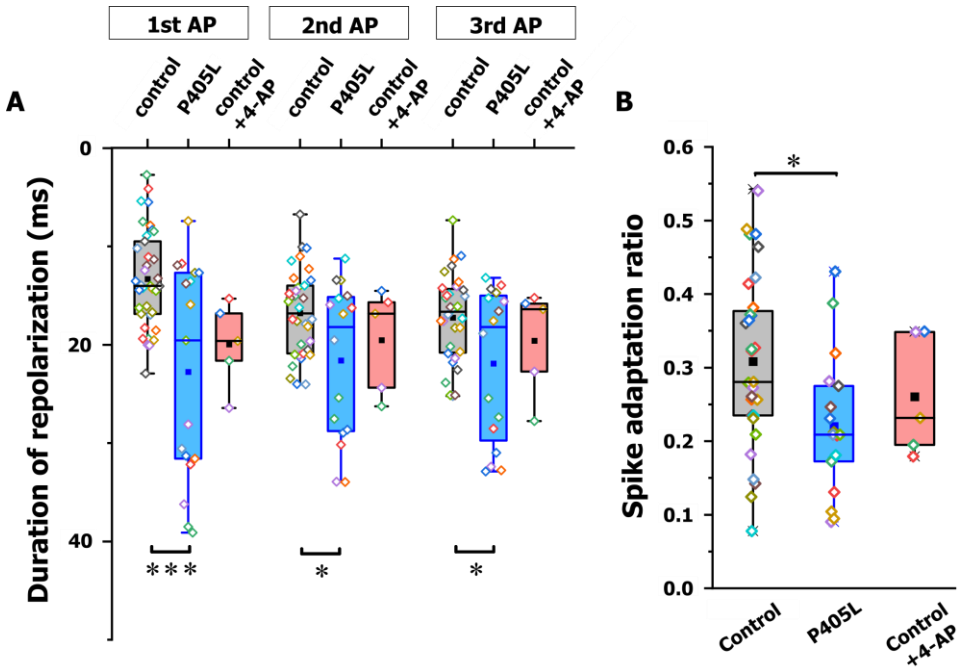

Figure 19. Changes in the repolarization phase of APs in the presence of 4-AP: (**A**) Box plot comparing the duration of the repolarization phase of 3 APs calculated from control (n = 30), P405L (n = 15) and control + 4-AP (n =5). AP firing response of current injection (125 pA, 800 ms) was used for the analysis. A significantly enhanced repolarization was observed in neurons overexpressing the P405L variant as compared to controls (1st AP, P < 0.001; ANOVA on ranks with Dunn's post hoc test. 2nd AP, P < 0.05; ANOVA on ranks with Dunn's post hoc test and 3rd AP, P < 0.05; ANOVA on ranks with Dunn's post hoc test), not in control + 4-AP. (**B**) Box plot represents the spike adaptation calculated from control, P405L (n = 18) and control + 4-AP (n =5). The current injection of 175 pA with 800 ms was used for analysis. A significant reduction in spike adaption was observed in P405L overexpressing neurons as compared to controls (P < 0.05; one-way ANOVA with Bonferroni's post hoc test).

3.1.7 Potassium currents recorded from cells overexpressing WT, and mutant (R297Q and P405L) $K_V1.2$ subunits

In addition to all electrophysiological parameters mentioned above, I have also recorded the potassium current from neurons overexpressing WT, and mutants (R297Q and P405L) $K_V1.2$ subunits (Figure 20). The voltage-clamp recording was obtained from each cell on which current-clamp experiments were performed by using the same intra- and extracellular solutions. No antagonists which block the A-current or M-current were used in this experimental procedure. Peak out-ward currents were evoked, from a holding potential of -70 mV, by 5-sec voltage steps from -60 mV to 20 mV. A minor increase in the recorded K^+ currents was observed in WT and R297Q overexpressing neurons in comparison to controls as well as a slight reduction in K^+ current from P405L cells. However, the comparison of the current amplitudes did not show any significant differences among the four groups (control, n = 20, WT, n = 4, R297Q, n = 4, and P405L, n = 17). The values of current amplitudes recorded at 20 mV for the four groups were as follows: control : 2.8 ± 0.3 nA, WT : 3.1 ± 0.2 nA, R297Q : 3.7 ± 0.3 nA, and P405L : 2.3 ± 0.2; one-way ANOVA with Bonferroni's post hoc test.

3.1.8 4-AP as an effective precision therapeutic option in *KCNA2* mediated epilepsies

4-aminopyridine (4-AP) is a licensed drug for symptomatic treatment of multiple sclerosis (Bostock *et al.*, 1981; Jensen *et al.*, 2014), which selectively blocks the K_V1 (Shaker, *KCNA*) and the K_V4 (Shal, *KCND*) channel families of voltage-activated K^+ channels. 4-AP has been investigated as a new precise therapeutic option for a highly pharmaco-resistant group of patients carrying *KCNA2*-related developmental and epileptic encephalopathy (Hedrich, Lauxmann et al., Sci Trans Med, under review). As a part of this study, I have examined the effect of 4-AP on $K_V1.2$ WT and R297Q overexpressing CHO cells to understand its single-channel specificity towards $K_V1.2$ channels in mammalian cells. CHO cells transfected with $K_V1.2$ WT and mutant R297Q subunits have been used in this experiment (Figure 21). K^+ current recorded in CHO cells were evoked by voltage steps from -110 mV to 60 mV with 10 mV increments and cells were held at -90 mV. Application of 1 mM 4-AP led to a significant reduction (paired t-tests) of current amplitude (at 60 mV) in both WT (before 4-AP : 14.5 ± 0.4 nA and after 1mM 4AP : 8.7 ± 0.9 nA, n=7, $P < 0.001$) and R297Q (before 4-AP : 17.4 ± 0.3 nA and after 1mM 4AP : 10.7 ± 0.7 nA, n = 9, $P < 0.001$). The voltage dependence of the activation curve showed a significant shift to more depolarized potentials in both WT ($P < 0.001$; two-way ANOVA with Tukey post hoc test) and R297Q ($P < 0.001$)

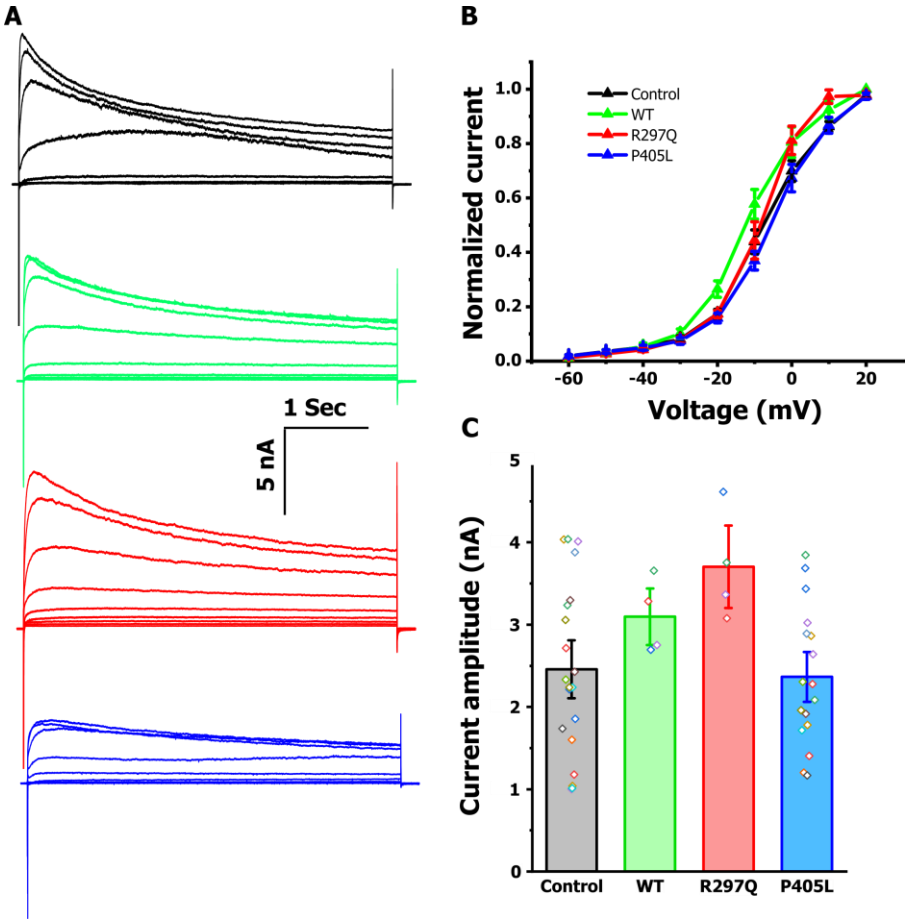

Figure 20. Voltage dependence of K_V activation in neurons overexpressing K_V1.2 WT, R297Q and P405L subunits: (**A**) Representative current traces recorded from control (black) neurons, neurons overexpressing K_V1.2 WT (green), R297Q (red) and P405L (blue) mutant subunits. (**B**) The graphical representation of normalized current-voltage relationship as a response of voltage step (hold at -70 mV) from -60 mV to 20 mV with a duration of 5 sec, among control (n= 20), WT (n = 4), R297Q (n = 4) and P405L (n = 17). No significant difference was observed among the groups. (**C**) Bar graph comparing the current amplitude from control, WT, R297Q and P405L; one-way ANOVA with Bonferroni's post hoc test). All data are shown as mean ± SEM.

after the application of 1 mM 4-AP. The $V_{1/2}$ were also significantly changed (paired t-tests) in both WT (before 4-AP : -9.4 ± 2.1 mV and after 1mM 4AP : -3.9 ± 3.4 mV, n=7, $P < 0.01$) and R297Q (before 4-AP : -50.1 ± 3.3 and after 1mM 4AP : -32.9 ± 2.4, n = 9, $P < 0.001$). The resting membrane potential (R_m) of CHO cells was significantly hyperpolarized in R297Q channels expressed cells ($P < 0.001$) as compared to the WT overexpressed cells. In addition, application of 1 mM 4-AP led to a significant reduction of resting membrane potentials for both WT (n =7, $P < 0.01$) and R297Q (n =9, $P < 0.01$; two-way ANOVA) overexpressing cells. These observations show the specificity of 4-AP on K_V1.2 channels.

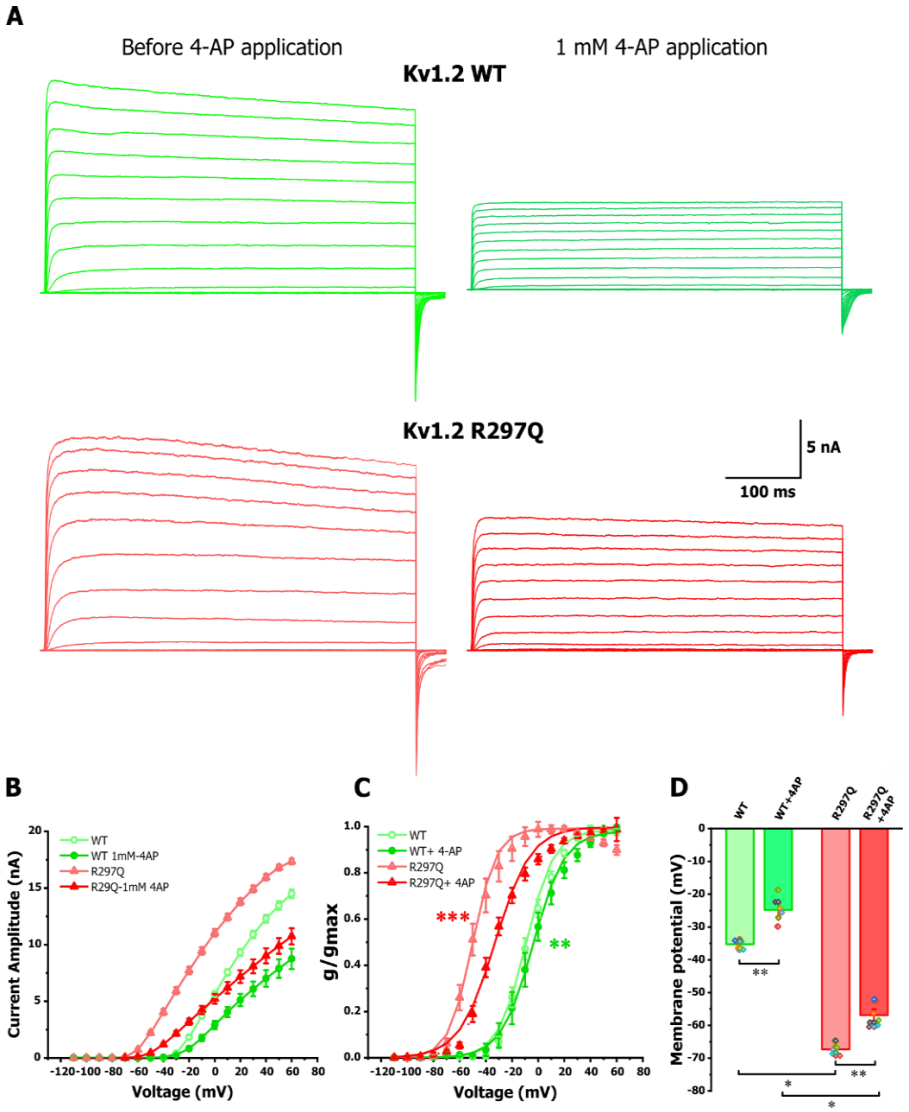

Figure 21. Effects of 4-AP on WT and R297Q Kv1.2 channels expressed in CHO cells: (**A**) Representative current traces of WT (green, top) and R297Q (red, bottom) channels recorded in CHO cells evoked by voltage steps from -110 mV to 60 mV, held at -90 and 10 mV increments. (**B**) Graphical representation of the current-voltage relationship of WT (n = 7) and R297Q (n =9) before and after application of 1 mM 4-AP. (**C**) The graph shows the mean voltage dependence of $K_V1.2$ channel activation for WT and R297Q before and after application of 1mM 4-AP. Data are shown as means ± SEM. Lines represent a Boltzmann fit to data points. The voltage dependence of the activation curve was significantly shifted to depolarized potentials in both WT ($P < 0.001$) and R297Q ($P < 0.001$) overexpressing cells (two-way ANOVA with Tukey post hoc test) after the application of 1 mM 4-AP. Green and red stars represent the statistical significance of $V_{1/2}$ observed in WT ($P < 0.01$, n =7) and R297Q ($P < 0.001$, n = 9), respectively, after the application of 4-AP (paired t-tests). (**D**) Changes in resting membrane potentials in WT and R297Q before and after the application of 4-AP. R_m of CHO cells overexpressing R297Q channels was significantly hyperpolarized ($P < 0.001$) as compared to those expressing WT channels. In both cells expressing WT (n =7, $P < 0.01$) and R297Q (n =9, $P < 0.01$), Rm was significantly shifted to more depolarized potentials after the application of 1mM 4-AP (two-way ANOVA).

3.1.9 Application of 4-AP recovers the regular firing pattern in K_V1.2 WT overexpressing neurons

Regarding the further validation of 4-AP as a therapeutic option, I have applied 4-AP on K_V1.2 WT electroporated neurons. Preliminary results of these experiments showed that the neurons with WT overexpression significantly recovered from its hypo excitability after the application of 100 µM 4-AP (Figure 22). Application of 4-AP also induced some effect in control cells, such as increased AP number, AP duration and elongation of the repolarization phase. Since the number of cells was low (WT : n =3), no statistical analysis was performed in these experiments. However, the application of 4-AP restored the regular firing pattern in all three cells. These data suggest the effective precision therapeutic use of 4-AP in *KCNA2*-mediated epilepsies.

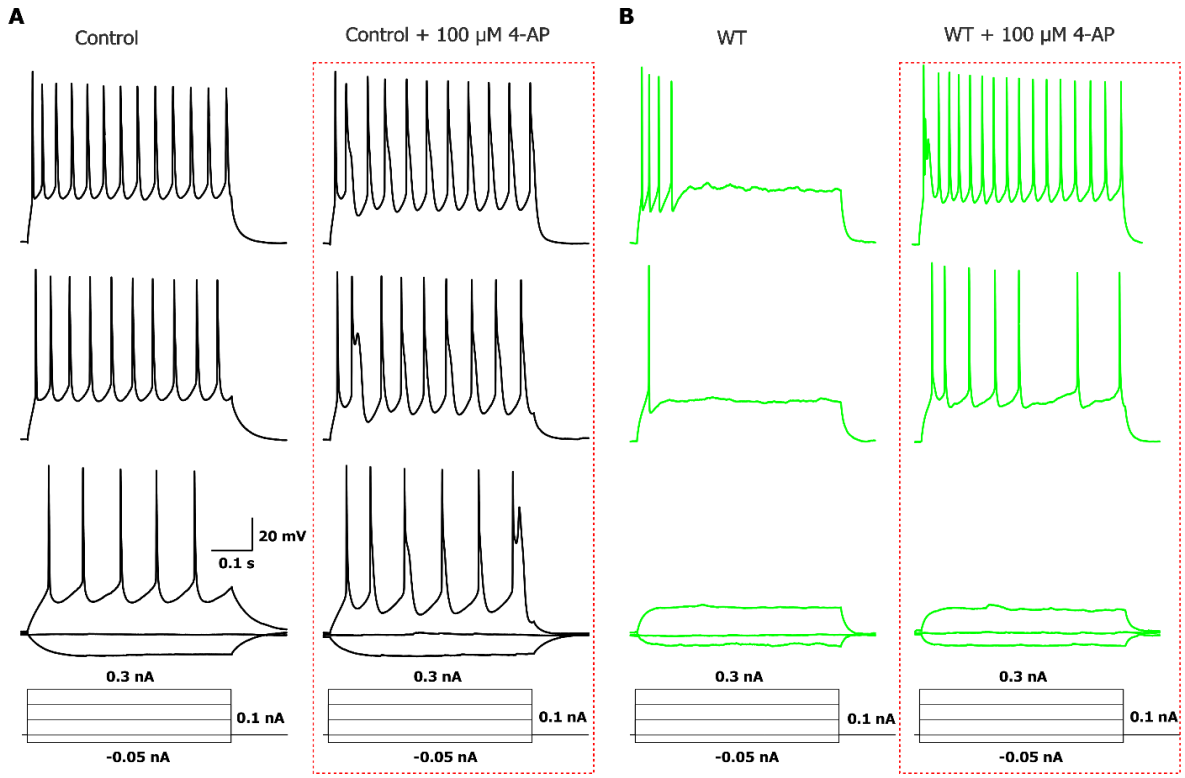

Figure 22. Effect of 4-AP on control neurons and neurons overexpressing K_V1.2 WT channels: (**A**) Representative AP traces recorded from control and control + 100 µM 4-AP as a response of current injection (-0.05 nA-0.3 nA, 500 ms duration). (**B**) Representative AP response recorded from neurons overexpressing K_V1.2 WT and WT + 100 µM 4-AP. Current protocols used in this experiment are shown as schematic at the bottom.

3.2 Effect of $Na_V1.1$ variants on thalamocortical up-states

Loss-of-function variants in the *SCN1A* gene can lead to generalized epilepsy with febrile seizures plus (GEFS+) (Escayg et al., 2000) as the mildest syndrome caused by missense mutations and severe myoclonic epilepsy of infancy (SMEI) as the most severe form caused by missense/nonsense mutations (Claes *et al.,* 2001; Ogiwara *et al.,* 2007; Yu *et al.,* 2006). Gain-of-function mutation in the $Na_V1.1$ channel can also cause a severe type of a migraine with aura (familial hemiplegic migraine type 3, FHM3) (Dichgans *et al.,* 2005; Fan *et al.,* 2015). In addition to seizures and FHM3, individuals carrying *SCN1A* mutations often experience disturbance in physiological functions such as sleep, suggesting its essential role in the neuronal pathways involved in the regulation of normal physiology. The consequences of *SCN1A* variants on the neuronal network are still unclear. Therefore, this part of the thesis aims to gain insight into the effect of *SCN1A* expressing neurons and the influence of both loss and gain-of-function mutations on neuronal network properties.

For the regulation of both sleep and epilepsy, the thalamocortical network and its participating inhibitory neurons play a crucial role (Steriade, 2005). Previous experimental studies showed that $Na_V1.1$ (encoded by *SCN1A* gene) is the primary Na^+ channel in GABAergic interneurons and its alteration leads to a ubiquitous disinhibition in the hippocampus and the thalamocortical (TC) loop (Yu *et al.*, 2006; Kalume *et al.*, 2007; Hedrich *et al.*, 2014). Hence, studying the alterations of TC network activities in *SCN1A* mouse models may reveal a link between epilepsy and sleep. The frequency of up-states recorded in thalamocortical slices (*in vitro*) can be used as a correlate for the frequency of those occurring *in vivo* during slow-wave sleep or anesthesia (Diekelmann and Born, 2010; Sanchez-Vives and McCormick, 2000; Wilson, 2008). These studies have facilitated the preliminary understanding at the slice level about the effect of *SCN1A* mutations on slow-wave sleep patterns. Therefore, in this part of the thesis, I have studied the LOF (R1648H, causing GEFS+) and GOF (L1649Q, causing FHM3) effect of $Na_V1.1$ on TC network activities by recording the up- and down-states (*in-vitro*) in TC brain slices prepared from the corresponding mouse models.

3.2.1 Effect of $Na_V1.1$ LOF and GOF mutations on thalamocortical (TC) up-states recorded in acute slices

To get a first insight about how $Na_V1.1$ LOF and GOF mutations may alter slow-wave sleep (SWS) in the intact brain due to altered inhibitory neuronal firing, I have recorded the up- and down-states from TC brain slices. Such experiments can provide information about an impairment of slow-wave oscillations (< 1 Hz) during NREM sleep (Sanchez-Vives and McCormick, 2000). Acute TC brain slices from animals carrying LOF (R1648H) or GOF (L1649Q) mutations and their WT littermates (P13-P20) were prepared (Agmon and Connors,

1991), by preserving the whole TC network. TC up-states were recorded using an extracellular electrode from SSC L5 neurons and NRT of the thalamus. The recordings from NRT were always followed by a long-lasting silent state, which were excluded from the analysis. In acute brain slices, the persistent TC network activities were limited to 50% of slices. Plateau depolarizing potentials lasting more than 300 ms were considered as an up-state, and the silent phase after each up-state as a down-state (Figure 23A). Comparing slices of R1648H LOF heterozygous (+/-), L1649Q GOF heterozygous (+/-) and WT (+/+) animals showed a significant reduction in the up-state frequency in both slices of R1648H ($P < 0.01$) and L1649Q ($P < 0.001$) animals (WT: 0.07 ± 0.01 Hz, number of slices (n) = 25; R1648H: 0.03 ± 0.00 Hz, n= 6; and L1649Q: 0.04 ± 0.00 Hz, n = 12, ANOVA on ranks with Dunn's post hoc test, ($P < 0.01$). The comparison of the up-state duration recorded from slices of WT (3.9 ± 0.2 S, n = 25), R1648H (2.6 ± 0.4 S, n = 6) and L1649Q (3.5 ± 0.5 S, n = 12) animals did not show a significant difference among three groups (one-way ANOVA with Bonferroni's post hoc test; $P > 0.05$). These results show a clear effect of *SCN1A* variants and altered inhibitory neuronal firing on TC up-states (Cestèle *et al.*, 2013; Hedrich *et al.*, 2014).

3.2.2 Effect of $Na_V1.1$ LOF and GOF mutations on TC up-state in organotypic brain slice culture

As a validation of the findings in acute brain slices, the same experiments were performed in organotypic TC brain slice cultures. In acute brain slices, the persistent TC network activities were limited to 50% of slices. This issue with acute slices demands many animals to perform experiments. The organotypic brain slice culture of TC slices can be used as an alternative to the acute experiments by providing prominent TC network activity in 90% of slices. Also, the technique of organotypic slice cultures has been largely adopted and recognized as a good model to perform comparable experiments (Humpel, 2015; Magalhães *et al.*, 2018). Slices were cultured from animals at the age of 5-6 days and up-states were subsequently recorded after 8 ± 1 days *in-vitro* (DIV). The TC up-states recorded in organotypic brain slices were very prominent with a higher frequency and duration than in acute slices. The up-state frequency comparison among WT (0.28 ± 0.03 Hz, n = 19), R1648H (0.06 ± 0.01 Hz, n = 5) and L1649Q (0.13 ± 0.01 Hz, n = 24) using one-way ANOVA with Bonferroni's post hoc test showed a significant reduction in the frequency of the up-states in slices of both R1648H heterozygous ($P < 0.001$) and L1649Q heterozygous ($P < 0.001$) animals as compared to WT. Similar to acute slice experiments, the duration of the recorded up-states was not significantly different among slices of WT (2.17 ± 0.50 S), R1648H (2.04 ± 0.40 S) and L1649Q (1.56 ± 0.22) animals (ANOVA on ranks with Dunn's post hoc test; $P > 0.05$) (Figure 24). These results

from organotypic slice culture experiments confirm a significant effect of *SCN1A* variants on TC up-state properties.

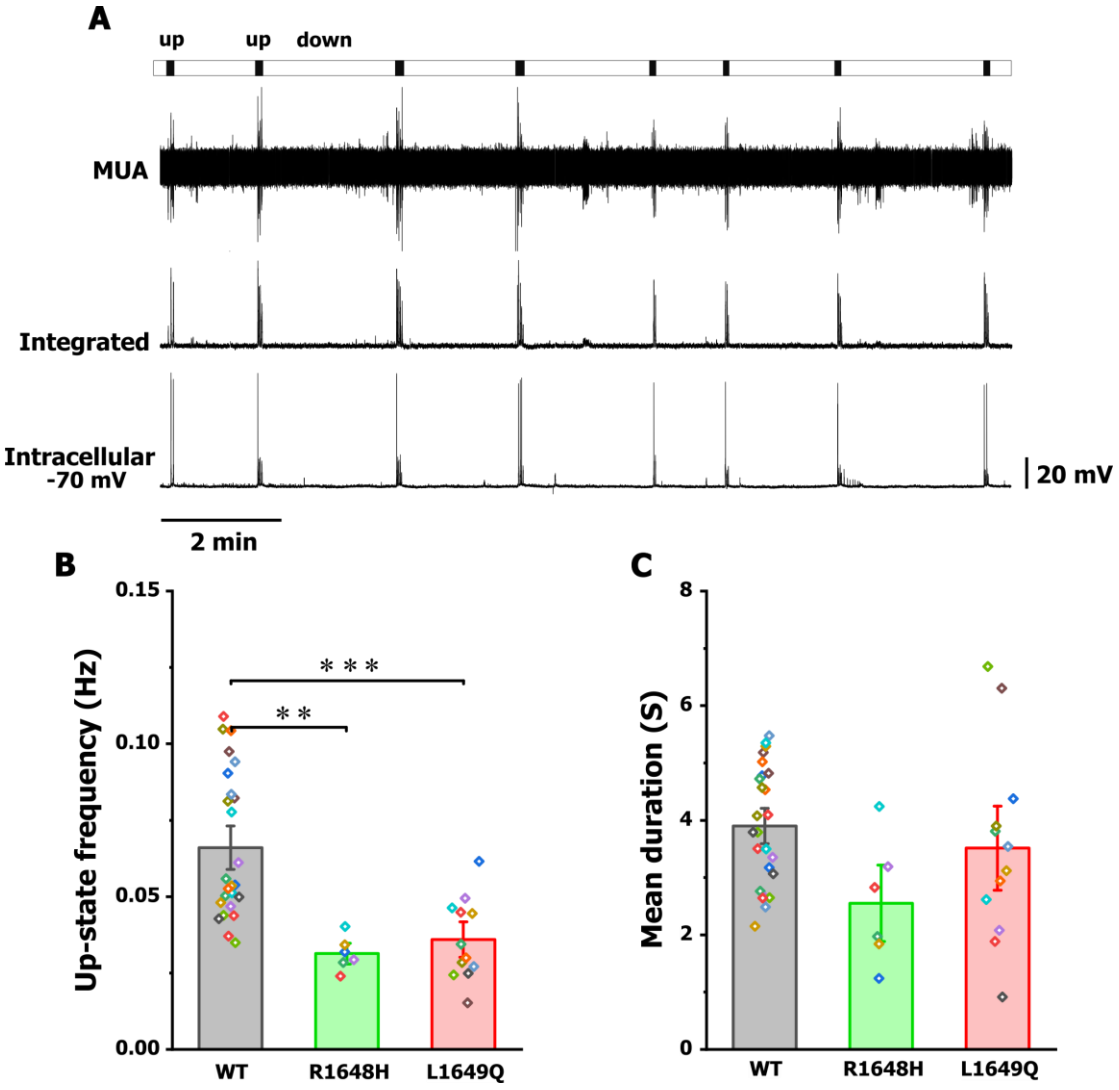

Figure 23. Effect of $Na_V1.1$ LOF and GOF mutations on thalamocortical (TC) up-states: (**A**) Representative traces of multiunit (MU) extracellular recordings of up-states in close vicinity of the intracellular recording. Up- and down-states from MU activity (MUA) and their integrated traces are denoted with the black box (top). Integrated traces are noisy baseline blanked signals from MU extracellular recordings, which are presented in a unidirectional manner. (**B**) Boxplots comparing the up-state frequency recorded in TC slices from R1648H LOF, L1649Q GOF and WT mice. The frequency of up-states was significantly reduced in both R1648H (n = 6) ($P < 0.01$) and L1649Q (n = 12, $P < 0.001$) acute slices compared to the WT (n =25); ANOVA on ranks with Dunn's post hoc test. (**C**) Box plots comparing the up-state duration recorded in TC slices from R1648H LOF (n = 6), L1649Q GOF (n = 12) and WT (n = 25) mice. The up-state duration was not significantly different among three groups ($P > 0.05$; one-way ANOVA with Bonferroni's post hoc test).

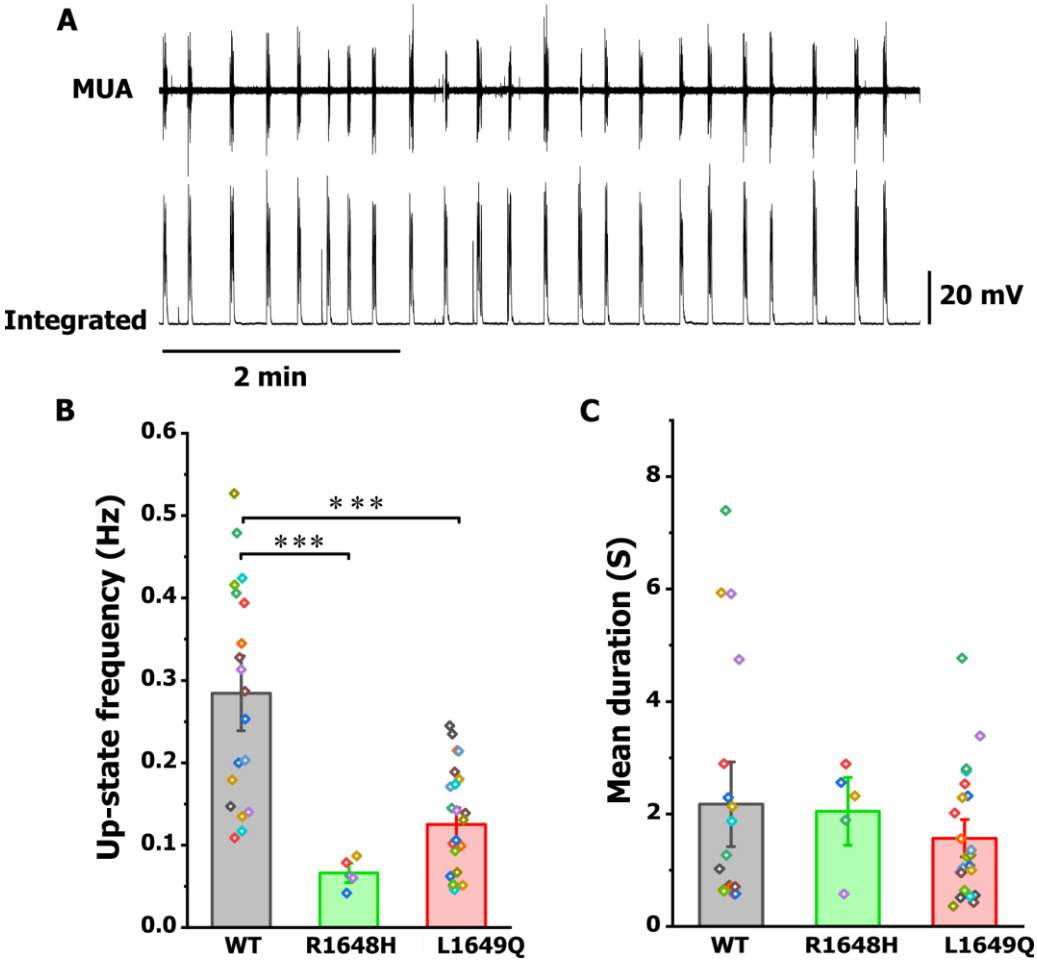

Figure 24. Effect of Nav1.1 LOF and GOF mutations on TC up-states recorded in organotypic brain slice cultures: (**A**) Representative traces of extracellular multiunit activity (MUA) of up-states and their integrated form. Integrated traces are noisy baseline blanked signals from multiunit extracellular recordings, which are presented in a unidirectional manner. (**B**) Bar graphs comparing the up-state frequency recorded in organotypic TC slices from R1648H LOF, L1649Q GOF and WT mice. The up-state frequency was significantly reduced in slices of both R1648H (n = 5) and L1649Q (24) animals as compared to slices of WT (n =19) animals ($P < 0.001$; one-way ANOVA with Bonferroni's post hoc test). (**C**) Bar graphs comparing the up-state duration recorded in organotypic TC slices from R1648H LOF, L1649Q GOF and WT mice. The up-state duration was not significantly different among R1648H LOF (5), L1649Q GOF (n = 24) and WT (n = 19) slices ($P > 0.05$; ANOVA on ranks with Dunn's post hoc test).

3.2.3 Application of picrotoxin (PTX) mimics LOF effect in TC up-states recorded in organotypic slice cultures of WT animals

To confirm the inhibitory modulation of emergent TC up-states, the LOF conditions were mimicked in organotypic slice cultures of WT animals by application of PTX. PTX is a plant toxin that inhibits $GABA_A$ receptors, which selectively block inhibitory synaptic

transmission (Newland and Cull-Candy, 1992; Atherton et al., 2016). The inhibition in slices of WT animals was reduced dose-dependently by the application of different PTX concentrations (from 1 – 5 µM). Dose-dependency was tested in one of recorded TC slices (Figure 25C) and then decided to compare 0 vs 5 µM PTX. Application of 5 µM PTX significantly reduced the up-state frequency ($P < 0.05$; paired t-tests) in slices of WT animals (before PTX : 0.35 ± 0.04 Hz and after PTX : 0.21 ± 0.04 Hz, n = 13) (Figure 25C). The duration of up-states was also significantly reduced in slices of WT animals after the application of 5 µM PTX (before PTX : 2.59 ± 0.55 S and after PTX : 0.83 ± 0.16 S, n = 13, $P < 0.05$; paired t-tests). Overall, these results suggest that a reduction of inhibition in slices of WT animals reduced the up-state frequency and duration, which were similar to the slices of LOF (R1648H) mutated condition.

3.2.4 Application of picrotoxin (PTX) changes the frequency of TC up-states recorded in organotypic slice culture of GOF animals

Similar to LOF, I have followed the same PTX approach in organotypic slices of GOF (L1649Q, +/-) animals. GOF of $Na_V1.1$ increased neuronal firing in transfected mature (Cestèle *et al.*, 2013) and inhibitory cortical neurons (Auffenberg, Hedrich et al., in preparation). Application of 5 µM PTX antagonized the increased inhibitory effects and significantly increased the firing frequency of up-states in slices of L1649Q animals (before PTX : 0.11 ± 0.02 Hz and after PTX : 0.17 ± 0.03 Hz, n = 15, $P < 0.01$; paired t-tests). However, the duration of up-states did not show any significant changes due to the application of PTX (before PTX : 1.43 ± 0.21 S and after PTX : 1.40 ± 0.28 S, n = 15, $P > 0.05$; paired t-tests) (Figure 26). These findings again confirm the crucial role of *SCN1A* variants in the regulation of TC up-states.

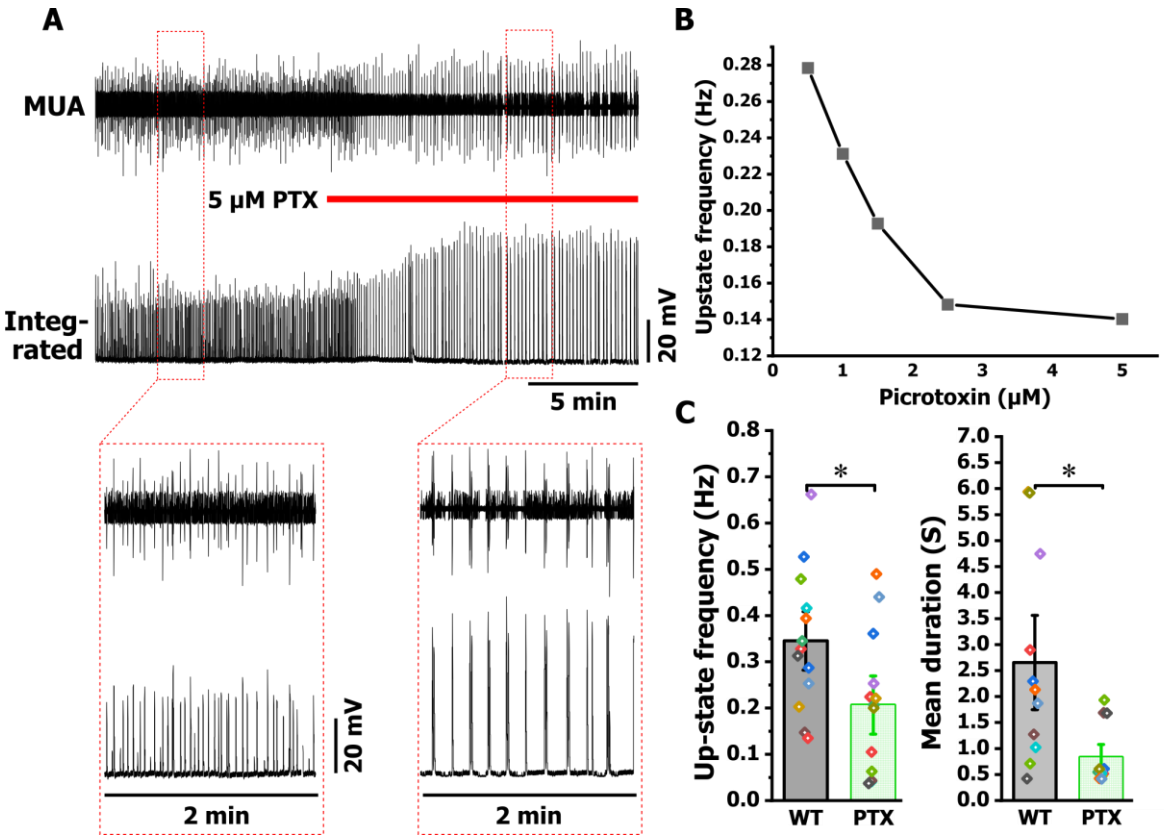

Figure 25. Effect of disinhibition on TC up-states recorded in organotypic brain slice cultures: (**A**) Representative voltage traces of multiunit activity (MUA) recordings of up-states and their integrated form before and after the application of 5 µM PTX concentration. Integrated traces are noisy baseline blanked signals from multiunit extracellular recordings, which are presented in a unidirectional manner. Bottom traces represent the enlarged view of the up-state frequency before and after the application of 5 µM PTX. (**B**) Graphical representation of the dose-effect of PTX (0.5, 1, 1.5, 2.5 and 5 µM) recorded from one of WT organotypic slices. (**C**) Bar graphs comparing the frequency and the duration of up-states recorded in organotypic TC slices of WT animals in the presence of 5 µM PTX. The up-state frequency was significantly reduced in slices of WT animals after PTX application (n = 13, $P < 0.05$; paired t-tests), which were less than that observed in slices of R1648H animals (See Figure 24). The up-state duration was also significantly reduced in slices of WT animals in the presence of 5 µM PTX (n = 13, $P < 0.05$; paired t-tests). Data are shown as mean ± SEM.

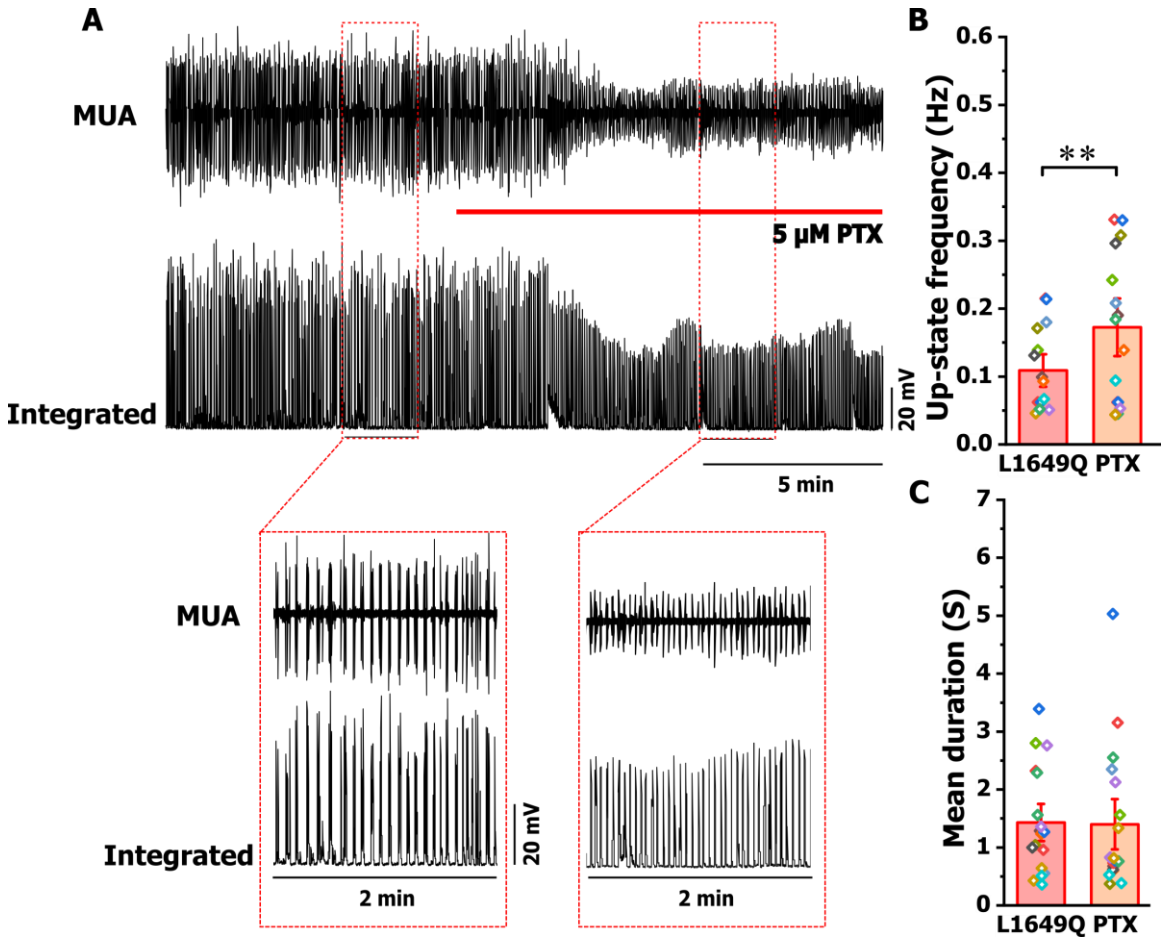

Figure 26. Effect of reduced inhibition on TC up-states recorded in slice cultures of L1649Q (GOF) animals: (**A**) Representative voltage traces show the multiunit activity (MUA) of up-states, their integrated form before and after the application of PTX (5 µM) (top) and their enlarged view (shown in red boxes) (bottom). Integrated traces are noisy baseline blanked signals from multiunit extracellular recordings, which are presented in a unidirectional manner (**B)** Bar graph comparing the frequency of up-states recorded in organotypic TC slices of heterozygous L1649Q animals in the presence of 5 µM PTX. The up-state frequency was significantly increased in slices of L1649Q animals after application of 5 µM PTX ($n = 15$, $P < 0.01$; paired t-tests). (**C**) Bar graph comparing the up-state duration recorded in organotypic TC slices of heterozygous L1649Q animals before and after application of 5 µM PTX. The up-state duration was not significantly different after application of 5 µM PTX ($n = 15$, $P > 0.05$; paired t-tests). Data are shown as mean ± SEM.

4. Discussion

4.1 Understanding the pathophysiology of *KCNA2* mediated epilepsies

The first part of the thesis aimed to understand the pathophysiological role of *KCNA2* variants in developmental and epileptic encephalopathies. The *KCNA2* gene encodes the voltage-gated potassium channel subunit $K_V1.2$ that mediates the rapid repolarization phase of an action potential and partially determines the resting membrane potential (Hodgkin and Huxley, 1952; Maljevic and Lerche, 2013). *De novo* variants in the *KCNA2* gene have been reported previously in cases of developmental epileptic encephalopathies (DEE) (Syrbe *et al.*, 2015; Masnada *et al.*, 2017). The $K_V1.2$ channel subunit is ubiquitously expressed in all crucial brain regions including both excitatory and inhibitory neurons (Nashmi *et al.*, 2000; Lorincz and Nusser, 2008; Trimmer, 2015). The clinical spectrum of *KCNA2* DEE varies largely in patients as evident from a previous study (Masnada *et al.*, 2017). Even though the large variability in phenotypic spectra are connected to *KCNA2* LOF, GOF and GOF-LOF variants, the cellular basis of neuronal dysfunction due to any of them is not clear. Therefore, the current thesis reported the first insights into the changes in neuronal intrinsic firing properties of SSC L2/3 pyramidal neurons due to overexpression of $K_V1.2$ WT, LOF and GOF variants. The studied *KCNA2* variants (P405L and R297Q) are the most recurrent LOF and GOF mutations observed in patients.

The current study targeted the SSC L2/3 pyramidal neurons in the developing brain through IUE and achieved an overexpression of $K_V1.2$ channel subunits. The experimental results (both morphological and electrophysiological) from $K_V1.2$ WT, R297Q and P405L subunits electroporated neurons showed that the neurons overexpressing the $K_V1.2$ WT and GOF subunits exhibited an impairment of the dendritic morphology in contrast to the control and LOF mutation as well as affected their passive membrane properties. The changes in AP firing were prominent in neurons overexpressing $K_V1.2$ subunits, such as earlier triggering of repolarization phase in R297Q cells, the reduced AP number in neurons overexpressing $K_V1.2$ WT and R297Q subunits, and an elongated AHP and repolarization in neurons overexpressing the P405L variant. These results provide first results of *KCNA2*-mediated disease mechanisms on a cellular level. In addition, a therapeutic strategy with 4-AP was successful and rescued neurons from their hypoexcitablity to regular firing in $K_V1.2$ WT overexpressing neurons.

4.1.1 $K_V1.2$ WT and GOF overexpression alter the morphological features of SSC L 2/3 pyramidal neurons

The direct involvement of ion-channel variants in neurodevelopmental disorders has been reported previously (Reid *et al.*, 2014; Scheffer *et al.*, 2017). The psychomotor

developmental delay or a stagnation was observed in *KCNA2*-related DEE (Masnada *et al.*, 2017). The pathophysiological consequence of *KCNA2* mutations in neurodevelopment was studied through morphological analysis of neurons overexpressing $K_V1.2$ WT subunits, their GOF (R297Q) and LOF (P405L) variants, and untransfected neurons in the electroporated area were used as controls. The morphological analysis revealed that neurons overexpressing $K_V1.2$ WT subunits and the R297Q variant showed a reduced dendritic arborization in contrast to controls and P405L overexpressing neurons. The overexpression of $K_V1.2$ WT channels in the neuronal membrane enhances the outflow of K^+ ions, similar to the R297Q variant and hence represents a less strong GOF condition. In more detail, WT and R297Q overexpressing neurons presented less dendritic arborization, and both the number of dendritic branches and total branch length were reduced. The overexpression of $K_V1.2$ subunits (R297Q variant) induced impairment in overall dendritic morphology regardless of apical and basal dendritic compartments.

The observed structural changes of the brain in patients MRIs carrying *KCNA2* variants were unremarkable for LOF, showed a marked cerebellar atrophy for GOF and a strong and more progressive cerebellar atrophy, which began in the early childhood for the mixed GOF-LOF group (Pena and Coimbra, 2015; Syrbe *et al.*, 2015; Corbett *et al.*, 2016; Hundallah *et al.*, 2016; Masnada *et al.*, 2017). There were no morphological changes in neurons overexpressing the LOF compared to controls; however, GOF overexpression induced significant changes in the dendritic morphology. The dendritic alterations due to the GOF variants may progress to cell death (Chopra *et al.*, 2018). Seizure induced chronic hyperexcitability can also limit the dendritic arborization by altering different growth signaling pathways (Nishimura *et al.,* 2008). Both of these two possibilities may contribute to the neuronal atrophy in DEE patients with ataxia (Dell'Orco *et al.*, 2015). However, these results need further validation experiments in gene-targeted mouse models carrying corresponding *KCNA2* mutations, which will further open the possibility to understand the spatial and temporal processes of dendritic alterations and related excitability changes in neurons.

4.1.2 $K_V1.2$ R297Q and P405L overexpression changes the neuronal passive membrane properties in SSC L2/3 pyramidal neurons

$K_V1.2$ subunits are crucial in regulating the resting membrane potential in neurons by allowing the out-flow of intracellular K^+ ions in response to neuronal depolarization. They activate at the resting membrane potential or towards more depolarized potential (Shen *et al.*, 2004; Al-Sabi *et al.*, 2013). Because of these electrophysiological characteristics of the $K_V1.2$ channel subunit, they may have a crucial role in regulating the neuronal passive

membrane properties. To understand the contribution of $K_V1.2$ in the regulation of these properties, I have recorded R_m, R_{in} and the membrane time constant from neurons overexpressing $K_V1.2$ WT subunits, their GOF (R297Q) and LOF (P405L) variants. $K_V1.2$ WT and R297Q overexpressing neurons showed hyperpolarized R_m in comparison to neurons overexpressing the P405L variant. This is consistent with previous findings, in which the expression of $K_V1.2$ WT and R297Q channels hyperpolarized the membrane potential of oocytes (Syrbe *et al.*, 2015). Similar results were observed in WT and R297Q overexpressing CHO cells. These findings confirm the role of $K_V1.2$ channels in the regulation of R_m by allowing an excess out-flow of K^+ ions at R_m. It has been reported that the application of 4-AP (100 µM) also depolarizes the R_m in cortical layer V pyramidal neurons (Bekkers and Delaney, 2001), which is consistent with our experiment showing the same effect of 4-AP in both $K_V1.2$ WT and R297Q overexpressing CHO cells. The R_m analysis in medial nucleus of the trapezoid body (MNTB) neurons of *Kcna2* knockout mice (+/- and -/-) did not show significant variation compared to neurons of its +/+ littermates (Brew *et al.*, 2007). However, R_m analysis of *Kcna2*−/− spiral ganglion neurons (SGNs) of the *Pingu* mouse (carries a missense LOF-I402T mutation in the S6 segment) showed a hyperpolarized R_m compared to recordings from neurons of the WT SGNs. This is in contrast to the current findings. The authors suggest that these unexpected R_m changes may be cell-specific to SGNs and hyperpolarized R_m is due to the dominated heteromeric interactions of $K_V1.2$ and $K_V1.4$ subunits, which further define features of K_V1 channels in SGNs (Wang *et al.*, 2013). It has been hypothesized that $K_V1.2$ channels might contribute largely in presynaptic transmitter release by clamping the terminal R_m (Xie *et al.*, 2010). This hypothesis can be explained in future studies to understand the interrelation between $K_V1.2$-regulated changes in R_m and presynaptic neurotransmitter release, which will only be possible by measuring R_m directly at the presynaptic terminal patch-clamping in knock-out or knock-in $K_V1.2$ mouse models.

The mean R_{in} in neurons overexpressing the R297Q variant was significantly reduced compared to those overexpressing P405L. This can be explained by the opening of $K_V1.2$ channels at more hyperpolarized potential than R_m due to the GOF effect, leading to diminished cellular excitability. Apart from R_{in}, the membrane time constant was also significantly smaller in neurons overexpressing $K_V1.2$ WT and R297Q subunits as compared to controls and P405L neurons, indicating a faster voltage change. Therefore, a GOF may attenuate the current-evoked voltage faster than for controls and LOF.

4.1.3 Overexpression of K_V1.2 WT, R297Q and P405L subunits changes AP properties

Previous studies have shown that K_V1.2 channels are enriched in axon initial segments (Gu *et al.*, 2003; Robbins and Tempel, 2012). Also, the role of the K_V1 channel family mediated delayed rectifier potassium current (I_K) has been studied with regard to somatic AP generation (Saviane *et al.*, 2003; Goldberg *et al.*, 2008; Cudmore *et al.*, 2010). In neurons, K_V1.2 subunits are usually building functional channels with other subunits of the K_V1 channel family. The specific role of K_V1.2 subunits in AP generation was studied in K_V1.2 WT, R297Q and P405L overexpressing neurons. The AP threshold did not vary among the control, WT, R297Q and P405L cells. This is in contrast to a previous study which showed that the application of α-DTX (blocking K_V1.1, K_V1.2 and K_V1.6) significantly lowered the voltage threshold for an AP in neocortical pyramidal neurons (Guan *et al.*, 2007). These results may indicate that other potassium channels of the K_V1 family play a more important role for the excitability of SSC L2/3 pyramidal neurons via regulation of the AP threshold and near-threshold responsiveness than K_V1.2 (Gittelman and Tempel, 2006; Goldberg *et al.*, 2008). The AP amplitude was significantly reduced in neurons overexpressing the R297Q variant as compared to controls, which suggests an early activation of K_V1.2 channels during the repolarization phase of an AP due to the GOF effects. The AP-width was significantly reduced in K_V1.2 WT overexpressing neurons in comparison to control cells, which hints towards the enhanced speed of the repolarization phase due to the fast outflow of K^+ ions. I did not find a reduction in AP-width for R297Q overexpressing neurons, which may be due to a relatively small number of recorded neurons overexpressing R297Q channels. Although K_V1.2-mediated currents activate at the beginning of the repolarization phase, the AP width comparison did not show any significant difference in LOF conditions. However, I found changes in AHP, indicating these K_V1.2 subunits have a prominent role during the final phases of the repolarization. Similar observations about the K_V1 channel family were reported on the later phase of the AP repolarization during the previous studies using α-DTX and 4-AP application on neocortical and hippocampal pyramidal neurons (Spain *et al.*, 1991; Bekkers and Delaney, 2001; Mitterdorfer and Bean, 2002).

4.1.4 K_V1.2 channels control the repetitive neuronal firing

The K_V1 channel family regulates the repolarization phase, which influences repetitive AP firing by inducing long-lasting afterhyperpolarizations (Pathak *et al.*, 2016). Also, it was predicted that the α-DTX-sensitive current has a strong influence on regulating interspike intervals (ISIs) during AP repetitive firing (Mitterdorfer and Bean, 2002). The repetitive firing characteristics of K_V1.2 channels in SSC L2/3 pyramidal neurons were examined in neurons

overexpressing $K_V1.2$ WT, R297Q and P405L subunits using current stimuli of different intensities. Neurons overexpressing $K_V1.2$ WT and R297Q subunits showed a significant reduction in the number of elicited APs compared to controls and P405L cells for all stimulus intensities (see Figure 16). In $K_V1.2$ WT overexpressing cells, the voltage at which the firing block was observed was significantly depolarized as compared to neurons overexpressing the R297Q variant and was at the level of AP threshold potential. This may indicate the inability of neurons overexpressing $K_V1.2$ WT and R297Q to reach the threshold potential, due to an increased K^+ outflow. These observed changes in the voltage at which the firing block occurred may be due to the differences in channel gating properties. Besides this, the reduced input resistance, which was discussed in the previous section, supported the reduced excitability of R297Q overexpressing neurons. To date, there is no gene-targeted mouse model for a GOF variant or experiments were reported, which closely mimics the observed $K_V1.2$ GOF effect. Overall, these results show that the GOF effect of $K_V1.2$ channels induces a firing deficiency in SSC L2/3 pyramidal neurons.

Also, the P405L overexpressing neurons elicited a considerably reduced number of APs compared to controls. In addition to the reduced excitability, P405L overexpressing cells exhibited an increased AHP and an elongated repolarization phase. The observed reduced AP numbers are similar to the hypoexcitablity found in $K_V1.2$ knockout glycinergic neurons (Brew *et al.*, 2007). The blockade of the delayed potassium current with TEA had a similar impact on the neuronal excitability, which was comparable to P405L overexpressing neurons. TEA significantly elongated and broadened the APs, which was explained by the inhibitory effect of TEA on the fast calcium-activated K^+ current (Storm, 1987). I have also found the same elongation and broadening of the AP repolarization phase in P405L overexpressing neurons. The possible reason for the considerably reduced AP firing in neurons overexpressing the P405L variant could be the changes in AHP due to the prolonged opening of voltage-gated calcium channels, which increase the intracellular calcium level and further enhance the opening of calcium-activated potassium channels (Hille, 1978; Lancaster *et al.*, 1991; Sah, 1995; Xia *et al.*, 1998). The increased AHP amplitude measured in the P405L overexpressing neurons complements these prospects of AHP.

Spike frequency adaptation is mediated by activation of a slow calcium-activated potassium conductance (Sah and Bekkers, 1996) and neurons showing an increased AHP can induce a strong spike adaptation (Nicoll, 1988). As I have observed a prominent AHP in P405L overexpressing neurons, I have further investigated the changes in spike adaptation in these neurons. Spike adaptation was significantly reduced in P405L cells. This finding is consistent with previous experiments performed in the callosal-projecting neurons of the visual cortex,

which showed the blockade of the delayed rectifier potassium current (I_K) with 4-AP (50 µM) reduced the spike adaptation (Locke and Nerbonne, 1997). These results show that the overexpression of the P405L variant induces enhanced AHP and elongated repolarization phase in neurons while presenting a reduced spike adaptation.

Overall the repetitive firing properties show that GOF variants reduce the AP number in neurons. This could be relevant particularly in inhibitory neurons, thereby explaining the occurrence of seizures by reduced inhibition. It was predicted previously that LOF primarily affects the excitatory pathway, where it impairs the cellular excitability (Masnada *et al.*, 2017). However, considerably reduced AP firing observed in the LOF variant suggests that LOF might also affect inhibitory neurons as speculated in GOF patients. The different degrees of phenotypic severity (LOF is correlated with milder phenotypes while GOF with severe features) observed in *KCNA2*-related DEE support the above hypothesis that LOF partially impairs neuronal firing with reduced AP number, whereas GOF severely abolishes the firing properties of inhibitory neurons.

4.1.5 Application of 4-AP restores the regular firing pattern in K_V1.2 WT overexpressing neurons

4-AP is a licensed drug for symptomatic treatment of multiple sclerosis (Bostock *et al.*, 1981; Jensen *et al.*, 2014), which quite selectively blocks the K_V1 and K_V4 family of voltage-gated K^+ channels. 4-AP has been investigated by our group as a new precision therapy for a highly pharmaco-resistant group of patients carrying *KCNA2* GOF related DEE (Hedrich, Lauxmann et al., Sci Trans Med, under revision). In the current study, the effect of 4-AP on K_V1.2 channels was examined in CHO cells overexpressing WT and R297Q variants. The results showed that 1 mM 4-AP was sufficient to block about half of the K_V1.2 current for WT and R297Q overexpressing cells. As a therapeutic option for *KCNA2*-mediated epilepsy, I could antagonize the K_V1.2 WT overexpression induced effect in electroporated neurons. Application of 4-AP (100 µM) rescued neurons from their hypoexcitablity. This underlines a therapeutic effect of 4-AP in patients with the *KCNA2* GOF variants. However, more investigations are needed in IUE electroporated neurons as well as gene-targeted *KCNA2* GOF mouse models to obtain detailed insights into the pathophysiology. Even though overexpression of K_V1.2 WT subunits impairs the dendritic arborization, application of 4-AP can rescue the neurons from their hypoexcitablity. These studies suggest the early need for effective precision therapy in *KCNA2*-related developmental and epileptic encephalopathy with 4-AP.

4.2 Effect of $Na_V1.1$ variants on thalamocortical (TC) up-states

In the second part of the thesis, I aimed to investigate the effect of $Na_V1.1$ variants on TC up-states. The obtained results provided a first-level understanding of how the epileptic variants alter the slow oscillatory patterns generated by the cortical network *in vitro*, which may predict possible consequences of $Na_V1.1$ variants on slow-wave phase of NREM sleep. Previous experimental studies showed that $Na_V1.1$ (encoded by *SCN1A* gene) is the primary Na^+ channel in GABAergic interneurons and its LOF leads to a ubiquitous disinhibition in the hippocampus and the thalamocortical (TC) loop (Yu *et al.,* 2006; Kalume *et al.,* 2007; Hedrich *et al.,* 2014) while its GOF increased inhibitory neuronal firing in the cortex and CA1 region of hippocampus (Auffenberg, Hedrich et al., in preparation). The findings of the present study in acute TC brain slices further confirmed that mouse models carrying both LOF and GOF mutations in the *SCN1A* gene*,* which alter the function of the $Na_V1.1$ channel, play a role for TC up-states. Both LOF (R1648H) and GOF (L1649Q) variants of $Na_V1.1$ reduced the frequency of TC up-states in TC acute brain slices. A similar set of experiments performed in organotypic brain slice cultures also provided the same results as observed in acute brain slices and verified the mutation derived reduction of the frequency of TC up-states. The pharmacological experiment with PTX in WT organotypic slices, which mimics the LOF condition, confirmed the results obtained in slices of animals carrying the LOF variant. Similarly, the PTX application to GOF-TC organotypic brain slices increased the frequency of up-states suggesting that the frequency reduction observed in GOF slices is due to enhanced inhibitory neuronal firing.

4.2.1 The $Na_V1.1$ LOF variant reduces the frequency of thalamocortical (TC) up-states

TC up- and down- states were recorded as extracellular multiunit activity (MUA) from SSC L5 neurons of acute brain slices of mouse models carrying epileptic *SCN1A* variants. These experiments helped to understand how $Na_V1.1$ LOF and GOF mutations alter the SWS in the intact brain due to the impaired inhibitory neuronal firing. Acute TC brain slices from *SCN1A* LOF (R1648H), GOF (L1649Q) and WT littermates (P13-P20) were prepared (Agmon and Connors, 1991), which preserved the whole TC network. The frequency of up- and down-states (< 1 Hz) recorded in TC slices (*in vitro*) are correlates of slow-wave oscillations (SWS) during the NREM sleep (*in vivo*) (Steriade *et al.*, 1993; Sanchez-Vives and McCormick, 2000).

Acute TC brain slices were prepared from mice at P13-P20 because it was shown that during this period, TC up-states manifested a ten-fold increase in occurrence, which represents the maximum level of up-state activity throughout the lifespan of a mouse (Rigas *et al.*, 2015). The TC up-states in cortical layer 5 pyramidal neurons are tightly regulated by the thalamic relay neurons as well as the intracortical inhibitory neuronal inputs (Sanchez-

Vives and McCormick, 2000; Rigas and Castro-Alamancos, 2007; Watson *et al.*, 2008). Hence, the recordings were obtained from SSC L5 pyramidal neurons. 200-300 ms (which was used as up-state selection criteria) is the minimum time window required for the interaction among multiple brain regions and allows intercommunication of feedforward stream from the thalamus to the feedback stream of higher cortical areas (Oikonomou *et al.*, 2014).

The frequency of up-states was significantly reduced in TC acute brain slices of R1648H (+/-) mice compared to slices of WT (+/+) animals. The comprehensive characterization of R1648H (+/-) showed ubiquitous disinhibition in the hippocampus and the thalamocortical loop presumably induced by a deficit of AP firing in axon initial segments of GABAergic interneurons as the cellular key mechanism (Hedrich *et al.*, 2014). The reduction of up-state frequency may be due to the reduced inhibitory neuronal firing as a consequence of the *SCN1A* LOF mutation. A previous study supports the above findings by showing that the progressive decrease in inhibition with bicuculine resulted in a parametric reduction in the duration and frequency of up-states in ferret cortical slices. The reduced inhibition impairs the synchronized network activity due to the concurrent increase in excitatory firing during the up-states, which led to shorter and less frequent up-states (Sanchez-Vives *et al.*, 2010). The enhanced excitatory neuronal firing during the up-states leads to the active recruitment of calcium-dependent potassium channels, which further promotes the transformation of an up- to down-state and reduces the up-state duration (Compte *et al.*, 2003; Cunningham *et al.*, 2006). The up-states duration in my experiments did not show a significant reduction, which may differ due to the difference in the mode of inhibition between genetic and pharmacological approaches. In pharmacological analyses with bicuculline and picrotoxin, the inhibition is mainly mediated through synaptic GABA receptors (Mann *et al.*, 2009) whereas, in R1648H mice, it was initiated due to the decreased neuronal firing of inhibitory neurons (Yu *et al.*, 2006; Kalume *et al.*, 2007; Hedrich *et al.*, 2014).

As a validation for the findings of acute slices of R1648H (+/-) animals, I have repeated similar experiments in organotypic brain slice cultures. In acute brain slices, the persistent TC network activities were limited to 50% of slices, which demands many animals for the experiments. The organotypic brain slice culture of TC slices can be an accurate alternative to the acute experiments by providing a prominent TC network up-state in 90 % of slices. Slices were cultured from animals at the age of 5-6 days and the up-states were subsequently recorded after 8 ± 1 days *in-vitro* (DIV), thus corresponding to the age of the acute brain slice preparation. TC up-states recorded from organotypic brain slice cultures also showed a similar trend of the experiments in acute slices. The frequency of TC up-states was significantly reduced, while the duration remained the same. These findings were further validated in

organotypic brain slice culture using PTX. The application of PTX on slices of WT (+/+) animals mimics the LOF conditions similar to the R1648H variant. Application of 5 µM PTX significantly reduced the frequency of up-states and their duration in slices of WT animals. These results confirm the inhibitory modulation of emergent TC up-states, similar to the findings observed previously in bicuculline-meditated inhibitory reduction (Sanchez-Vives *et al.*, 2010).

4.2.2 The $Na_V1.1$ GOF variant also reduce the frequency of thalamocortical (TC) up-states

Interestingly, the TC up-states recorded in acute slices of *SCN1A* GOF (L1649Q, +/-) animals also showed a significant reduction of their frequency without affecting the duration compared to slices of WT (+/+) animals. The electrophysiological characterization of L1649Q (+/-) showed increased inhibitory neuronal firing in the hippocampal CA1 region and SSC layer 4 (Cestèle *et al.*, 2013, Auffenberg, Hedrich et al., in preparation/personal communication). The dominating inhibitory input during the network activity of up-states may be the reason for the reduced up-state frequency. So far, no animal model or pharmacological experiments investigated an enhanced inhibitory effect on TC up-states. Similar to acute slice experiments, the frequency of TC up-states decreased in organotypic slice cultures of L1649Q (+/-) animals while the up-state duration remained the same. The increased inhibitory neuronal effect was antagonized in organotypic slice cultures of L1649Q (+/-) animals by using 5 µM PTX. The addition of PTX significantly increased the frequency of TC up-states, without changing the duration. These observations endorse the role of increased inhibitory input in reducing the incidence of up-states during network synchronization.

Overall, these results indicate an important influence of inhibitory neurons in maintaining balanced firing patterns of the neural network as an essential aspect for TC up- and down- states. The mutated *SCN1A* gene induces $Na_V1.1$ channel dysfunction, which consequently alters balanced network synchronization. The TC network is an essential brain structure crucial for sensory processing, which regulates many physiological and pathophysiological conditions such as sleep and epilepsy (Steriade *et al.*, 1993). The reduced delta waves and spindles during NREM sleep and the increased awakening observed in *Scn1a* mouse models represent *in vivo* examples of imbalanced network activities (Papale *et al.*, 2013; Kalume *et al.*, 2015). However, it was not clear whether the disturbed sleep can be mainly explained by the dysfunction of interneurons or by the occurrence of seizure activity during sleep stages. The results obtained from TC slices provide insights that recurrent seizures may not be the only reason for a disturbed sleep in epileptic patients carrying a mutant *SCN1A* gene, but also the involvement of mutation-derived TC network dysfunction.

5. References

Agmon, A, and B.W. Connors. 1991. "Thalamocortical Responses of Mouse Somatosensory (Barrel) Cortexin Vitro." *Neuroscience* 41 (2–3): 365–79. doi:10.1016/0306-4522(91)90333-j.

Allen, Nicholas M, Judith Conroy, Amre Shahwan, Bryan Lynch, Raony G Correa, Sergio DJ Pena, Dara McCreary, et al. "Unexplained Early Onset Epileptic Encephalopathy: Exome Screening and Phenotype Expansion." *Epilepsia* 57, no. 1 (2016): e12–17. https://doi.org/10.1111/epi.13250.

Allou, L., S. Julia, D. Amsallem, S. El Chehadeh, L. Lambert, J. Thevenon, Y. Duffourd, et al. "Rett-like Phenotypes: Expanding the Genetic Heterogeneity to the *KCNA2* Gene and First Familial Case of CDKL5-related Disease." *Clinical Genetics* 91, no. 3 (2017): 431–40. https://doi.org/10.1111/cge.12784.

Al-Sabi, Ahmed, Seshu Kaza, Oliver J Dolly, and Jiafu Wang. 2013. "Pharmacological Characteristics of Kv1.1- and Kv1.2-Containing Channels Are Influenced by the Stoichiometry and Positioning of Their α Subunits." *Biochemical Journal* 454 (1): 101–8. doi:10.1042/BJ20130297.

Balamurugan, E, Meena Aggarwal, Anurag Lamba, Nitika Dang, and Manjari Tripathi. 2013. "Perceived Trigger Factors of Seizures in Persons with Epilepsy." *Seizure* 22 (9): 743–47. doi:10.1016/j.seizure.2013.05.018.

Baronas, Victoria A., Brandon R. McGuinness, G. Stefano Brigidi, Rachel N. Gomm Kolisko, Yury Y. Vilin, Robin Y. Kim, Francis C. Lynn, Shernaz X. Bamji, Runying Yang, and Harley T. Kurata. "Use-Dependent Activation of Neuronal K_V1.2 Channel Complexes." *The Journal of Neuroscience* 35, no. 8 (2015): 3515–24. https://doi.org/10.1523/JNEUROSCI.4518-13.2015.

Bekkers, John M., and Andrew J. Delaney. 2001. "Modulation of Excitability by α-Dendrotoxin-Sensitive Potassium Channels in Neocortical Pyramidal Neurons." *Journal of Neuroscience* 21 (17): 6553–60. doi:10.1523/jneurosci.21-17-06553.2001.

Berg, Anne T., Samuel F. Berkovic, Martin J. Brodie, Jeffrey Buchhalter, J. Helen Cross, Walter Van Emde Boas, Jerome Engel, et al. "Revised Terminology and Concepts for Organization of Seizures and Epilepsies: Report of the ILAE Commission on Classification and Terminology, 2005–2009." *Epilepsia* 51, no. 4 (2010): 676–85. https://doi.org/10.1111/j.1528-1167.2010.02522.x.

Borrell, Víctor, Yumiko Yoshimura, and Edward M Callaway. 2004. "Targeted Gene Delivery to Telencephalic Inhibitory Neurons by Directional in Utero Electroporation." *Journal of Neuroscience Methods* 143 (2): 151–58. doi:10.1016/j.jneumeth.2004.09.027.

Bostock, H, T A Sears, and R M Sherratt. 1981. "The Effects of 4-Aminopyridine and Tetraethylammonium Ions on Normal and Demyelinated Mammalian Nerve Fibres." *The Journal of Physiology* 313 (1): 301–15. doi:10.1113/jphysiol.1981.sp013666.

Brew, Helen M, Joshua X Gittelman, Robert S Silverstein, Timothy D Hanks, Vas P Demas, Linda C Robinson, Carol A Robbins, et al. "Seizures and Reduced Life Span in Mice Lacking the Potassium Channel Subunit K_V1.2, but Hypoexcitability and Enlarged Kv1 Currents in Auditory Neurons." *Journal of Neurophysiology* 98, no. 3 (2007): 1501–25. https://doi.org/10.1152/jn.00640.2006.

Buoni, S, A Orrico, L Galli, R Zannolli, L Burroni, J Hayek, A Fois, and V Sorrentino. "*SCN1A* (2528delG) Novel Truncating Mutation with Benign Outcome of Severe Myoclonic Epilepsy of Infancy." *Neurology* 66, no. 4 (2006): 606–7. https://doi.org/10.1212/01.wnl.0000198504.41315.b1.

Capovilla, Giuseppe, Peter Wolf, Francesca Beccaria, and Giuliano Avanzini. "The History of the Concept of Epileptic Encephalopathy." *Epilepsia* 54, no. s8 (2013): 2–5. https://doi.org/10.1111/epi.12416.

Catterall, William A, Franck Kalume, and John C Oakley. "Na_V1.1 Channels and Epilepsy." *The Journal of Physiology* 588, no. 11 (2010): 1849–59. https://doi.org/10.1113/jphysiol.2010.187484.

Cestèle, Sandrine, Emanuele Schiavon, Raffaella Rusconi, Silvana Franceschetti, and Massimo Mantegazza. "Nonfunctional $Na_V1.1$ Familial Hemiplegic Migraine Mutant Transformed into Gain of Function by Partial Rescue of Folding Defects." *Proceedings of the National Academy of Sciences* 110, no. 43 (2013): 17546–51. https://doi.org/10.1073/pnas.1309827110.

Chang, Bernard S., and Daniel H. Lowenstein. "Epilepsy." *The New England Journal of Medicine* 349, no. 13 (2003): 1257–66. https://doi.org/10.1056/nejmra022308.

Chen, Fuyi, Brady J Maher, and Joseph J LoTurco. 2014. "PiggyBac Transposon-Mediated Cellular Transgenesis in Mammalian Forebrain by in Utero Electroporation." *Cold Spring Harbor Protocols* 2014 (7): 741–49. doi:10.1101/pdb.prot073650.

Chopra, Ravi, David D Bushart, and Vikram G Shakkottai. 2018. "Dendritic Potassium Channel Dysfunction May Contribute to Dendrite Degeneration in Spinocerebellar Ataxia Type 1." *PLOS ONE* 13 (5): e0198040. doi:10.1371/journal.pone.0198040.

Claes, L, J Del-Favero, B Ceulemans, L Lagae, C Van Broeckhoven, and P De Jonghe. "De Novo Mutations in the Sodium-Channel Gene *SCN1A* Cause Severe Myoclonic Epilepsy of Infancy." *American Journal of Human Genetics* 68, no. 6 (2001): 1327–32. https://doi.org/10.1086/320609.

Clark, Brian D., Ethan M. Goldberg, and Bernardo Rudy. "Electrogenic Tuning of the Axon Initial Segment." *The Neuroscientist* 15, no. 6 (2009): 651–68. https://doi.org/10.1177/1073858409341973.

Compte, Albert, Maria V Sanchez-Vives, David A McCormick, and Xiao-Jing Wang. 2003. "Cellular and Network Mechanisms of Slow Oscillatory Activity (<1 Hz) and Wave Propagations in a Cortical Network Model." *Journal of Neurophysiology* 89 (5): 2707–25. doi:10.1152/jn.00845.2002.

Consortium, Epi4K, Epilepsy Phenome/Genome Project, Andrew S Allen, Samuel F Berkovic, Patrick Cossette, Norman Delanty, Dennis Dlugos, et al. "De Novo Mutations in Epileptic Encephalopathies." *Nature* 501, no. 7466 (2013): 217–21. https://doi.org/10.1038/nature12439.

Coppola, Antonietta, and Solomon L. Moshé. "Chapter 4 Animal Models." *Handbook of Clinical Neurology* 107 (2012): 63–98. https://doi.org/10.1016/b978-0-444-52898-8.00004-5.

Corbett, Mark A, Susannah T Bellows, Melody Li, Renée Carroll, Silvana Micallef, Gemma L Carvill, Candace T Myers, et al. "Dominant *KCNA2* Mutation Causes Episodic Ataxia and Pharmacoresponsive Epilepsy." *Neurology* 87, no. 19 (2016): 1975–84. https://doi.org/10.1212/WNL.0000000000003309.

Cudmore, Robert H, Laure Fronzaroli-Molinieres, Pierre Giraud, and Dominique Debanne. 2010. "Spike-Time Precision and Network Synchrony Are Controlled by the Homeostatic Regulation of the D-Type Potassium Current." *The Journal of Neuroscience : The Official Journal of the Society for Neuroscience* 30 (38): 12885–95. doi:10.1523/jneurosci.0740-10.2010.

Cunningham, M O, D D Pervouchine, C Racca, N J Kopell, C H Davies, R S G Jones, R D Traub, and M A Whittington. 2006. "Neuronal Metabolism Governs Cortical Network Response State." *Proceedings of the National Academy of Sciences of the United States of America* 103 (14): 5597–5601. doi:10.1073/pnas.0600604103.

Dell'Orco, James M, Aaron H Wasserman, Ravi Chopra, Melissa A C Ingram, Yuan-Shih Hu, Vikrant Singh, Heike Wulff, Puneet Opal, Harry T Orr, and Vikram G Shakkottai. 2015. "Neuronal Atrophy Early in Degenerative Ataxia Is a Compensatory Mechanism to Regulate Membrane Excitability." *The Journal of Neuroscience : The Official Journal of the Society for Neuroscience* 35 (32): 11292–307. doi:10.1523/jneurosci.1357-15.2015.

Delemotte, Lucie, Werner Treptow, Michael L Klein, and Mounir Tarek. "Effect of Sensor Domain Mutations on the Properties of Voltage-Gated Ion Channels: Molecular Dynamics Studies of the

Potassium Channel $K_V1.2$." *Biophysical Journal* 99, no. 9 (2010): L72–74. https://doi.org/10.1016/j.bpj.2010.08.069.

Dichgans, Martin, Tobias Freilinger, Gertrud Eckstein, Elena Babini, Bettina Lorenz-Depiereux, Saskia Biskup, Michel D Ferrari, et al. "Mutation in the Neuronal Voltage-Gated Sodium Channel *SCN1A* in Familial Hemiplegic Migraine." *The Lancet* 366, no. 9483 (2005): 371–77. https://doi.org/10.1016/s0140-6736(05)66786-4.

Diekelmann, Susanne, and Jan Born. "The Memory Function of Sleep." *Nature Reviews Neuroscience* 11, no. 2 (2010): 114–26. https://doi.org/10.1038/nrn2762.

Dilekoz, Ergin, Thijs Houben, Katharina Eikermann-Haerter, Mustafa Balkaya, A. Mariette Lenselink, Michael J. Whalen, Sabine Spijker, Michel D. Ferrari, Arn M.J.M. van den Maagdenberg, and Cenk Ayata. "Migraine Mutations Impair Hippocampal Learning Despite Enhanced Long-Term Potentiation." *The Journal of Neuroscience* 35, no. 8 (2015): 3397–3402. https://doi.org/10.1523/jneurosci.2630-14.2015.

Dodson, Paul D, Brian Billups, Zoltán Rusznák, Géza Szucs, Matthew C Barker, and Ian D Forsythe. "Presynaptic Rat $K_V1.2$ Channels Suppress Synaptic Terminal Hyperexcitability Following Action Potential Invasion." *The Journal of Physiology* 550, no. 1 (2003): 27–33. https://doi.org/10.1113/jphysiol.2003.046250.

Doyle, Declan A., João Morais Cabral, Richard A. Pfuetzner, Anling Kuo, Jacqueline M. Gulbis, Steven L. Cohen, Brian T. Chait, and Roderick MacKinnon. 1998. "The Structure of the Potassium Channel: Molecular Basis of K^+ Conduction and Selectivity." *Science* 280 (5360): 69–77. doi:10.1126/science.280.5360.69.

Duflocq, Amandine, Barbara Le Bras, Erika Bullier, François Couraud, and Marc Davenne. "$Na_V1.1$ Is Predominantly Expressed in Nodes of Ranvier and Axon Initial Segments." *Molecular and Cellular Neuroscience* 39, no. 2 (2008): 180–92. https://doi.org/10.1016/j.mcn.2008.06.008.

Escayg, Andrew, Bryan T. MacDonald, Miriam H. Meisler, Stéphanie Baulac, Gilles Huberfeld, Isabelle An-Gourfinkel, Alexis Brice, et al. "Mutations of *SCN1A*, Encoding a Neuronal Sodium Channel, in Two Families with GEFS+2." *Nature Genetics* 24, no. 4 (2000): 343–45. https://doi.org/10.1038/74159.

Fan, Chunxiang, Stefan Wolking, Frank Lehmann-Horn, Ulrike BS Hedrich, Tobias Freilinger, Holger Lerche, Guntram Borck, Christian Kubisch, and Karin Jurkat-Rott. "Early-Onset Familial Hemiplegic Migraine Due to a Novel *SCN1A* Mutation." *Cephalalgia* 36, no. 13 (2015): 1238–47. https://doi.org/10.1177/0333102415608360.

Fan, Denggui, Fucheng Liao, and Qingyun Wang. "The Pacemaker Role of Thalamic Reticular Nucleus in Controlling Spike-Wave Discharges and Spindles." *Chaos: An Interdisciplinary Journal of Nonlinear Science* 27, no. 7 (2017): 073103. https://doi.org/10.1063/1.4991869.

Fan, Longchang, Xiaowei Guan, Wei Wang, Jian-Yuan Zhao, Hongkang Zhang, Vinod Tiwari, Paul N Hoffman, Min Li, and Yuan-Xiang Tao. "Impaired Neuropathic Pain and Preserved Acute Pain in Rats Overexpressing Voltage-Gated Potassium Channel Subunit $K_V1.2$ in Primary Afferent Neurons." *Molecular Pain* 10, no. 1 (2014): 8. https://doi.org/10.1186/1744-8069-10-8.

Fisher, Robert S, Walter van Emde Boas, Warren Blume, Christian Elger, Pierre Genton, Phillip Lee, and Jerome Engel. 2005. "Epileptic Seizures and Epilepsy: Definitions Proposed by the International League Against Epilepsy (ILAE) and the International Bureau for Epilepsy (IBE)." *Epilepsia* 46 (4): 470–72. doi:10.1111/j.0013-9580.2005.66104.x.

Fisher, Robert S., Carlos Acevedo, Alexis Arzimanoglou, Alicia Bogacz, J. Helen Cross, Christian E. Elger, Jerome Engel, et al. "ILAE Official Report: A Practical Clinical Definition of Epilepsy." *Epilepsia* 55, no. 4 (2014): 475–82. https://doi.org/10.1111/epi.12550.

Fisher, Robert S., J. Helen Cross, Jacqueline A. French, Norimichi Higurashi, Edouard Hirsch, Floor E. Jansen, Lieven Lagae, et al. "Operational Classification of Seizure Types by the International League Against Epilepsy: Position Paper of the ILAE Commission for Classification and Terminology." *Epilepsia* 58, no. 4 (2017): 522–30. https://doi.org/10.1111/epi.13670.

Freilinger, T., N. Ackl, A. Ebert, C. Schmidt, B. Rautenstrauss, M. Dichgans, and A. Danek. "A Novel Mutation in CACNA1A Associated with Hemiplegic Migraine, Cerebellar Dysfunction and Late-Onset Cognitive Decline." *Journal of the Neurological Sciences* 300, no. 1–2 (2011): 160–63. https://doi.org/10.1016/j.jns.2010.09.032.

Freilinger, T, M Bohe, B Wegener, B Müller-Myhsok, M Dichgans, and H Knoblauch. "Expansion of the Phenotypic Spectrum of the CACNA1A T666M Mutation: A Family with Familial Hemiplegic Migraine Type 1, Cerebellar Atrophy and Mental Retardation." *Cephalalgia* 28, no. 4 (2008): 403–7. https://doi.org/10.1111/j.1468-2982.2008.01540.x.

Gittelman, Joshua X, and Bruce L Tempel. 2006. "Kv1.1-Containing Channels Are Critical for Temporal Precision during Spike Initiation." *Journal of Neurophysiology* 96 (3): 1203–14. doi:10.1152/jn.00092.2005.

Goldberg, Ethan M, Brian D Clark, Edward Zagha, Mark Nahmani, Alev Erisir, and Bernardo Rudy. 2008. "K^+ Channels at the Axon Initial Segment Dampen Near-Threshold Excitability of Neocortical Fast-Spiking GABAergic Interneurons." *Neuron* 58 (3): 387–400. doi:10.1016/j.neuron.2008.03.003.

Gu, Chen, Yuh Nung Jan, and Lily Yeh Jan. 2003. "A Conserved Domain in Axonal Targeting of Kv1 (Shaker) Voltage-Gated Potassium Channels." *Science (New York, N.Y.)* 301 (5633): 646–49. doi:10.1126/science.1086998.

Guan, D, J C F Lee, M H Higgs, W J Spain, and R C Foehring. 2007. "Functional Roles of Kv1 Channels in Neocortical Pyramidal Neurons." *Journal of Neurophysiology* 97 (3): 1931–40. doi:10.1152/jn.00933.2006.

Guerrini, Renzo, Carla Marini, and Massimo Mantegazza. "Genetic Epilepsy Syndromes Without Structural Brain Abnormalities: Clinical Features and Experimental Models." *Neurotherapeutics* 11, no. 2 (2014): 269–85. https://doi.org/10.1007/s13311-014-0267-0.

Gulbis, Jacqueline M., Ming Zhou, Sabine Mann, and Roderick MacKinnon. "Structure of the Cytoplasmic β Subunit--T1 Assembly of Voltage-Dependent K^+ Channels." *Science* 289, no. 5476 (2000): 123–27. https://doi.org/10.1126/science.289.5476.123.

Hille, B. 1978. "Ionic Channels in Excitable Membranes. Current Problems and Biophysical Approaches." *Biophysical Journal* 22 (2): 283–94. doi:10.1016/s0006-3495(78)85489-7.

He, Na, Zhi-Jian Lin, Jie Wang, Feng Wei, Heng Meng, Xiao-Rong Liu, Qian Chen, et al. "Evaluating the Pathogenic Potential of Genes with de Novo Variants in Epileptic Encephalopathies." *Genetics in Medicine* 21, no. 1 (2019): 17–27. https://doi.org/10.1038/s41436-018-0011-y.

Hedrich, Ulrike, Camille Liautard, Daniel Kirschenbaum, Martin Pofahl, Jennifer Lavigne, Yuanyuan Liu, Stephan Theiss, et al. "Impaired Action Potential Initiation in GABAergic Interneurons Causes Hyperexcitable Networks in an Epileptic Mouse Model Carrying a Human $Na_V1.1$ Mutation." *The Journal of Neuroscience*, no. 45 (2014). https://doi.org/10.1523/JNEUROSCI.0721-14.2014.

Helbig, Ingo, Ingrid E Scheffer, John C Mulley, and Samuel F Berkovic. "Navigating the Channels and beyond: Unravelling the Genetics of the Epilepsies." *The Lancet Neurology* 7, no. 3 (2008): 231–45. https://doi.org/10.1016/s1474-4422(08)70039-5.

Helbig, Katherine L, Ulrike Hedrich, Deepali N Shinde, Ilona Krey, Anne-Christin Teichmann, Julia Hentschel, Julian Schubert, et al. "A Recurrent Mutation in *KCNA2* as a Novel Cause of Hereditary

Spastic Paraplegia and Ataxia." *Annals of Neurology* 80, no. 4 (2016). https://doi.org/10.1002/ana.24762.

Heron, Sarah E., Ingrid E. Scheffer, Samuel F. Berkovic, Leanne M. Dibbens, and John C. Mulley. "Channelopathies in Idiopathic Epilepsy." *Neurotherapeutics* 4, no. 2 (2007): 295–304. https://doi.org/10.1016/j.nurt.2007.01.009.

Hodgkin, A. L., and A. F. Huxley. "Currents Carried by Sodium and Potassium Ions through the Membrane of the Giant Axon of Loligo." *The Journal of Physiology* 116, no. 4 (1952): 449–72. https://doi.org/10.1113/jphysiol.1952.sp004717.

Horne, Andrew James, Christian Joseph Peters, Thomas William Claydon, and David Fedida. 2010. "Fast and Slow Voltage Sensor Rearrangements during Activation Gating in Kv1.2 Channels Detected Using Tetramethylrhodamine Fluorescence." *The Journal of General Physiology* 136 (1): 83–99. doi:10.1085/jgp.201010413.

Huguenard, John. "Current Controversy: Spikes, Bursts, and Synchrony in Generalized Absence Epilepsy: Unresolved Questions Regarding Thalamocortical Synchrony in Absence Epilepsy." *Epilepsy Currents* 19, no. 2 (2019): 105–11. https://doi.org/10.1177/1535759719835355.

Humpel, C. 2015. "Organotypic Brain Slice Cultures: A Review." *Neuroscience* 305: 86–98. doi:10.1016/j.neuroscience.2015.07.086.

Hundallah, Khaled, Asma'a Alenizi, Amal AlHashem, and Brahim Tabarki. "Severe Early-Onset Epileptic Encephalopathy Due to Mutations in the *KCNA2* Gene: Expansion of the Genotypic and Phenotypic Spectrum." *European Journal of Paediatric Neurology* 20, no. 4 (2016): 657–60. https://doi.org/10.1016/j.ejpn.2016.03.011.

Huntsman, Molly M., Darrell M. Porcello, Gregg E. Homanics, Timothy M. DeLorey, and John R. Huguenard. "Reciprocal Inhibitory Connections and Network Synchrony in the Mammalian Thalamus." *Science* 283, no. 5401 (1999): 541–43. https://doi.org/10.1126/science.283.5401.541.

Jensen, Henrik Boye, Mads Ravnborg, Ulrik Dalgas, and Egon Stenager. 2014. "4-Aminopyridine for Symptomatic Treatment of Multiple Sclerosis: A Systematic Review." *Therapeutic Advances in Neurological Disorders* 7 (2): 97–113. doi:10.1177/1756285613512712.

Kalume, Franck, John C. Oakley, Ruth E. Westenbroek, Jennifer Gile, Horacio O. de la Iglesia, Todd Scheuer, and William A. Catterall. "Sleep Impairment and Reduced Interneuron Excitability in a Mouse Model of Dravet Syndrome." *Neurobiology of Disease* 77 (2015): 141–54. https://doi.org/10.1016/j.nbd.2015.02.016.

Kalume, Franck, Frank H. Yu, Ruth E. Westenbroek, Todd Scheuer, and William A. Catterall. "Reduced Sodium Current in Purkinje Neurons from $Na_V1.1$ Mutant Mice: Implications for Ataxia in Severe Myoclonic Epilepsy in Infancy." *The Journal of Neuroscience* 27, no. 41 (2007): 11065–74. https://doi.org/10.1523/jneurosci.2162-07.2007.

Kataria, Lynn, and Bradley V. Vaughn. "Sleep and Epilepsy." *Sleep Medicine Clinics* 11, no. 1 (2016): 25–38. https://doi.org/10.1016/j.jsmc.2015.10.008.

Khalili-Araghi, Fatemeh, Emad Tajkhorshid, and Klaus Schulten. "Dynamics of K^+ Ion Conduction through $K_V1.2$." *Biophysical Journal* 91, no. 6 (2006): L72–74. https://doi.org/10.1529/biophysj.106.091926.

Kreusch, Andreas, Paul J. Pfaffinger, Charles F. Stevens, and Senyon Choe. "Crystal Structure of the Tetramerization Domain of the Shaker Potassium Channel." *Nature* 392, no. 6679 (1998): 945–48. https://doi.org/10.1038/31978.

Krosigk, M von, T Bal, and DA McCormick. "Cellular Mechanisms of a Synchronized Oscillation in the Thalamus." *Science* 261, no. 5119 (1993): 361–64. https://doi.org/10.1126/science.8392750.

Kuba, Hiroshi, Rei Yamada, Go Ishiguro, and Ryota Adachi. "Redistribution of Kv1 and Kv7 Enhances Neuronal Excitability during Structural Axon Initial Segment Plasticity." *Nature Communications* 6, no. 1 (2015): 8815. https://doi.org/10.1038/ncomms9815.

Lancaster, B, RA Nicoll, and DJ Perkel. 1991. "Calcium Activates Two Types of Potassium Channels in Rat Hippocampal Neurons in Culture." *The Journal of Neuroscience* 11 (1): 23–30. doi:10.1523/jneurosci.11-01-00023.1991.

Landisman, Carole E., Michael A. Long, Michael Beierlein, Michael R. Deans, David L. Paul, and Barry W. Connors. "Electrical Synapses in the Thalamic Reticular Nucleus." *Journal of Neuroscience* 22, no. 3 (2002): 1002–9. https://doi.org/10.1523/jneurosci.22-03-01002.2002.

Lanigar, Sean, and Susanta Bandyopadhyay. 2017. "Sleep and Epilepsy: A Complex Interplay." *Missouri Medicine* 114 (6): 453–57.

Lerche, Holger, Mala Shah, Heinz Beck, Jeff Noebels, Dan Johnston, and Angela Vincent. "Ion Channels in Genetic and Acquired Forms of Epilepsy." *The Journal of Physiology* 591, no. 4 (2013): 753–64. https://doi.org/10.1113/jphysiol.2012.240606.

Locke, R E, and J M Nerbonne. 1997. "Role of Voltage-Gated K^+ Currents in Mediating the Regular-Spiking Phenotype of Callosal-Projecting Rat Visual Cortical Neurons." *Journal of Neurophysiology* 78 (5): 2321–35. doi:10.1152/jn.1997.78.5.2321.

Long, Stephen B., Ernest B. Campbell, and Roderick MacKinnon. "Crystal Structure of a Mammalian Voltage-Dependent *Shaker* Family K^+ Channel." *Science* 309, no. 5736 (2005): 897–903. https://doi.org/10.1126/science.1116269.

"Voltage Sensor of $K_V1.2$: Structural Basis of Electromechanical Coupling." *Science* 309, no. 5736 (2005): 903–8. https://doi.org/10.1126/science.1116270.

Long, Stephen B., Xiao Tao, Ernest B. Campbell, and Roderick MacKinnon. "Atomic Structure of a Voltage-Dependent K^+ Channel in a Lipid Membrane-like Environment." *Nature* 450, no. 7168 (2007): 376–82. https://doi.org/10.1038/nature06265.

Lorincz, Andrea, and Zoltan Nusser. "Cell-Type-Dependent Molecular Composition of the Axon Initial Segment." *The Journal of Neuroscience* 28, no. 53 (2008): 14329–40. https://doi.org/10.1523/JNEUROSCI.4833-08.2008.

Magalhães, Daniela M., Noémia Pereira, Diogo M. Rombo, Cláudia Beltrão-Cavacas, Ana M. Sebastião, and Cláudia A. Valente. 2018. "Ex Vivo Model of Epilepsy in Organotypic Slices—a New Tool for Drug Screening." *Journal of Neuroinflammation* 15 (1): 203. doi:10.1186/s12974-018-1225-2.

Maljevic, Snezana, and Holger Lerche. 2013. "Potassium Channels: A Review of Broadening Therapeutic Possibilities for Neurological Diseases." *Journal of Neurology* 260 (9): 2201–11. doi:10.1007/s00415-012-6727-8.

Mann, Edward O, Michael M Kohl, and Ole Paulsen. 2009. "Distinct Roles of GABA(A) and GABA(B) Receptors in Balancing and Terminating Persistent Cortical Activity." *The Journal of Neuroscience : The Official Journal of the Society for Neuroscience* 29 (23): 7513–18. doi:10.1523/jneurosci.6162-08.2009.

Manole, Andreea, Roope Männikkö, Michael G Hanna, SYNAPS study group, Dimitri M Kullmann, and Henry Houlden. "De Novo *KCNA2* Mutations Cause Hereditary Spastic Paraplegia." *Annals of Neurology* 81, no. 2 (2017): 326–28. https://doi.org/10.1002/ana.24866.

Martin, Melinda S, Karoni Dutt, Ligia A Papale, Céline M Dubé, Stacey B Dutton, Georgius de Haan, Anupama Shankar, et al. 2010. "Altered Function of the *SCN1A* Voltage-Gated Sodium Channel Leads to Gamma-Aminobutyric Acid-Ergic (GABAergic) Interneuron Abnormalities." *The Journal of Biological Chemistry* 285 (13): 9823–34. doi:10.1074/jbc.m109.078568.

Masnada, Silvia, Ulrike B S Hedrich, Elena Gardella, Julian Schubert, Charu Kaiwar, Eric W Klee, Brendan C Lanpher, et al. "Clinical Spectrum and Genotype–Phenotype Associations of *KCNA2*-Related Encephalopathies." *Brain* 140, no. 9 (2017): 2337–54. https://doi.org/10.1093/brain/awx184.

McTague, Amy, Katherine B Howell, J Helen Cross, Manju A Kurian, and Ingrid E Scheffer. "The Genetic Landscape of the Epileptic Encephalopathies of Infancy and Childhood." *The Lancet Neurology* 15, no. 3 (2016): 304–16. https://doi.org/10.1016/s1474-4422(15)00250-1.

Mitterdorfer, Jörg, and Bruce P. Bean. 2002. "Potassium Currents during the Action Potential of Hippocampal CA3 Neurons." *Journal of Neuroscience* 22 (23): 10106–15. doi:10.1523/jneurosci.22-23-10106.2002.

Meeren, Hanneke K M, Jan Pieter M Pijn, Egidius L J M Van Luijtelaar, Anton M L Coenen, and Fernando H Lopes da Silva. 2002. "Cortical Focus Drives Widespread Corticothalamic Networks during Spontaneous Absence Seizures in Rats." *The Journal of Neuroscience : The Official Journal of the Society for Neuroscience* 22 (4): 1480–95. doi:10.1523/jneurosci.22-04-01480.2002.

Mullen, Saul A., Samuel F. Berkovic, and the ILAE Genetics Commission. "Genetic Generalized Epilepsies." *Epilepsia* 59, no. 6 (2018): 1148–53. https://doi.org/10.1111/epi.14042.

Muona, Mikko, Samuel F Berkovic, Leanne M Dibbens, Karen L Oliver, Snezana Maljevic, Marta A Bayly, Tarja Joensuu, et al. "A Recurrent de Novo Mutation in KCNC1 Causes Progressive Myoclonus Epilepsy." *Nature Genetics* 47, no. 1 (2015): 39–46. https://doi.org/10.1038/ng.3144.

Myatt, Darren R, Tye Hadlington, Giorgio A Ascoli, and Slawomir J Nasuto. 2012. "Neuromantic – from Semi-Manual to Semi-Automatic Reconstruction of Neuron Morphology." *Frontiers in Neuroinformatics* 6: 4. doi:10.3389/fninf.2012.00004.

Nashmi, Raad, Owen T. Jones, and Michael G. Fehlings. "Abnormal Axonal Physiology Is Associated with Altered Expression and Distribution of Kv1.1 and $K_V1.2$ K^+ Channels after Chronic Spinal Cord Injury." *European Journal of Neuroscience* 12, no. 2 (2000): 491–506. https://doi.org/10.1046/j.1460-9568.2000.00926.x.

Nieh, Sahar Esmaeeli, and Elliott H. Sherr. "Epileptic Encephalopathies: New Genes and New Pathways." *Neurotherapeutics* 11, no. 4 (2014): 796–806. https://doi.org/10.1007/s13311-014-0301-2.

Nicoll, R. 1988. "The Coupling of Neurotransmitter Receptors to Ion Channels in the Brain." *Science* 241 (4865): 545–51. doi:10.1126/science.2456612.

Nishimura, Masataka, James Owens, and John W Swann. 2008. "Effects of Chronic Network Hyperexcitability on the Growth of Hippocampal Dendrites." *Neurobiology of Disease* 29 (2): 267–77. doi:10.1016/j.nbd.2007.08.018.

Oikonomou, Katerina D, Mandakini B Singh, Enas V Sterjanaj, and Srdjan D Antic. 2014. "Spiny Neurons of Amygdala, Striatum, and Cortex Use Dendritic Plateau Potentials to Detect Network UP States." *Frontiers in Cellular Neuroscience* 8: 292. doi:10.3389/fncel.2014.00292.

Ogiwara, Ikuo, Hiroyuki Miyamoto, Noriyuki Morita, Nafiseh Atapour, Emi Mazaki, Ikuyo Inoue, Tamaki Takeuchi, et al. "$Na_V1.1$ Localizes to Axons of Parvalbumin-Positive Inhibitory Interneurons: A Circuit Basis for Epileptic Seizures in Mice Carrying an *Scn1a* Gene Mutation." *The Journal of Neuroscience* 27, no. 22 (2007): 5903–14. https://doi.org/10.1523/jneurosci.5270-06.2007.

Ogiwara, Ikuo, Hiroyuki Miyamoto, Tetsuya Tatsukawa, Tetsushi Yamagata, Tojo Nakayama, Nafiseh Atapour, Eriko Miura, et al. "$Na_V1.2$ Haplodeficiency in Excitatory Neurons Causes Absence-like Seizures in Mice." *Communications Biology* 1 (2018). https://doi.org/10.1038/s42003-018-0099-2.

Oyrer, Julia, Snezana Maljevic, Ingrid E. Scheffer, Samuel F. Berkovic, Steven Petrou, and Christopher A. Reid. "Ion Channels in Genetic Epilepsy: From Genes and Mechanisms to Disease-Targeted Therapies." *Pharmacological Reviews* 70, no. 1 (2018): 142–73. https://doi.org/10.1124/pr.117.014456.

Papale, Ligia A, Christopher D Makinson, Christopher J Ehlen, Sergio Tufik, Michael J Decker, Ketema N Paul, and Andrew Escayg. "Altered Sleep Regulation in a Mouse Model of *SCN1A*-derived Genetic Epilepsy with Febrile Seizures plus (GEFS+)." *Epilepsia* 54, no. 4 (2013). https://doi.org/10.1111/epi.12060.

Pathak, Dhruba, Dongxu Guan, and Robert C Foehring. 2016. "Roles of Specific Kv Channel Types in Repolarization of the Action Potential in Genetically Identified Subclasses of Pyramidal Neurons in Mouse Neocortex." *Journal of Neurophysiology* 115 (5): 2317–29. doi:10.1152/jn.01028.2015.

Pena, S D, and R L Coimbra. "Ataxia and Myoclonic Epilepsy Due to a Heterozygous New Mutation in *KCNA2*: Proposal for a New Channelopathy." *Clinical Genetics* 87, no. 2 (2015): e1-3. https://doi.org/10.1111/cge.12542.

Polack, Pierre-Olivier, Isabelle Guillemain, Emilie Hu, Colin Deransart, Antoine Depaulis, and Stéphane Charpier. 2007. "Deep Layer Somatosensory Cortical Neurons Initiate Spike-and-Wave Discharges in a Genetic Model of Absence Seizures." *The Journal of Neuroscience : The Official Journal of the Society for Neuroscience* 27 (24): 6590–99. doi:10.1523/jneurosci.0753-07.2007.

Prüss, Harald, Gisela Grosse, Irene Brunk, Rüdiger W. Veh, and Gudrun Ahnert-Hilger. "Age-Dependent Axonal Expression of Potassium Channel Proteins during Development in Mouse Hippocampus." *Histochemistry and Cell Biology* 133, no. 3 (2010): 301–12. https://doi.org/10.1007/s00418-009-0668-z.

Ragona, Francesca, Daniela Brazzo, Ilaria De Giorgi, Monica Morbi, Elena Freri, Federica Teutonico, Elena Gennaro, et al. "Dravet Syndrome: Early Clinical Manifestations and Cognitive Outcome in 37 Italian Patients." *Brain and Development* 32, no. 1 (2010): 71–77. https://doi.org/10.1016/j.braindev.2009.09.014.

Rasband, Matthew N., and Elior Peles. "The Nodes of Ranvier: Molecular Assembly and Maintenance." *Cold Spring Harbor Perspectives in Biology* 8, no. 3 (2016): a020495. https://doi.org/10.1101/cshperspect.a020495.

Rigas, Pavlos, and Manuel A. Castro-Alamancos. 2007. "Thalamocortical Up States: Differential Effects of Intrinsic and Extrinsic Cortical Inputs on Persistent Activity." *The Journal of Neuroscience* 27 (16): 4261–72. doi:10.1523/jneurosci.0003-07.2007.

Rigas, Pavlos, Dimitrios A Adamos, Charalambos Sigalas, Panagiotis Tsakanikas, Nikolaos A Laskaris, and Irini Skaliora. 2015. "Spontaneous Up States in Vitro: A Single-Metric Index of the Functional Maturation and Regional Differentiation of the Cerebral Cortex." *Frontiers in Neural Circuits* 9: 59. doi:10.3389/fncir.2015.00059.

Reid, Christopher A., Bryan Leaw, Kay L. Richards, Robert Richardson, Verena Wimmer, Christiaan Yu, Elisa L. Hill-Yardin, et al. 2014. "Reduced Dendritic Arborization and Hyperexcitability of Pyramidal Neurons in a *Scn1b*-Based Model of Dravet Syndrome." *Brain* 137 (6): 1701–15. doi:10.1093/brain/awu077.

Reid, Christopher A., Samuel F. Berkovic, and Steven Petrou. "Mechanisms of Human Inherited Epilepsies." *Progress in Neurobiology* 87, no. 1 (2009): 41–57. https://doi.org/10.1016/j.pneurobio.2008.09.016.

Rezazadeh, Saman, Harley T. Kurata, Thomas W. Claydon, Steven J. Kehl, and David Fedida. "An Activation Gating Switch in $K_V1.2$ Is Localized to a Threonine Residue in the S2-S3 Linker." *Biophysical Journal* 93, no. 12 (2007): 4173–86. https://doi.org/10.1529/biophysj.107.116160.

Robbins, Carol A, and Bruce L Tempel. "Kv1.1 and $K_V1.2$: Similar Channels, Different Seizure Models." *Epilepsia* 53, no. s1 (2012): 134–41. https://doi.org/10.1111/j.1528-1167.2012.03484.x.

Sachdev, Monisha, Marina Gaínza-Lein, Dmitry Tchapyjnikov, Yong-Hui Jiang, Tobias Loddenkemper, and Mohamad A. Mikati. "Novel Clinical Manifestations in Patients with *KCNA2* Mutations." *Seizure* 51 (2017): 74–76. https://doi.org/10.1016/j.seizure.2017.07.018.

Sah, P. 1995. "Properties of Channels Mediating the Apamin-Insensitive Afterhyperpolarization in Vagal Motoneurons." *Journal of Neurophysiology* 74 (4): 1772–76. doi:10.1152/jn.1995.74.4.1772.

Sah, Pankaj, and John M Bekkers. 1996. "Apical Dendritic Location of Slow Afterhyperpolarization Current in Hippocampal Pyramidal Neurons: Implications for the Integration of Long-Term Potentiation." *The Journal of Neuroscience* 16 (15): 4537–42. doi:10.1523/jneurosci.16-15-04537.1996.

Saito, T, and N Nakatsuji. 2001. "Efficient Gene Transfer into the Embryonic Mouse Brain Using in Vivo Electroporation." *Developmental Biology* 240 (1): 237–46. doi:10.1006/dbio.2001.0439.

Saito, Tetsuichiro. 2006. "In Vivo Electroporation in the Embryonic Mouse Central Nervous System." *Nature Protocols* 1 (3): 1552–58. doi:10.1038/nprot.2006.276.

Salkoff, Lawrence, and Robert Wyman. "Genetic Modification of Potassium Channels in Drosophila Shaker Mutants." *Nature* 293, no. 5829 (1981): 228–30. https://doi.org/10.1038/293228a0.

Sanchez-Vives, Maria V, Maurizio Mattia, Albert Compte, Maria Perez-Zabalza, Milena Winograd, Vanessa F Descalzo, and Ramon Reig. 2010. "Inhibitory Modulation of Cortical Up States." *Journal of Neurophysiology* 104 (3): 1314–24. doi:10.1152/jn.00178.2010.

Sanchez-Vives, MV, and DA McCormick. "Cellular and Network Mechanisms of Rhythmic Recurrent Activity in Neocortex." *Nature Neuroscience* 3, no. 10 (2000): 1027–34. https://doi.org/10.1038/79848.

Saviane, Chiara, Majid H Mohajerani, and Enrico Cherubini. 2003. "An ID-like Current That Is Downregulated by $Ca2^+$ Modulates Information Coding at CA3-CA3 Synapses in the Rat Hippocampus." *The Journal of Physiology* 552 (Pt 2): 513–24. doi:10.1113/jphysiol.2003.051045.

Scanziani, Massimo, and Michael Häusser. 2009. "Electrophysiology in the Age of Light." *Nature* 461 (7266): 930–39. doi:10.1038/nature08540.

Scheffer, Ingrid E., Samuel Berkovic, Giuseppe Capovilla, Mary B. Connolly, Jacqueline French, Laura Guilhoto, Edouard Hirsch, et al. "ILAE Classification of the Epilepsies: Position Paper of the ILAE Commission for Classification and Terminology." *Epilepsia* 58, no. 4 (2017): 512–21. https://doi.org/10.1111/epi.13709.

Sejnowski, Terrence J, Patricia S Churchland, and J Anthony Movshon. 2014. "Putting Big Data to Good Use in Neuroscience." *Nature Neuroscience* 17 (11): 1440–41. doi:10.1038/nn.3839.

Sengupta, Biswa, A Aldo Faisal, Simon B Laughlin, and Jeremy E Niven. 2013. "The Effect of Cell Size and Channel Density on Neuronal Information Encoding and Energy Efficiency." *Journal of Cerebral Blood Flow and Metabolism : Official Journal of the International Society of Cerebral Blood Flow and Metabolism* 33 (9): 1465–73. doi:10.1038/jcbfm.2013.103.

Shen, N.Vivienne, and Paul J Pfaffinger. "Molecular Recognition and Assembly Sequences Involved in the Subfamily-Specific Assembly of Voltage-Gated K^+ Channel Subunit Proteins." *Neuron* 14, no. 3 (1995): 625–33. https://doi.org/10.1016/0896-6273(95)90319-4.

Shen, Weixing, Salvador Hernandez-Lopez, Tatiana Tkatch, Joshua E Held, and James D Surmeier. "K_V1.2-Containing K^+ Channels Regulate Subthreshold Excitability of Striatal Medium Spiny Neurons." *Journal of Neurophysiology* 91, no. 3 (2004): 1337–49. https://doi.org/10.1152/jn.00414.2003.

Shimogori, Tomomi, and Masaharu Ogawa. 2008. "Gene Application with in Utero Electroporation in Mouse Embryonic Brain." *Development, Growth & Differentiation* 50 (6): 499–506. doi:10.1111/j.1440-169x.2008.01045.x.

SHOLL, DA. 1953. "Dendritic Organization in the Neurons of the Visual and Motor Cortices of the Cat." *Journal of Anatomy* 87 (4): 387–406.

Siddiqi, Faez, Fuyi Chen, Abraham W Aron, Christopher G Fiondella, Komal Patel, and Joseph J LoTurco. 2012. "Fate Mapping by PiggyBac Transposase Reveals That Neocortical GLAST+ Progenitors Generate More Astrocytes than Nestin+ Progenitors in Rat Neocortex." *Cerebral Cortex (New York, N.Y. : 1991)* 24 (2): 508–20. doi:10.1093/cercor/bhs332.

Spain, W J, P C Schwindt, and W E Crill. 1991. "Two Transient Potassium Currents in Layer V Pyramidal Neurones from Cat Sensorimotor Cortex." *The Journal of Physiology* 434 (1): 591–607. doi:10.1113/jphysiol.1991.sp018488.

Starace, Dorine M, and Francisco Bezanilla. "A Proton Pore in a Potassium Channel Voltage Sensor Reveals a Focused Electric Field." *Nature* 427, no. 6974 (2004): 548–53. https://doi.org/10.1038/nature02270.

Steriade, M. "Corticothalamic Resonance, States of Vigilance and Mentation." *Neuroscience* 101, no. 2 (2000): 243–76. https://doi.org/10.1016/s0306-4522(00)00353-5.

Steriade, M, DA McCormick, and TJ Sejnowski. 1993. "Thalamocortical Oscillations in the Sleeping and Aroused Brain." *Science* 262 (5134): 679–85. doi:10.1126/science.8235588.

Steriade, Mircea. 2005. "Sleep, Epilepsy and Thalamic Reticular Inhibitory Neurons." *Trends in Neurosciences* 28 (6): 317–24. doi:10.1016/j.tins.2005.03.007.

Storm, J F. 1987. "Action Potential Repolarization and a Fast After-Hyperpolarization in Rat Hippocampal Pyramidal Cells." *The Journal of Physiology* 385 (1): 733–59. doi:10.1113/jphysiol.1987.sp016517.

Suarez-Delgado, Esteban, Teriws G Rangel-Sandin, Itzel G Ishida, Gisela E Rangel-Yescas, Tamara Rosenbaum, and Leon D Islas. "K_V1.2 Channels Inactivate through a Mechanism Similar to C-Type Inactivation." *BioRxiv*, 2019, 784249. https://doi.org/10.1101/784249.

Syrbe, Steffen, Ulrike BS Hedrich, Erik Riesch, Tania Djémié, Stephan Müller, Rikke S Møller, Bridget Maher, et al. "De Novo Loss- or Gain-of-Function Mutations in *KCNA2* Cause Epileptic Encephalopathy." *Nature Genetics* 47, no. 4 (2015): 393–99. https://doi.org/10.1038/ng.3239.

Tabata, H, and K Nakajima. 2001. "Efficient in Utero Gene Transfer System to the Developing Mouse Brain Using Electroporation: Visualization of Neuronal Migration in the Developing Cortex." *Neuroscience* 103 (4): 865–72. doi:10.1016/s0306-4522(01)00016-1.

Tombola, Francesco, Medha M Pathak, and Ehud Y Isacoff. "Voltage-Sensing Arginines in a Potassium Channel Permeate and Occlude Cation-Selective Pores." *Neuron* 45, no. 3 (2005): 379–88. https://doi.org/10.1016/j.neuron.2004.12.047.

Trimmer, James S. "Subcellular Localization of K^+ Channels in Mammalian Brain Neurons: Remarkable Precision in the Midst of Extraordinary Complexity." *Neuron* 85, no. 2 (2015): 238–56. https://doi.org/10.1016/j.neuron.2014.12.042.

Vacher, Helene, Durga P Mohapatra, and James S Trimmer. "Localization and Targeting of Voltage-Dependent Ion Channels in Mammalian Central Neurons." *Physiological Reviews* 88, no. 4 (2008): 1407–47. https://doi.org/10.1152/physrev.00002.2008.

Vanmolkot, Kaate R.J., Elena Babini, Boukje de Vries, Anine H. Stam, Tobias Freilinger, Gisela M. Terwindt, Lisa Norris, et al. "The Novel p.L1649Q Mutation in the *SCN1A* Epilepsy Gene Is Associated with Familial Hemiplegic Migraine: Genetic and Functional Studies." *Human Mutation* 28, no. 5 (2007): 522–522. https://doi.org/10.1002/humu.9486.

Wang, Wenying, Hyo Kim, Ping Lv, Bruce Tempel, and Ebenezer N Yamoah. 2013. "Association of the Kv1 Family of K^+ Channels and Their Functional Blueprint in the Properties of Auditory Neurons as Revealed by Genetic and Functional Analyses." *Journal of Neurophysiology* 110 (8): 1751–64. doi:10.1152/jn.00290.2013.

Wang, Xiu-Chao, Shan Wang, Ming Zhang, Fang Gao, Chun Yin, Hao Li, Ying Zhang, San-Jue Hu, and Jian-Hong Duan. "A-Dendrotoxin-Sensitive Kv1 Channels Contribute to Conduction Failure of Polymodal Nociceptive C-Fibers from Rat Coccygeal Nerve." *Journal of Neurophysiology* 115, no. 2 (2015): 947–57. https://doi.org/10.1152/jn.00786.2014.

Watson, Brendon O, Jason N MacLean, and Rafael Yuste. 2008. "UP States Protect Ongoing Cortical Activity from Thalamic Inputs." *PloS One* 3 (12): e3971. doi:10.1371/journal.pone.0003971.

Wilson, Charles. "Up and down States." *Scholarpedia Journal* 3, no. 6 (2008): 1410.

Xie, Gang, John Harrison, Steven J Clapcote, Yun Huang, Jin-Yi Zhang, Lu-Yang Wang, and John C Roder. "A New K_V1.2 Channelopathy Underlying Cerebellar Ataxia." *Journal of Biological Chemistry* 285, no. 42 (2010): 32160–73. https://doi.org/10.1074/jbc.M110.153676.

Xia, X -M, B Fakler, A Rivard, G Wayman, T Johnson-Pais, J E Keen, T Ishii, et al. 1998. "Mechanism of Calcium Gating in Small-Conductance Calcium-Activated Potassium Channels." *Nature* 395 (6701): 503–7. doi:10.1038/26758.

Yellen, Gary. "The Voltage-Gated Potassium Channels and Their Relatives." *Nature* 419, no. 6902 (2002): 35–42. https://doi.org/10.1038/nature00978.

Yu, Frank H, Massimo Mantegazza, Ruth E Westenbroek, Carol A Robbins, Franck Kalume, Kimberly A Burton, William J Spain, G Stanley McKnight, Todd Scheuer, and William A Catterall. "Reduced Sodium Current in GABAergic Interneurons in a Mouse Model of Severe Myoclonic Epilepsy in Infancy." *Nature Neuroscience* 9, no. 9 (2006): 1142–49. https://doi.org/10.1038/nn1754.

Zhang, Gaofeng, Mathew Edmundson, Vsevolod Telezhkin, Yu Gu, Xiaoqing Wei, Paul J. Kemp, and Bing Song. "The Role of K_V1.2 Channel in Electrotaxis Cell Migration." *Journal of Cellular Physiology* 231, no. 6 (2016): 1375–84. https://doi.org/10.1002/jcp.25259.

Acknowledgments

First and foremost, I would like to thank my family especially my parents and my wife, Dr. Gurpreet Kaur who extended their confidence and infinite support in every aspect of my thesis and making my mind relax during the hard times.

I owe my heartiest gratitude to my mentor Prof. Dr. Holger Lerche for giving me the opportunity and facilities to pursue Ph.D. studies in the Department of Neurology and Epileptology. I highly appreciate his intellectual guidance, time-to-time critical evaluation and valuable suggestions throughout the course of my research work. I am equally indebted to Dr. Ulrike Hedrich-Klimosch for her extremely helpful discussions, scientific expertise and friendly support, which made my work fruitful. Additionally, I am thankful to Prof. Dr. Cornelius Schwarz and Prof. Dr. Jan Benda for being members of my doctoral advisory board and their valuable suggestions.

It is a great pleasure to extend my thanks to Dr. Henner Koch for his suggestion in the sleep project and Dr. Thomas Wuttke for his help *in utero* electroporation experiments. I am grateful to Pu Yan, Dr. Julian Schubert, Dr. Mahmoud Koko Musa, Dr. Filip Rosa and Dr. Niklas Schwarz for their help and suggestions in molecular biology experiments. Special thanks to Heidi Loeffler for teaching the cell culture techniques. Many sincere thanks to my lab buddies Philipp Luehrs, Niklas Vogel, Jacqueline Bahr and Kornelijus Stanaitis for fun, emotional support and stress bursting sessions. I would also like to thank my other past and current lab members Dr. Snezana Maljevic, Dr. Cristina Elena Niturad, Simone Seiffert, Johanna Krueger, Dr. Yuanyuan Liu, Betül Uysal, Merle Harrer, Ana Fulgencio Maisch, Dr. Ahmed Eltokhi and Nikolas Layer.

I am also grateful to my brother Dr. Sunil Kumar. K, and my Master mentor Dr. R. Harikumaran Nair for their constant encouragement and guidance.

Above all, I also would like to specially thank my little scientist Aatika Preet. She joined us during my thesis and giving me infinite happiness and immense pleasure. I appreciate her for the patience she showed during my thesis writing.

Harshad P.A.